NASA CONTRACTOR REPORT

N73-16255
NASA CR-2156

NASA CR-2156

CAVITATION IN LIQUID CRYOGENS

II - Hydrofoil

by J. Hord

Prepared by
NATIONAL BUREAU OF STANDARDS
Boulder, Colo. 80302
for Lewis Research Center

NATIONAL AERONAUTICS AND SPACE ADMINISTRATION • WASHINGTON, D. C. • JANUARY 1973

1. Report No.	2. Government Accession No.	3. Recipient's Catalog No.
NASA CR-2156		

4. Title and Subtitle	5. Report Date
CAVITATION IN LIQUID CRYOGENS II - HYDROFOIL	December 1972 6. Performing Organization Code
7. Author(s)	8. Performing Organization Report No.
J. Hord	None
9. Performing Organization Name and Address	10. Work Unit No.
National Bureau of Standards Boulder, Colorado 80302	11. Contract or Grant No. C-39004B
12. Sponsoring Agency Name and Address	13. Type of Report and Period Covered
National Aeronautics and Space Administration Washington, D.C. 20546	Contractor Report 14. Sponsoring Agency Code

15. Supplementary Notes

Project Manager, Werner R. Britsch, Fluid System Components Division, NASA Lewis Research Center, Cleveland, Ohio

16. Abstract

This document constitutes the second of four volumes to be issued on the results of continuing cavitation studies. Boundary layer principles, along with two-phase flow concepts, are used to improve existing correlative theory for developed cavity data. Details concerning cavity instrumentation, data analysis, correlative techniques, and experimental and theoretical aspects of a cavitating hydrofoil are given. Both desinent and thermodynamic data, using liquid hydrogen and liquid nitrogen, are reported here. The thermodynamic data indicated that stable thermodynamic equilibrium exists throughout the vaporous cryogen cavities. The improved correlative formulae were used to evaluate these data. A new correlating parameter, based on consideration of mass limiting two-phase flow flux across the cavity interface, is proposed. This correlating parameter appears attractive for future correlative and predictive applications. Agreement between theory and experiment is discussed, and directions for future analysis are suggested. The front half of the cavities, developed on the hydrofoil, may be considered as parabolically shaped.

17. Key Words (Suggested by Author(s))		18. Distribution Statement
Cavitation	Pumps	Unclassified - unlimited
Cryogenics	Venturi	
Hydrofoil		
Nucleation		

19. Security Classif. (of this report)	20. Security Classif. (of this page)	21. No. of Pages	22. Price*
Unclassified	Unclassified	162	$3.00

* For sale by the National Technical Information Service, Springfield, Virginia 22151

CONTENTS

LIST OF FIGURES

LIST OF FIGURES (Continued)

LIST OF TABLES

CAVITATION IN LIQUID CRYOGENS
II - HYDROFOIL

J. Hord

1. SUMMARY

This document constitutes the second of four volumes to be issued on the results of continuing cavitation studies. The first volume dealt with venturi experiments, and this second volume is concerned with a 0.5-caliber hydrofoil.

Convective heat transfer and two-phase mass-flow flux limiting concepts are used to extend, and improve, existing formulae for correlating developed cavitation data. These correlative expressions are also suitable for predicting the cavitating performance of a particular piece of equipment from one fluid to another. Elementary boundary layer principles and two-phase flow models are used to derive these expressions. A new correlating parameter, MTWO, is derived; MTWO is a liquid phase velocity ratio that is deceptively similar to a Mach number and is derived from two-phase flow considerations.

Details of the hydrofoil-tunnel configuration, cavity instrumentation, data analysis, and correlative techniques are discussed.

Experimental data resulting from this study are presented in their entirety in tabular form. Selected data are also presented in graphical form. Both desinent and developed cavity data were acquired, using liquid hydrogen and liquid nitrogen test fluids. A mathematical technique, for correlating the desinent data, was developed and is explained in detail. The desinent data exhibit a nearly single-valued K_{iv}, for each fluid, at the maximum velocities, irrespective of fluid temperature. Similar results were obtained with the venturi. The desinent hydrogen data were more temperature-dependent than the

nitrogen data. Comparison of our desinent data with that of others--for higher boiling-point liquids--shows that cryogenic liquids require less subcooling to avoid cavitation, i. e. , less Net Positive Suction Pressure (NPSP) is required for the cryogens.

Thermodynamic data, consisting of pressure and temperature measurements within fully developed hydrogen and nitrogen cavities, indicated that stable thermodynamic equilibrium prevails throughout the vaporous cavities. These data were correlated using the extended theory derived herein. In certain instances, data correlation is improved by using liquid kinematic viscosity as a correlating parameter. Maximum benefit, in data correlation, is obtained by using the new MTWO parameter. When MTWO is used, it appears that only one other correlating parameter, cavity length, may be required. Use of MTWO, to correlate or predict the performance of cavitating equipment, is recommended in all future work.

Correlative expressions, experimentally evaluated, are in fair agreement with those derived from the boundary layer analysis. More analysis is needed to explain the subtleties, of the combined mass and heat transfer processes, that govern the cavitation process.

$K_{c,min}$ is known to vary widely with equipment geometry. This study demonstrates that $K_{c,min}$ can also vary appreciably with flow conditions, although the equipment geometry is fixed. This information, coupled with that of others, indicates that current predictive techniques must be used with prudence, i. e. , the techniques that rely upon constant $K_{c,min}$ admit an additional source of error for some equipment geometries.

Photographic studies, performed during this experiment, indicate that the cavities formed on the hydrofoil have an elliptical shape. The

front halves of these cavities are adequately represented by a simple algebraic expression of parabolic form.

2. INTRODUCTION

Vaporous cavitation is the formation of the vapor phase within a flowing liquid, due to a reduction in pressure. Since the formation and collapse of vapor cavities alters flow patterns, cavitation may reduce the efficiency of pumping machinery [1][1] and reduce the precision of flow measuring devices. Collapse of these vapor cavities can also cause serious erosion damage [2] to fluid-handling equipment. While the noncavitating performance of hydraulic equipment may be predicted from established similarity laws, cavitating performance is much more difficult to predict from fluid-to-fluid. Recent advances in this area have been made by NASA-LeRC personnel [3-6] and others [7-9], but additional work is required to improve the current technique for predicting cavitating performance of equipment from fluid-to-fluid. The effects of fluid properties on cavitation performance are well recognized [10-19] and require more understanding to develop improved similarity relations [19] for equipment behavior. Much more knowledge is needed to extend this predictive capability from one piece of equipment to another, i.e., a more general predictive technique, applicable to equipment design, must include the effects of equipment geometry and size, in addition to fluid properties.

NASA has undertaken a program [1] to determine the cavitation characteristics of various hydrodynamic bodies and the thermodynamic behavior of different fluids, in an effort to obtain improved design criteria to aid in the prediction of cavitating pump performance. The experimental and analytical study described herein was conducted in support of this program.

---

[1] Numbers in brackets indicate references at the end of this paper.

Liquid hydrogen and liquid nitrogen were chosen as test fluids for this study for the following reasons: (1) the ultimate goal of this program is to acquire sufficient knowledge to permit intelligent design of pumps for near-boiling liquids, and (2) predictive analyses indicated [1] that the physical properties of hydrogen and nitrogen make them particularly desirable test fluids. The objectives of this study were 1) to experimentally determine the flow and thermodynamic conditions required to induce desinent (or incipient) and developed cavitation on various hydrodynamic bodies, 2) to improve existing correlative expressions for the prediction of cavitating performance of hydraulic equipment, and 3) to establish, if possible, a technique for predicting the fluid-handling capability of different cavitating equipment using different fluids. The latter two items are extensions of the state-of-the-art and the last objective is highly optimistic, i. e., accounting for the effects of equipment geometry and size in the predictive expressions.

This report covers the work performed on a two dimensional body (hydrofoil). Similar results, using a transparent plastic venturi, were presented in Volume I of this report series [20].

In the desinent (or incipient) cavity studies, the test section inlet velocity was varied from 103.7 to 200.5 ft/s (31.6 to 61.1 m/s) with hydrogen, and from 24.2 to 74.1 ft/s (7.4 to 22.6 m/s) with nitrogen. Inlet fluid temperatures were varied from 36.58 to 41.60 R (20.32 to 23.11 K) with hydrogen, and from 137.45 to 160.06 R (76.36 to 88.92 K) with nitrogen. Both incipient and desinent cavitation data were acquired with hydrogen and nitrogen test fluids; however, the incipient nitrogen data were not used in the final data correlations--see appendix C. A slight hysteresis effect was detected with nitrogen, but there was no noticeable hysteresis in the hydrogen data; i. e., for hydrogen the flow

conditions associated with barely visible cavities did not vary, even though the data point was approached from noncavitating (incipient) flow, and from developed cavitating (desinent) flow. In this report, desinence refers to barely visible cavities, and for convenience the terms incipience and desinence are used interchangeably.

Pressure and temperature profiles, within fully developed cavities, were measured and are referred to herein as developed cavitation data. Cavity lengths varied from 0.35 to 1.75 inches (0.89 to 4.45 cm) with hydrogen and from 0.45 to 2.00 inches (1.14 to 5.08 cm) with nitrogen. Test section inlet velocities were varied from 113.2 to 219.1 ft/s (34.5 to 66.8 m/s) with hydrogen and from 26.7 to 80.2 ft/s (8.1 to 24.4 m/s) with nitrogen. Inlet liquid temperatures were varied from 36.47 to 41.53 R (20.26 to 23.07 K) with hydrogen and from 137.41 to 159.79 R (76.34 to 88.7 K) with nitrogen. The bulkstream vapor pressure exceeds the measured cavity pressure and the saturation pressure corresponding to the measured cavity temperature; therefore, the measured pressure depressions within the cavity, and also the pressure depressions corresponding to the measured temperature depressions, are called "pressure depressions." Alternatively, the pressure depression may be expressed in terms of its equivalent equilibrium "temperature depression." Contrary to the venturi tests [20, 21], no thermodynamic metastability was detected within the vaporous hydrogen or nitrogen cavities developed on the hydrofoil; i.e., measured temperatures and pressures within the cavitated regions, appeared to be in thermodynamic equilibrium.

A similarity equation, based upon the B-factor concept of Stahl and Stepanoff [11], has been developed [19] for correlating cavitation data for a particular test item from fluid-to-fluid; this correlation is

also useful in extending the velocity and temperature range of data for any given fluid. This correlative expression has been subjected to some criticism,[2] and obviously has some theoretical defects. In this report, thermal boundary layer considerations are used to place this correlative expression on a firmer analytical base; also, the similarity approach is extended to include the effects of convective heat transfer. Two additional correlating parameters, liquid viscosity and liquid-vapor surface tension, emerge from this analysis. A convection-oriented dimensional analysis is also performed and a two-phase liquid-vapor sonic velocity correlating parameter is introduced. Two-phase mass-flow flux limiting concepts are then used to combine this two-phase sonic velocity parameter, with the liquid inlet velocity parameter. A new and valuable correlating parameter, MTWO, results. The correlative expressions resulting from these analyses are evaluated using experimental data from this study.

3. ANALYTICAL CONSIDERATIONS

In this section, we shall endeavor to upgrade the theoretical framework for correlating developed cavitation data and the cavitating performance of equipment. The basic approach of Gelder, et al. [19], with some major improvements, will be used; this approach is an extension of the B-factor concept introduced by Stahl and Stepanoff [11]. A history of the development of the B-factor theory and an improved technique for calculating B-factor were recently published [23]; this article [23] indicates that the "quasi-static" vaporization model, based upon isentropic flashing of the liquid, is reasonably compatible with the physical processes of cavitation. Of some concern is the assumption that this isentropic vaporization occurs under stable thermodynamic

[2] See discussions at end of papers by Moore [5] and Ruggeri [22].

equilibrium conditions. There is experimental evidence [20] of slight thermodynamic metastabilities in the midregions of vaporous hydrogen cavities, although most data [19-21] indicate that thermodynamic equilibrium exists near the leading edge of vaporous cavities in a wide variety of liquids. Consequently, it appears that the B-factor concept is compatible with the physical processes of cavitation, so long as we restrict our attention to the leading edges of the cavity where vaporization most surely occurs. The B-factor concept may be viewed as an abstract quantity, analogous to entropy in the study of thermodynamics, used to obtain a simple solution to our complex and physically real problem. Further improvement of the B-factor approach is desirable because 1) the concept of isentropic vaporization at the leading edges of the cavity is reasonably compatible with the conditions of our problem, 2) this approach is well established [19] and provides good results when applied to cavitating equipment [4-6], and 3) current efforts to account for the dynamic effects of cavitation via bubble growth [9], or entrainment theory [24], have not yet resulted in a correlative technique that is less complex or less dependent upon experimental data. Also, it appears that the B-factor approach consistently provides the best correlative results [9]. Thus, it is the intention of this paper to provide a firmer theoretical foundation for an improved B-factor correlative approach.

It will be shown that the simple thermal conduction model used by Gelder, et al., [19] is a special case of a more general 'convection' model developed herein. The fundamentals of boundary layer theory and convective heat transfer are used to derive the appropriate parametric expressions. Because it is correlating parameters that we seek, it is not necessary to concern ourselves with the mathematical rigors of an exact and specific boundary layer analysis; however, application of the thermal boundary layer concepts should yield the pertinent

heat transfer correlating parameters, thereby placing the B-factor approach on firmer ground. Under certain engineering assumptions, we shall establish a convective heat transfer model believed applicable to the developed cavitation process. In those areas where assumptions are required, and little or no information exists, it will be apparent that there is a willingness of the author to be guided by experimental data. From this analysis, liquid viscosity and surface tension emerge as additional correlating parameters. A dimensional analysis confirms the boundary layer analysis and introduces the possibility of still an additional correlating parameter--the liquid-vapor two-phase acoustic velocity.

3.1 Convection Model (boundary layer analysis)

That convective heat transfer must be involved in the cavitation process is apparent. It is therefore equally apparent that the conductive heat transfer model used by Gelder, et al., [19] is inadequate.[3] Despite its shortcomings, the method of Gelder, et al., has been surprisingly successful in predicting the cavitating performance of liquid pumps. From this, we can only conclude that their correlative expression, though simplified, contains the essential correlating parameters. The conduction model used by Gelder, et al., [19] was based on an analysis performed by Eisenberg and Pond [25]; this analysis simply relates the heat extracted from a liquid film, of constant thickness, to the bulk-stream velocity, and to the heat transferred through this film by conduction. Gelder, et al., [19] also assumed that the cavity thickness did not vary with length; it has subsequently been shown [26] that correlation of experimental data with theory can be materially improved, by assuming an appropriate shape for the cavity. In the analysis that

[3] See discussions at end of paper by Ruggeri [22].

follows, a forced convection heat transfer model is proposed; this model features a liquid film with dimensions proportional to the thermal boundary layer, and a parabolic-shaped cavity. The resulting expressions permit the computation of B-factor which is then related through the entropy calculations [23] to the physical cavitation process, i.e., to the cavity pressure depression, or temperature depression, and ultimately to the predicted [3-5] equipment operating conditions.

The two-dimensional model is shown in figure 3.1a; figure 3.1b will be used later in considering the axisymmetric case. A number of engineering assumptions are required to proceed with the analysis, and each is sufficiently important to be discussed in detail. Referring to figure 3.1a, we will assume that flow is forced over the flat plate by an imposed pressure gradient in the bulkstream liquid, i.e., by external means unrelated to the temperature field in the liquid. Body forces are hereby neglected, and it will be further assumed that the vapor-filled cavity springs from the leading edge of the flat plate (or submerged body)--the latter is in good agreement with experimental results. We will then assume that the liquid flows over the cavity as if it were a solid body. Sufficient heat transfer must occur to vaporize enough liquid molecules to sustain the cavity under steady flow conditions; therefore, we will assume the existence of a thermal boundary layer in the liquid flowing over the liquid-vapor interface (cavity wall). Because of the uncertainty of the flow patterns, circulation, etc., of the vapor within the cavity, it is difficult to assess the virtue of this assumption. Certainly, the vaporous cavity must lubricate the liquid flow, and the relative velocity of liquid/vapor is unknown; consequently, it is possible that the liquid flow at the cavity interface may be laminar even though the bulkstream liquid is highly turbulent. It is also possible that the

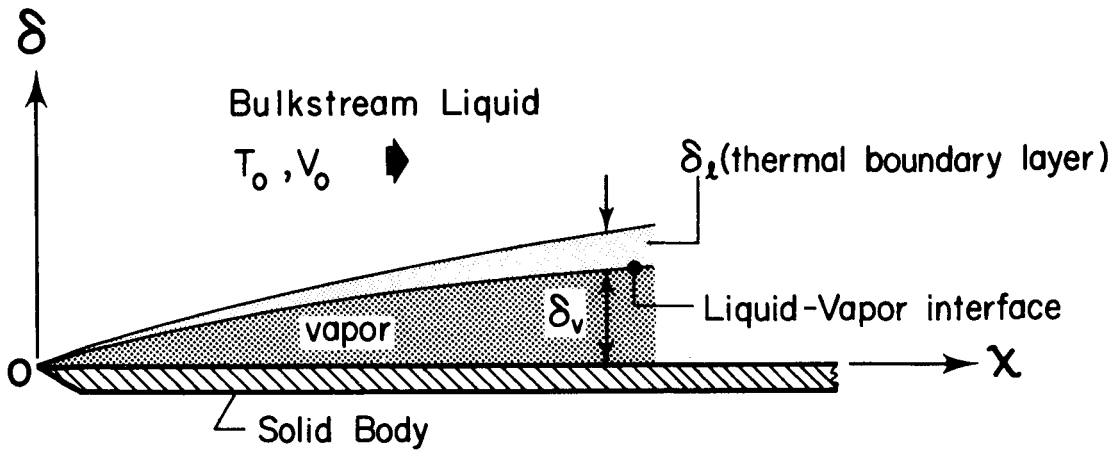

3.1a Basic flat plate model.

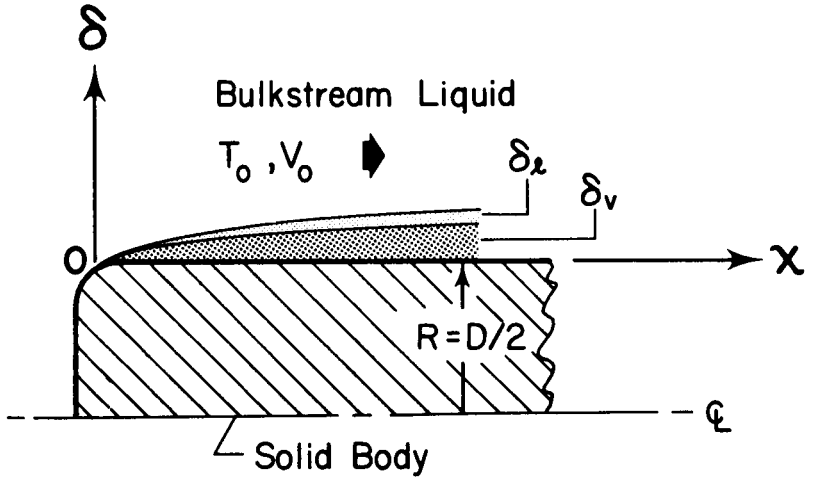

3.1b Axisymmetric model.

Figure 3.1 Convective heat transfer model--thermal boundary layer analysis.

liquid flow at the liquid-vapor interface is turbulent; therefore, we shall examine both laminar and turbulent thermal boundary layers in the liquid flowing over the liquid-vapor interface. Under these assumptions, the roughness of the interface (cavity wall) can also influence the turbulence level and affect the heat transfer coefficient [27--p. 75]. The fluid bulkstream Reynolds number will be turbulent, i.e., $> 10^6$ in most cavitating systems, but the possibility of laminar flow is not to be discounted.

In connection with the foregoing assumption, we shall permit no blowing or suction at the interface; in effect, this means that no mass transfer from the liquid to vapor phase will be allowed at the interface. Obviously, this assumption is violated because the liquid must have a velocity component normal to the interface, and there must be some mass exchange between the liquid and vapor phases to sustain the cavity; however, the liquid/vapor density ratio is large for all liquids, and the cavity may easily be sustained by the vaporization of relatively few molecules of liquid in the thermal boundary layer. This justification is less valid as we approach the fluid critical point and the liquid/vapor density ratio decreases. Again, this 'no-suction' assumption is difficult to evaluate, because we have insufficient knowledge concerning the net flow of vapor through the cavity and the rate of vaporization required to sustain this vapor flow and hence the developed vaporous cavity. With due consideration to the foregoing arguments, and to the other assumptions required in this particular analysis, the introduction of mass transfer concepts does not appear warranted. This decision becomes even more plausible when we recall that we only seek correlating parameters--the functional relationship will be established empirically.

We shall also assume that this limited vaporization, at the interface, has negligible effect on the shape and thickness of the thermal boundary layer and the vaporous cavity. For simplicity, we shall also neglect the curvature of the liquid-vapor interface in deriving an expression for the thermal boundary layer thickness; this interface curvature is retained in describing the cavity thickness. Neglecting interface curvature and considering the cavity as a solid body that springs from the leading edge of the hydrodynamic body, reduces our problem to that of flow over a wedge. The cavity will always originate at or near the leading edge of the hydrodynamic body, and the foregoing assumptions essentially eliminate the geometrical configuration of the hydrodynamic body from our boundary layer analysis. The decision to neglect curvature of the interface, in the evaluation of boundary layer thickness, does not necessarily result in flow over a wedge--we could, for example, merely require that the curvature of the interface and the curvature of the boundary layer be sufficiently close that transformation to linear coordinates does not induce appreciable error. While the shape of the hydrodynamic body does not appear to be important to the boundary layer analysis, it certainly affects the shape of the attached vapor cavity; consequently, the cavity vapor volume and subsequent empirical results will be influenced by the body shape. We will therefore restrict our correlative results to applications where geometric and dynamic similarity can be reasonably assured, i. e., where identical or similar hydraulic equipment is used.

We will assume that the vapor cavity is relatively thin, so that we may approximate our problem--for any arbitrary shape--by considering forced flow over a flat plate. The thermal boundary layer in the liquid will also be taken as sufficiently thin that interaction with

other boundary layers can be ignored, i.e., the body is immersed in a semi-infinite flow field (no bounding walls). The hydrodynamic and thermal boundary layers will be assumed to originate with the cavity, at the leading edge of the body, whether the flow be laminar or turbulent. This condition causes us to specify that the liquid-vapor interface be at constant temperature [27--p. 204, 234]. Experimental evidence [19-21] indicates the interface temperature varies slightly, but as previously noted we prefer to restrict our analysis to the leading edges of the cavity where little temperature variation occurs.

Consistent with this argument is the assumption that liquid properties remain constant as the liquid flows along the cavity wall. Fortunately, relatively small temperature-depressions, due to vaporization, occur along the cavity interface and the fluid properties cannot vary significantly. In addition, we have the option of evaluating the fluid properties at the reduced (cavity) temperature or at a mixed mean temperature if we so desire. Past experience indicates that the physical properties can be evaluated at the bulkstream temperature without sacrifice in the correlative results. To maintain constant fluid properties, we must also neglect liquid compressibility and limit our flow to relatively low velocities, i.e., the effects of kinetic energy and viscous energy dissipation are neglected. We will require the freestream velocity to be invariant along the cavity wall. The hydrodynamic boundary layer is thicker than the thermal boundary layer in laminar flow, but the two are of about the same thickness in turbulent flow [27--p. 234]. The latter situation results [27--p. 234] because the transfer mechanism through a turbulent boundary layer is primarily eddy diffusion, and the eddy diffusivities for heat and momentum are nearly equal where the liquid Prandtl number is in the range 0.5 to 10--our range of interest.

It is assumed that boundary layer separation (stall) does not occur, and that the isentropic flashing model [23] is applicable to the vaporization occurring at the leading edge of the cavity. Compatibility of this model with the actual cavitation process has already been discussed. We would like to emphasize that liquid-vapor thermodynamic equilibrium normally exists [19-21] near the cavity leading edge, with metastability occurring in some cases [20] in the central regions of the cavity. With due respect to this experimental data, we note that radial probing (temperature and pressure measurement normal to the cavity wall) has not been, and perhaps cannot be, accomplished; thus, we have no guarantee that stable thermodynamic equilibrium does or does not exist along the entire liquid-vapor interface. To the best of our knowledge, it is safe to assume that liquid-vapor equilibrium does exist along the leading edges of the cavity. Experimental data indicate, as would be expected [20], that slower liquid velocities promote liquid-vapor equilibrium throughout the developed cavities.

Under the stipulated assumptions, we cover a wide range of practical cavitating flow applications, e.g., flow over hydrofoils, turbines, inducers, impellers, cylinders, spheres, ogives, flow inside nozzles, etc. For simplicity, we will assume that the 'convective' heat transfer to bodies of arbitrary shape may be expressed in the form

$$Nu_x = C_o Re_x^{ml} Pr^{nl}, \qquad (3\text{-}1)$$

where C_o, ml and nl have different values for laminar and turbulent flows. This simple expression is universally accepted and needs no further justification. More specific Nusselt expressions, that include additional dimensionless numbers, could be used but would merely

clutter the analysis presented here; therefore, eq (3-1) will be used to complete this analysis. Subsequently, these generalized results may be modified to accommodate specific Nusselt expressions--examples are given. We will also assume that the characteristic thermal boundary layer thickness may be expressed in the form

$$\delta_t = C_1 \times Re_x^{-m2} Pr^{-n2} , \qquad (3\text{-}2)$$

where again C_1, m2, and n2 have different values for laminar and turbulent flows.

Using eq (3-1) and the proposed 'cavity model', it is easily shown that eq (3-2) has the appropriate algebraic form for the enthalpy and conduction thicknesses of the thermal boundary layer. Later, in this section, we shall see that a simplified boundary layer analysis may be employed without regard for the numerous foregoing assumptions; however, such an analysis does not provide the framework for modifying or improving the theory, nor does it shed light on the various physical characteristics of the cavitation process.

Equation (3-2) is the proper result for laminar flow over a flat plate, and is consistent with the reasoning advanced by Kays [27--p. 234, 244] for turbulent flow over a body of arbitrary shape. For light liquids and small values of n2, the Prandtl term in eq (3-2) approaches unity and δ_t is approximately equal to the hydrodynamic boundary layer thickness for turbulent flow over a flat plate--one of our basic assumptions. Recall that in laminar flow, molecular transport processes dominate, while in turbulent flow, eddy transport processes are dominant. Therefore, it is only in the sublayers of the turbulent boundary layer that Prandtl number has any influence. Since the sublayers comprise only a small portion of the turbulent boundary layer thickness,

the thermal and velocity boundary layers should have about the same thickness regardless of Prandtl number. To maintain generality, irrespective of flow mode, we will retain the Prandtl term in eq (3-2). Under the assumptions set forth herein, the generalized solutions [27--p. 222, 244] for heat transfer in laminar and turbulent flow, over bodies of arbitrary shape, reduce to the form given in eq (3-1).

Finally, let us assume that the volume (thickness) of liquid involved in the sustenance of the vaporous cavity is proportional to--not necessarily equivalent to--the characteristic thermal boundary layer thickness. It seems natural that more liquid can take part in the vaporization process as particles of liquid progress along the cavity wall, i.e., more time is available for heat to be transferred from liquid located further away from the liquid-vapor interface. Thus, we propose mating this physical concept of cavitation to the thermal boundary layer development in external flow. We will then require that the liquid-vapor interface (cavity wall) can be mathematically described by an expression of the form $\delta_v = C_2 x^p$. Data from Rouse and McNown [28], and data obtained in this study, indicate that this form is quite adequate and the value of p normally lies between 0.4 and 0.9 for a wide variety of hydrodynamic body shapes. For this analysis a mean value of $p \approx 0.65$ will be used. Later, we shall use a more general expression for the cavity shape to account for body size effects.

Admittedly, there is no shortage of assumptions to this point, but it must be equally obvious to the reader that a rigorous solution to our problem is hopelessly complicated. Accordingly, we seek correlating parameters, and eventually an empirical solution, for the prediction of the cavitating performance of hydrodynamic equipment. Before proceeding with the development of the correlating expressions, let us tabulate the pertinent assumptions that limit the scope of this analysis:

1) Liquid flow is forced over the hydrodynamic body by external means unrelated to the fluid temperature field (no body forces).

2) The liquid flow is steady, incompressible, with relatively low and constant free-stream velocity over a hydrodynamic body in a semi-infinite flow field. The flow may be laminar or turbulent.

3) Liquid flow over the vaporous cavity is treated as flow over a solid body. The thermal and velocity boundary layers originate with the cavity wall, at or near the leading edge of the hydrodynamic body.

4) The cavity wall is at constant temperature, all fluid properties are invariant and are evaluated at the free-stream temperature. Liquid Prandtl numbers are $\lesssim 10$.

5) Depletion of liquid molecules, due to vaporization, from the liquid film associated with the sustenance of a vaporous cavity, is assumed to have a negligible effect on the shape and thickness of this liquid film and the cavity, i.e., mass transfer across the liquid-vapor interface is neglected. Curvature of the liquid-vapor interface is also neglected in computing the thermal boundary layer thickness; the interface curvature is taken as parabolic in computing the cavity thickness.

6) Boundary layer separation (stall) does not occur.

7) Equations (3-1) and (3-2) are applicable to flow over developed cavities on bodies of arbitrary shape.

8) The thickness of the liquid film, involved in the sustenance of the vaporous cavity, is proportional to the characteristic thermal boundary layer thickness.

9) The "quasi-static" isentropic flashing theory is applicable to the cavitation process near the leading edges of the cavity.

10) The generalized results, obtained from flat plate or wedge-flow analyses, are applicable to bodies of arbitrary shape. Date correlation is applicable to hydrodynamic bodies with geometric and dynamic similitude, i.e., similarity of shapes, fluid motion and forces.

The B-factor is defined as the ratio of vapor to liquid volume associated with the sustenance of a fixed vaporous cavity in a liquid. Then, referring to figure 3.1a, we may write

$$B = \mathcal{V}_v/\mathcal{V}_\ell = \int_o^x \delta_v \, dx \Big/ \int_o^x \delta_\ell \, dx \tag{3-3}$$

for a plate of unit width (normal to the δ - x plane). Substituting eq (3-2) and the algebraic expression for δ_v into eq (3-3), we obtain

$$B = \left[C_2 \int_o^x x^p \, dx \right] \Big/ \left[C_1 \, Pr^{-n2} \int_o^x x Re_x^{-m2} \, dx \right] . \tag{3-4}$$

Evaluating Re_x and performing the integration in eq (3-4) produces

$$B = C_3 x^{p-1} Re_x^{m2} Pr^{n2} . \tag{3-5}$$

For the particular case where m2 = n2, the liquid viscosity is eliminated from Re_x and Pr and eq (3-5) reduces to

$$B = C_3 x^{p-1} (V_o x/\alpha)^{m2} . \tag{3-6}$$

If we now restrict eq (3-6) to laminar flow, m2 = 0.5, and if we follow Gelder, et al., [19] and take the cavity thickness as invariant, p = 0; performing the indicated algebra on eq (3-6), we get

$$B = C_3 (V_o/\alpha x)^{0.5} . \tag{3-7}$$

This particular solution is the same result obtained by Gelder, et al., using the conductive model. Had Gelder, et al., assumed that the liquid-vapor interface varied linearly with length (p = 1), they would have obtained

$$B = C_3 (V_o \, x/\alpha)^{0.5} , \tag{3-8}$$

a result which has the appropriate arrangement of parameters as verified by subsequent experiments [3, 19-21]. Note that the product of Re_x and Pr is the Peclet number, $Pe = V_o x/\alpha$, and it is this number upon which the Gelder, et al., [19] correlative technique is based.

Referring back to eq (3-5), we will combine the dimensionless numbers to derive the appropriate correlating parameters for the general case

$$B = C_3 \alpha^{-n2} V_o^{m2} x^{p-1+m2} (\rho/\mu)^{m2-n2} . \qquad (3\text{-}9)$$

The similarity constant for the cavitating body, C_3, may now be eliminated and empirical evaluation made possible [19] by relating the predicted B to a reference value evaluated from experimental data

$$B = B_{ref} \left(\frac{\alpha_{ref}}{\alpha} \right)^{E1} \left(\frac{V_o}{V_{o,ref}} \right)^{E2} \left(\frac{x}{x_{ref}} \right)^{E3} \left(\frac{\nu_{ref}}{\nu} \right)^{E4} , \qquad (3\text{-}10)$$

where E1 = n2, E2 = m2, E3 = p-1+m2, E4 = m2-n2, and $\nu = \mu/\rho$, the kinematic viscosity. An additional correlating parameter, ν, is introduced.

To obtain estimates of the exponent values in eq (3-10), let us consider both laminar and turbulent flows and evaluate eq (3-2) in three different ways. We will use only the simplest flat plate theory and the conventional relations [27] for the conduction, enthalpy, and thermal boundary layer thicknesses. Using a mean value for p (≈ 0.65) and performing the necessary algebra, we obtain the estimated range of values for each exponent as indicated in table 3.1.

Table 3.1: Estimated (analytic) exponent values.

Flow	n2 = E1	m2 = E2	E3	E4	Comments
Laminar (m1 = 0.50, n1 = 0.33, p = 0.65)	0.33	0.50	0.15	0.17	*
	0.67	0.50	0.32	-0.17	**
	0.33	0.50	0.15	0.17	***
Turbulent (m1 = 0.80, n1 = 0.60, p = 0.65)	0.60	0.80	0.45	0.20	*
	0.40	0.20	-0.15	-0.20	**
	0.00	0.20	-0.15	0.20	***
(Laminar or Turbulent)	0.00 to 0.67	0.20 to 0.80	-0.15 to 0.45	-0.20 to 0.20	Estimated range of Exponent Values

* - Evaluated from conduction thickness of thermal boundary layer.

** - Evaluated from enthalpy thickness of thermal boundary layer.

*** - Evaluated from thermal boundary layer thickness.

The most physically relevant method of evaluating δ_ℓ may be indicated by comparison of experimental data with analytical results given in table 3.1. Then, if the proposed model is reasonably valid, the heat transfer mechanism that limits heat transfer to the cavity interface may be revealed. A convection-limited process should be best represented by exponents evaluated from the enthalpy thickness, while

a conduction-limited process should favor the use of conduction thickness. The location, within the boundary layer, of the major source of resistance to heat transfer will vary with the Reynolds and Prandtl numbers. In turbulent flow, where Pr > 1, most of the thermal resistance resides in the laminar sublayers of the boundary layer; thus, use of the conduction thickness is suggested. In laminar flow, the thermal resistance is distributed over the entire thickness of the thermal boundary layer, and conduction and convection are of equal importance. Because most cavitating flows are turbulent, one is tempted to prefer the fourth row of exponents in table 3.1; however, in reality, the liquid flow is vapor-lubricated and the shapes of the hydrodynamic and thermal boundary layers are uncertain. Allowing for vapor lubrication--irrespective of the liquid flow mode--the liquid velocity must be nonzero at the liquid-vapor interface, and the thermal boundary layer must be somewhat characteristic of laminar flow. This consideration would encourage us to use the enthalpy thickness and expect the second and fifth rows of exponents in table 3.1 to bracket experimental data.

Obviously, the theoretical values given in table 3.1 can vary with the method of evaluating δ_ℓ, cavity shape, and the appropriate Nusselt relationship for each specific cavitating system.

It is also apparent from the foregoing analysis that eq (3-10) contains only the most common correlating parameters. Other Nusselt relationships, or cavity shape formulations, could easily introduce additional correlating parameters as indicated by the following discussion.

If we were so inclined, we could assume that the heat exchange at the liquid-vapor interface retains the salient features of both nucleate boiling and forced convection; nucleate boiling is selected because the liquid-to-vapor ΔT is generally within the nucleate regime. Using the

superposition theorem [29], we would add the individual contributions of the boiling and convection processes to obtain the combined heat transfer coefficient. This coefficient will decrease, with increasing liquid surface tension [29], in a manner dependent upon the contribution of the boiling coefficient to the combined heat transfer coefficient. Since we are empirically evaluating each correlating parameter in eq (3-10), we may introduce surface tension (σ) as a simple ratio to test its importance as a correlating parameter. If the boiling coefficient strongly influences the heat exchange, at the cavity wall, this addition will be valuable because the boiling coefficient is $\propto \sigma^{-E5}$. Following the development that led us to eq (3-10), we may conclude that $B \propto \sigma^{-E5}$. Use of the boiling coefficient would also introduce other parameters that we have not considered, namely vapor density, latent heat of vaporization, and appropriate fluid pressures and temperatures. All of these parameters, excluding σ, are in essence used to compute B (hereafter called BFLASH) in the isentropic flashing model [23]. To evaluate [20] the exponents on eq (3-10), we force B as computed from eq (3-10) to match BFLASH as closely as possible. Thus, σ is the only parameter in the boiling coefficient expression that is unused in the correlative expression. Use of the boiling coefficient is not considered entirely appropriate because the boiling process differs from the cavitation process. The latter is the formation of a vapor phase inside an originally uniform temperature field, while boiling occurs in an originally nonuniform temperature field (surface being hotter than bulk); however, a radially nonuniform temperature field surrounds the developed cavity, so that the concept of a boiling heat transfer component is tenable. Whether the mechanism of vapor generation is mainly attributable to a pressure reduction, or to a temperature difference induced by the pressure reduction, is of little importance to us.

It is also quite likely that σ could enter the correlative expression through δ_v. Dynamic analysis of the stability of the liquid-vapor interface may reveal a dependency, of the cavity shape, upon the Weber and/or Bond numbers. Because the inertia forces are usually much larger than the gravitational forces, the Weber number should prevail. The dimensional analysis performed herein confirms that σ enters through the Weber number. $We_x = \rho V_o^2 x/\sigma$ is important in the study of bubble formation, breakup of liquid jets, liquid surface ripples, etc., and has long been recognized [30] as a potential correlating parameter. Use of the Weber number or the boiling heat transfer coefficient introduces only one new correlating parameter, σ. Equation (3-10) may be written to include σ as follows

$$B = B_{ref}\left(\frac{\alpha_{ref}}{\alpha}\right)^{E1}\left(\frac{V_o}{V_{o,ref}}\right)^{E2}\left(\frac{x}{x_{ref}}\right)^{E3}\left(\frac{\nu_{ref}}{\nu}\right)^{E4}\left(\frac{\sigma_{ref}}{\sigma}\right)^{E5} . \quad (3\text{-}11)$$

The numerical value of E5 may be estimated from the boiling heat transfer data as ≈ 0.5 to 1.0.

Gravitational forces may easily be included in this correlative expression by permitting the Nusselt number to be a function of the Froude number [24]; however, the ratio of dynamic/gravitational forces, of the cavitation model, is normally large and this refinement does not appear warranted. Note that use of the Bond number in describing the shape of the cavity would introduce both gravity and σ.

Next, we direct our attention to the body size effects that were neglected in assuming that $\delta_v = C_2 x^p$. Under our assumption of similar dimensions, velocities, forces, etc., we can follow the logic of Moore and Ruggeri [31] and assert that cavity thickness and cavity length will vary directly with scale size, i.e., with some characteristic dimension, D, of the cavitating body. Then, similar cavitation performance occurs

with similar bodies of different size when x/D is held constant. Moore and Ruggeri [31] show that this 'model similarity' reasoning merely introduces a $(D/D_{ref})^{E6}$ term into eq (3-11). In developing eq (3-5), we assumed that $\delta_v = C_2 x^p$ adequately represents the shape of the cavity wall, irrespective of body shape or size. We also assumed that the cavity wall originates near the leading edge--actually near the minimum pressure point--of the hydrodynamic body; then it is obvious that the radius of curvature of the cavity wall, near the point of origin, varies with the radius of curvature of the body. Geometrical analysis of a family of parabolic-shaped curves indicates that we can satisfy this size requirement by replacing C_2 with $C_2' D^{E6}$, where E6 (like p) may have a particular value for each body shape. Since we are neglecting the effect of cavity wall curvature when evaluating the thermal boundary layer thickness, the size effect will not enter into the liquid volume calculation, and $B \propto D^{E6}$--see eq (3-4) and eq (3-5). Then, accounting for size, eq (3-11) may be revised

$$B = B_{ref}\left(\frac{\alpha_{ref}}{\alpha}\right)^{E1}\left(\frac{V_o}{V_{o,ref}}\right)^{E2}\left(\frac{x}{x_{ref}}\right)^{E3}\left(\frac{\nu_{ref}}{\nu}\right)^{E4}\left(\frac{\sigma_{ref}}{\sigma}\right)^{E5}\left(\frac{D}{D_{ref}}\right)^{E6}. \tag{3-12}$$

The size term is identical to that obtained by Moore and Ruggeri [31].

The foregoing examples clearly indicate that the constituent parameters of the chosen Nusselt expression, and cavity shape formulation, must appear in the correlative expression, eq (3-10).

So far, our analysis has been restricted to two-dimensional flow. Referring to figure 3.1b, we consider the axisymmetric body. Rewriting eq (3-3) for the axisymmetric body produces

$$B = \left[\pi\int_o^x\left\{\left(\delta_v + R\right)^2 - R^2\right\}dx\right] \Big/ \left[\pi\int_o^x\left\{\left(\delta_v + \delta_\ell + R\right)^2 - \left(\delta_v + R\right)^2\right\}dx\right]. \tag{3-13}$$

Rearranging terms, we obtain,

$$B = \left[\int_o^x \delta_v \left(\delta_v + 2R\right) dx\right] \Big/ \left[\int_o^x \delta_\ell \left(\delta_\ell + 2\delta_v + 2R\right) dx\right] . \qquad (3\text{-}14)$$

Comparing eq (3-14) with eq (3-3), we note that some second-order terms have appeared; therefore, for first order approximations, eq (3-14) reduces to eq (3-3). Also, recalling that our problem deals with the cavity wall near its leading edges, we may argue that in most cavitating equipment $2R \gg \delta_v$ and $2R \gg \delta_\ell$; thus, eq (3-14) reduces to eq (3-3). In consideration of the various assumptions used in this analysis, the refinement offered by eq (3-14) does not appear warranted; so we shall assume that eq (3-3) and subsequent expressions, through eq (3-12), are applicable to cavitating flow over plane-surface and axisymmetric bodies.

Before turning to dimensional analysis, it should be pointed out that the equations developed in this section may be derived in a simplified manner. It is only necessary to assume that the heat transfer at the cavity interface can be expressed in the general form given by eq (3-1), irrespective of body shape. No other assumptions concerning the 'cavity model' are necessary. Next, the conduction thickness of the thermal boundary layer is given [27--p. 50] as k/h_x; then $\delta_\ell \propto k/h_x$. Evaluating eq (3-1) to obtain h_x, and combining h_x with the foregoing relation for δ_ℓ, results in a functional expression for δ_ℓ that is identical to eq (3-2). Referring to eq (3-4), we note that $\int \delta_v \, dx$ does not contain any physical parameters[4] that are not contained in $1/\int \delta_\ell \, dx$. Then, to simply obtain correlating parameters, we may state that $B \propto (1/k) \int h_x \, dx$. So long as we are empirically evaluating exponents

[4] With the possible exception of D, for scale effects, and D can be introduced as per reference [31].

on each physical parameter, i.e., the initial values of m1, n1, m2, n2, etc., are unimportant; this particular expression will produce the same results as the generalized approach outlined herein.

From a practical viewpoint, $B \propto (1/k) \int h_x \, dx$ is all that we need to develop correlating parameters, but no other information is gained from this simplified approach. From a theoretical viewpoint, the general approach outlined herein provides detailed information concerning the 'cavity model'. The latter approach, after comparison of theory and experiment, may be modified to account for theoretical deficiencies--no such avenue exists for the simplified case. In the simpler case, only empirical adjustment of eq (3-1) is possible, and no physical explanation for the adjustment is visible; however, a variance in one or more of the numerous assumptions used in the detailed analysis may well synthesize experiment and theory. Although the detailed approach is preferable in a theoretical sense, the simplified view that $B \propto (1/k) \int h_x \, dx$ will be used to good advantage in our dimensional analysis.

3.2 Convection Model (dimensional analysis)

The primary strength of dimensional analysis is the formulation of dimensionless groups of variables, useful in the correlation of experimental data. A complete analytic solution does not result, but significant dimensionless numbers are identified, e.g., Reynolds number, Prandtl number, etc. The main weakness of dimensional analysis is that no information is gained on the inner mechanisms of the physical problem--thus, the functional dependency of each dimensionless number must be determined empirically. To apply dimensional analysis, it is necessary to know which parameters influence the problem, and the success of the method depends upon the intuitive selection of these parameters. One's confidence in the results is usually bolstered if

there exists a skeletal theory and/or some understanding of the physical problem to support the parameter selection. Because of the work in the previous section and existing correlating techniques [5, 7-9, 19, 22], we are in a good position to perform such an analysis. To determine the number of independent dimensionless groups required to describe the problem, we use the Buckingham π - theorem and the MLθT dimensional system--M = mass, L = length, θ = time and T = temperature. The Buckingham method produces n groups, π_1, π_2, $\pi_3 \ldots \pi_n$, of dimensionless variables and predicts a solution to the problem has the form $\pi_1 = f(\pi_2, \pi_3 \ldots \pi_n)$; n is determined by subtracting the number of primary dimensions, e.g., M, θ, T, from the total number of physical variables. Table 3.2 summarizes the physical variables, primary dimensions and resultant π - groups for the cavitation problem.

The physical variables listed in this table are either geometric parameters or else they may be determined from appropriate pressure and temperature measurements. The first seven parameters listed are the fundamental convection variables. The eighth parameter introduces size effect, and the ninth parameter permits surface tension to influence the stability and heat exchange phenomena at the liquid-vapor interface. The tenth and last parameter is included because apparent 'shocks' have been experimentally observed [20] in cavitated regions of liquid hydrogen, and such 'shocks' are known to affect heat transfer [27--p. 271]. Also, at least two authors [7, 8] have developed correlation techniques based upon two-phase compressibility phenomenon.[5] Note that the first seven physical variables in table 3.2 require only four

[5] See reference [32] also.

Table 3.2 Physical parameters, primary dimensions and dimensionless groups resulting from dimensional analysis of the cavitation problem.

Physical Parameter	Primary Dimensions	Dimensionless Groups of Variables Resulting from Dimensional Analyses	
x	L		
V_o	L/θ		
k	$ML/\theta^3 T$	Nu_x	Nu_x
ρ	M/L^3	Re_x	Re_x
$C_{p,\ell}$	$L^2/\theta^2 T$	Pr	Pr
μ	$M/L\,\theta$		
$\hbar_x$	$M/\theta^3 T$		x/D
D	L		We_x
σ	M/θ^2		$M_{2\varphi}$
$V_{2\varphi}$	L/θ		

primary dimensions-- then, we anticipate that three π - groups will be required to correlate the data. Buckingham's rule assumes that

$$\pi = x^a V_o^b k^c \rho^d C_{p,\ell}^e \mu^f \hbar_x^g , \qquad (3\text{-}15)$$

where the exponents are to be evaluated to determine the individual π - groups, π_1, π_2, etc. Substituting the primary dimensions of each physical variable into eq (3-15), and then equating the sum of the exponents of each primary dimension to zero, produces a set of equations.

For π to be dimensionless, the sum of the exponents on each primary dimension must be zero. This procedure produces four equations, with seven unknowns; therefore, three of the exponents may be evaluated arbitrarily, so long as they are linearly independent. Simultaneous solution of these equations, in a fashion that assures the exponents are linearly independent, provides one of the π - groups. This process is repeated twice to evaluate π_2 and π_3. Table 3.2 shows that this method produces $\pi_1 = Nu_x$, $\pi_2 = Re_x$, and $\pi_3 = Pr$; from experience we know that $Nu_x = f(Re_x, Pr)$.

If we include size, surface tension, and two-phase sonic velocity in the list of physical variables and repeat the dimensional analysis, we get

$$Nu_x = f(Re_x, Pr, x/D, We_x, M_{2\varphi}). \tag{3-16}$$

The result is dimensionless groupings of our input parameters. Without prior theoretical work, we would have no idea of the functional relationship of the individual π - groups; however, to conform with the Nusselt relationship, we will assume that

$$Nu_x = (Re_x)^a (Pr)^b (x/D)^c (We_x)^d (M_{2\varphi})^e , \tag{3-17}$$

where the exponents are to be evaluated empirically. By evaluating each π- group in terms of physical parameters, rearranging, and combining exponents on each physical parameter in eq (3-17), we obtain

$$h_x = k \alpha^{-b} V_o^t x^u \nu^v (\rho/\sigma)^d (1/D)^c (1/V_{2\varphi})^e , \tag{3-18}$$

where $t = a + 2d + e$, $u = a + c + d - 1$ and $v = a - b$. Recalling that

$B \propto (1/k)\int \hbar_x dx$ and proceeding as in the development of eq (3-10), we obtain

$$B = B_{ref}\left(\frac{\alpha_{ref}}{\alpha}\right)^{b}\left(\frac{V_o}{V_{o,ref}}\right)^{t}\left(\frac{x}{x_{ref}}\right)^{u+1}\left(\frac{\nu}{\nu_{ref}}\right)^{v}\left(\frac{[\rho/\sigma]}{[\rho/\sigma]_{ref}}\right)^{d}\cdots$$

$$\cdots\left(\frac{D_{ref}}{D}\right)^{c}\left(\frac{V_{2\varphi,\,ref}}{V_{2\varphi}}\right)^{e}. \qquad (3\text{-}19)$$

Because ρ is contained in both the α and ν terms, there is little need to preserve ρ as an explicit parameter in eq (3-19). Alternatively, we could retain $k/C_{p,\ell}$ and ρ terms and eliminate α. To minimize the number of correlating parameters and thus simplify the correlative expression, we elect to retain α, a proven correlating parameter. The resultant expression is very similar to eq (3-12),

$$B = B_{ref}\left(\frac{\alpha_{ref}}{\alpha}\right)^{E1}\left(\frac{V_o}{V_{o,ref}}\right)^{E2}\left(\frac{x}{x_{ref}}\right)^{E3}\left(\frac{\nu}{\nu_{ref}}\right)^{E4}\cdots$$

$$\cdots\left(\frac{\sigma_{ref}}{\sigma}\right)^{E5}\left(\frac{D_{ref}}{D}\right)^{E6}\left(\frac{V_{2\varphi,\,ref}}{V_{2\varphi}}\right)^{E7}, \qquad (3\text{-}20)$$

where the exponents in eq (3-19) have been converted to those used in eq (3-12) and are to be evaluated empirically. So, without further struggle, the basic correlating parameters are produced, although some of the parameters are inverted.

The $V_{2\varphi}$ term emerges because of our assumption that it is a significant physical variable. This parameter may be related to the "characteristic velocity" discussed by Holl and Wislicenus [30] and thought to be important in cavitation studies. Jakobsen [8] and Spraker

[7] have enjoyed some success in the correlation of inducer and pump cavitation data using two-phase acoustical parameters; however, Chivers[6] is skeptical of the role of the acoustical parameter in the correlation of cavitation data. In this paper, we include the acoustical parameter in the B-factor expression, but do not rely upon it as a sole or primary correlating parameter. Computation of $V_{2\varphi}$ requires determination of fluid quality, a quantity that varies from zero to 100 percent across the liquid-vapor interface. Therefore, evaluation of $V_{2\varphi}$ is not straightforward, and the effect of $V_{2\varphi}$ on h_x and ultimately on B is not clear. A method of estimating $V_{2\varphi}$ is proposed in the following section of this paper.

The dimensionless groups in eq (3-17) may ultimately simplify correlation of cavitation data, but more insight into the mechanism of the problem is obtained by correlating on the individual physical variables. Thus, until further knowledge evolves, it is suggested that eq (3-20), or a modification thereof, be used for correlative purposes. Evaluation of exponents in the correlative expression is fully explained elsewhere [20], and use of the results for predicting cavitating performance of equipment has also been published [3-6].

3.3 Estimation of $V_{2\varphi}$

Computation of $V_{2\varphi}$ can only be performed in an abstract manner. This situation occurs because $V_{2\varphi}$ varies with fluid quality and the assumed thermodynamic process. For our problem, we cannot define the fluid quality or the thermodynamic process. Of the various thermodynamic models available [33], it is proposed that the homogeneous

---

[6] See discussion at end of papers by Chivers [9].

metastable model is the most appropriate. This model is selected because it works best [33, 34] for experimental systems with fluid qualities $\lesssim$ 0.10--our range of interest, as will be demonstrated. Also, it is based upon an isentropic flashing process, which is consistent with the BFLASH theory [23]. In this model, the liquid is assumed incompressible and an equivalent two-phase pressure-volume relationship, for an isentropic process, is used to derive the following relation [33],

$$G_c^2 = \left[\frac{ZC_{p,v} + C_{v,\ell}}{ZC_{v,v} + C_{v,\ell}} \right] \frac{P_1 \rho_v (Z+1)}{Z}, \tag{3-21}$$

where $Z = X/(1-X)$. Using the basic definitions of X and B, we readily obtain the algebraic expression

$$X = \frac{B}{B + (\rho_\ell / \rho_v)} = \frac{Z}{Z+1}, \tag{3-22}$$

$$\text{and } Z = B\rho_v / \rho_\ell . \tag{3-23}$$

Then eq (3-21) may be written as a function of fluid quality, X, or BFLASH, as we see fit. For our problem we have no independent way of estimating X but a proven method of estimating BFLASH [23]. G_c ($= \rho_{2\varphi} V_{2\varphi}$) is the choking (limiting) mass flow flux for two-phase flow, based upon the fluid quality as computed from eq (3-22). Thus, it is apparent that the two-phase acoustic velocity, $V_{2\varphi}$, is a function of BFLASH. Now, since BFLASH is a characteristic vapor/liquid volume ratio, for a prescribed cavity, it is clear that G_c is a parameter that is <u>characteristic</u> of this cavity and cannot vary locally along the cavity interface. Therefore, G_c ($= \rho_\ell V_\ell$) may be used to compute a <u>characteristic</u> liquid velocity component, V_ℓ, normal to the cavity interface. This liquid velocity component may be regarded as the

characteristic limiting rate at which liquid may approach the liquid-vapor interface. This velocity component is not to be confused with the actual limiting rate at which liquid crosses the interface, but should be considered as representative of that actual rate. Then, in this simplified and abstract fashion, we can account for mass transfer considerations that were neglected in the foregoing analyses. Figure 3.2 illustrates this mass flow flux limiting concept, i.e., mass transport to the liquid-vapor interface is limited by choking two-phase flow across the interface. Combining the characteristic mass-limiting liquid velocity, V_ℓ, with the liquid inlet velocity, V_o, forms the velocity ratio, V_o/V_ℓ. This velocity ratio will be designated MTWO, to emphasize that this ratio is similar to a Mach number and is proportional to the two-phase Mach number, $M_{2\varphi}$, i.e., MTWO = V_o/V_ℓ and $M_{2\varphi} = V_o/V_{2\varphi}$, then MTWO = $M_{2\varphi}V_{2\varphi}/V_\ell$. Because $G_c = \rho_{2\varphi}V_{2\varphi} = \rho_\ell V_\ell$, and $V_{2\varphi}/V_\ell = \rho_\ell/\rho_{2\varphi}$, we may alternatively state that MTWO = $M_{2\varphi}\rho_\ell/\rho_{2\varphi}$. Also, $V_\ell = G_c/\rho_\ell$ and

$$\text{MTWO} = V_o/V_\ell = V_o\rho_\ell/G_c . \tag{3-24}$$

Combining this expression and eq (3-21), we obtain

$$\text{MTWO} = \frac{V_o}{\left\{\left(\frac{ZC_{p,v} + C_{v,\ell}}{ZC_{v,v} + C_{v,\ell}}\right)\frac{P_1\rho_v}{\rho_\ell^2}\left(\frac{Z+1}{Z}\right)\right\}^{0.5}} . \tag{3-25}$$

Reasons for evaluating (and correlating on) the MTWO parameter, rather than the V_ℓ (or $V_{2\varphi}$) parameter, will be discussed in detail in a later section of this report.

Several thermodynamic models are available [33] for computing G_c and a fundamental relationship for acoustic velocity in a homogeneous

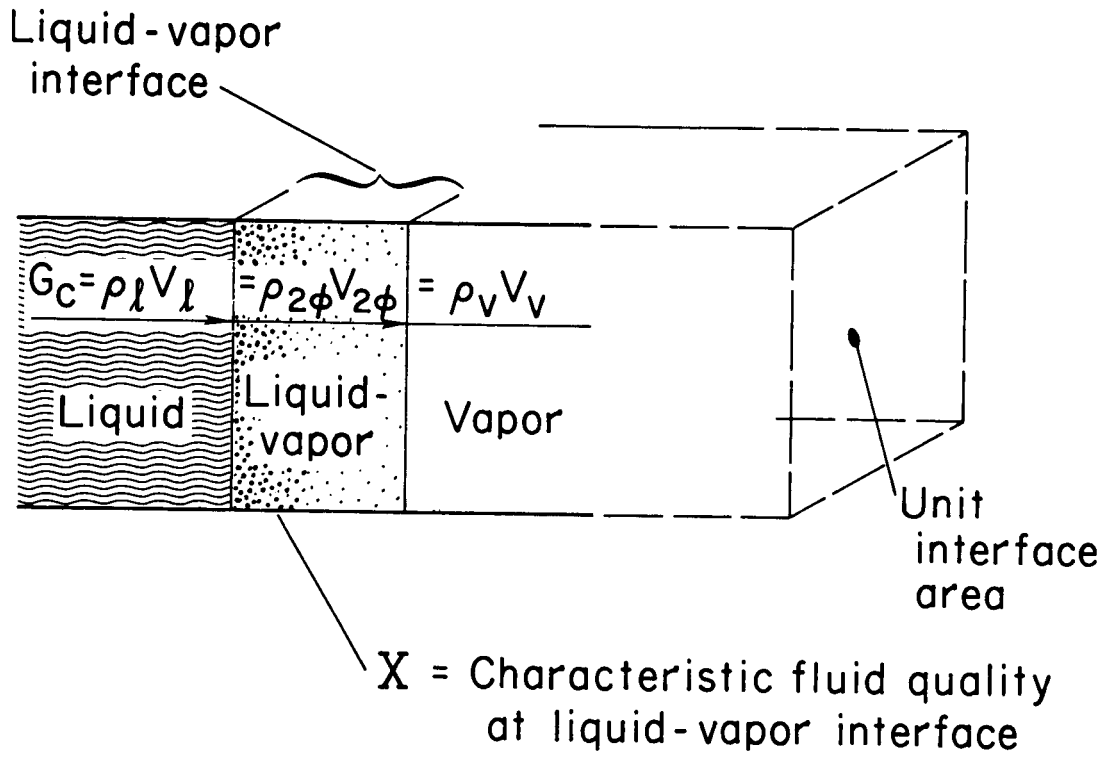

Figure 3.2 Illustration of how choking two-phase flow within the liquid-vapor boundary limits mass flow flux across the cavity interface.

compressible fluid was derived by Jakobsen [8]. Using the Jakobsen formula and eq (3-24), we obtain

$$\text{MTWO} = \frac{V_o}{a_\ell} \left\{ \frac{1 + Z(\rho_\ell / \rho_v)^2 (a_\ell / a_v)^2}{1 + Z} \right\}^{0.5} . \qquad (3\text{-}26)$$

Equation (3-25) is restricted to relatively low fluid qualities ($\lesssim 0.10$), but eq (3-26) bears no such restrictions. These two equations, evaluated with experimental data, produce almost identical trends (not equivalent values); therefore, they produce almost identical correlative results when used with the correlative expression, eq (3-20). Because eq (3-26) bears no fluid quality limitations and is no more complex than eq (3-25), it is recommended for future use. Introducing MTWO into the correlative expression of eq (3-20), and eliminating the V_o and $V_{2\varphi}$ terms, we obtain

$$B = B_{ref} \left(\frac{\alpha_{ref}}{\alpha} \right)^{E1} \left(\frac{\text{MTWO}}{\text{MTWO}_{ref}} \right)^{E2} \left(\frac{x}{x_{ref}} \right)^{E3} \cdots$$

$$\cdots \left(\frac{\nu}{\nu_{ref}} \right)^{E4} \left(\frac{\sigma_{ref}}{\sigma} \right)^{E5} \left(\frac{D_{ref}}{D} \right)^{E6} . \qquad (3\text{-}27)$$

Subsequently, we shall show that this expression is far superior to eq (3-12) in correlating the experimental cavitation data acquired in this study.

The two-phase thermodynamic models advocated by Smith [33], which are the vapor-choking, the homogeneous thermal equilibrium, and the homogeneous metastable models, have been tested with experimental

data from this study. Of these models, only the homogeneous metastable model produced beneficial correlative results. This model, evaluated with formulations for both compressible and incompressible fluids, correlated our experimental data with equal success. To test the validity of the two-phase-limited mass transport concept, the experimental data were correlated 1) using V_o/V_ℓ, 2) using $V_o/V_{2\varphi}$ and 3) using V_o/a_v. Beneficial correlative results were obtained only when V_o/V_ℓ was used, substantiating the choice of MTWO as a correlating parameter. Note that eq (3-25) and eq (3-26) are evaluated at the reduced pressure and temperature conditions at the cavity interface--in this study, these reduced fluid conditions are measured. BFLASH is also evaluated at the reduced fluid temperature.

It will be convenient, in a later discussion, to express eq (3-26) in a simplified form. This is accomplished by first noting that $\rho_\ell/\rho_v >> B$ for all of our experimental data, i.e., $B \lesssim 5$ and $\rho_\ell/\rho_v \gtrsim 40$. Then, from eq (3-22), $X \approx B\,\rho_v/\rho_\ell$ and from eq (3-23), $X \approx Z$. Also, $X \approx Z \lesssim 0.13$ for our experimental data--the choice of the homogeneous metastable two-phase model is made apparent. Referring to eq (3-26), we note that $(\rho_\ell a_\ell/\rho_v a_v)^2$ is a very large quantity ($\gtrsim 10^3$); therefore, for values of Z of interest (≈ 0.01 to 0.13), we may simplify eq (3-26) as follows

$$\mathrm{MTWO} \approx \frac{V_o \rho_\ell Z^{0.5}}{a_v \rho_v} \quad . \tag{3-28}$$

Recalling that $Z = B\,\rho_v/\rho_\ell$, we can conclude from eq (3-28) that

$$\mathrm{MTWO} \propto V_o\,(\mathrm{BFLASH})^{0.5} \quad , \tag{3-29}$$

and

$$V_{\ell} \propto (1/BFLASH)^{0.5} . \qquad (3\text{-}30)$$

These two relations will be useful in explaining data correlations, in another section of this report.

4. EXPERIMENTAL APPARATUS

The experimental apparatus used in this study was explained in detail in the first volume [20] of this report series. The experimental facility, instrumentation, error statements, visual and photographic aids, and test procedures are fully described in that document [20]. One additional error statement--concerning uncertainty in pressure measurement for nitrogen test fluid--is needed and given in section 5.2 of this report. Only the test section (tunnel) and hydrodynamic body (hydrofoil) details need to be discussed here. This tunnel was located between the supply and receiver dewars of a blowdown flow system, see reference [20].

4.1 Hydrofoil, Sting-Mount, and Tunnel

The 0.5-caliber hydrofoil, used in this experiment, was chosen so that developed cavitation test data could be obtained for external flow over a two-dimensional body. These data may ultimately be correlated with similar data for external flow over axisymmetric bodies (ogives) and for internal flow through a venturi. Also, the hydrofoil offers the ultimate opportunity to study the effect of cavity shape on the correlative formulae, i.e., the effects of flow assymmetries, fluid rotation, etc., should be minimized and the cavity thickness, as a function of length, velocity, etc., should be easily determined.

The two-dimensional body (hydrofoil) used in this experiment was a tapered plate with a cylindrical leading edge (0.5 caliber). Initially, the hydrofoil was designed as a flat plate with a cylindrical

leading edge; however, difficulties were encountered with tunnel cavitation, and it was necessary to slightly taper the plate. Using the maximum plate thickness, the length-to-thickness ratio of the hydrofoil is 8:1. A transparent plastic tunnel, and a rigid metallic sting-mount, were designed to experimentally complement the 0.5-caliber hydrofoil. Photographs of the hydrofoil and sting-mount assembly are shown in figure 4.1. A sketch of the instrumented hydrofoil and sting assembly is given on figure 4.2, and figure 4.3 shows photographs of the hydrofoil as installed and viewed during a test. Details concerning the tunnel, hydrofoil, and sting-mount are given below and on figures 4.4 through 4.7.

4.1.1 Design Considerations

The hydrofoil was initially designed as a flat plate with sufficient tunnel blockage to cause the hydrofoil to cavitate readily; however, preliminary tests indicated that cavities, developed on the hydrofoil, were sufficiently thick to cause tunnel cavitation. The tunnel (test section) cavitation is attributed to the pressure reduction that accompanies the acceleration of liquid between the cavity and tunnel walls. Selection of a thinner hydrofoil alleviates this Bernoulli effect in the vicinity of the cavity, but simultaneously decreases the hydrofoil cavitation number, K_{iv}--resulting in lower magnitudes of subcooling, $P_o - P_v$, in the tunnel inlet liquid, and therefore enhancing cavitation in the inlet and downstream regions of the tunnel. Thus, to perform experiments within the pressure and flow limitations of the existing facility, it was necessary to taper the hydrofoil, front-to-rear. This 1.817 degree taper provided sufficient relief to avoid tunnel cavitation, without detachment of the cavity on the hydrofoil, i.e., the cavity developed on the hydrofoil adhered to the taper--all tests were monitored via remote closed-circuit TV and motion picture cameras.

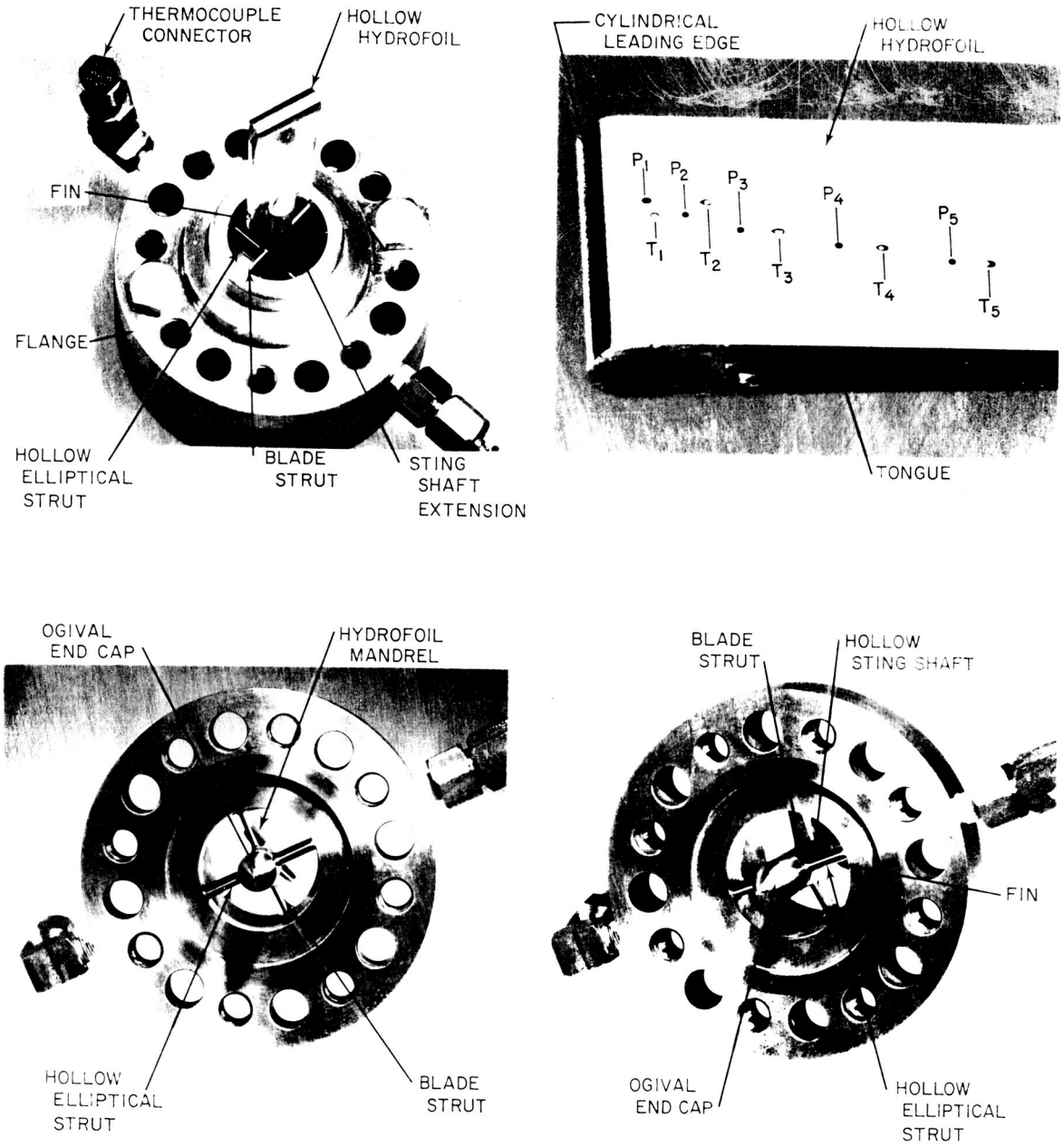

Figure 4. 1 Photographs of hydrofoil and sting-mount assembly.

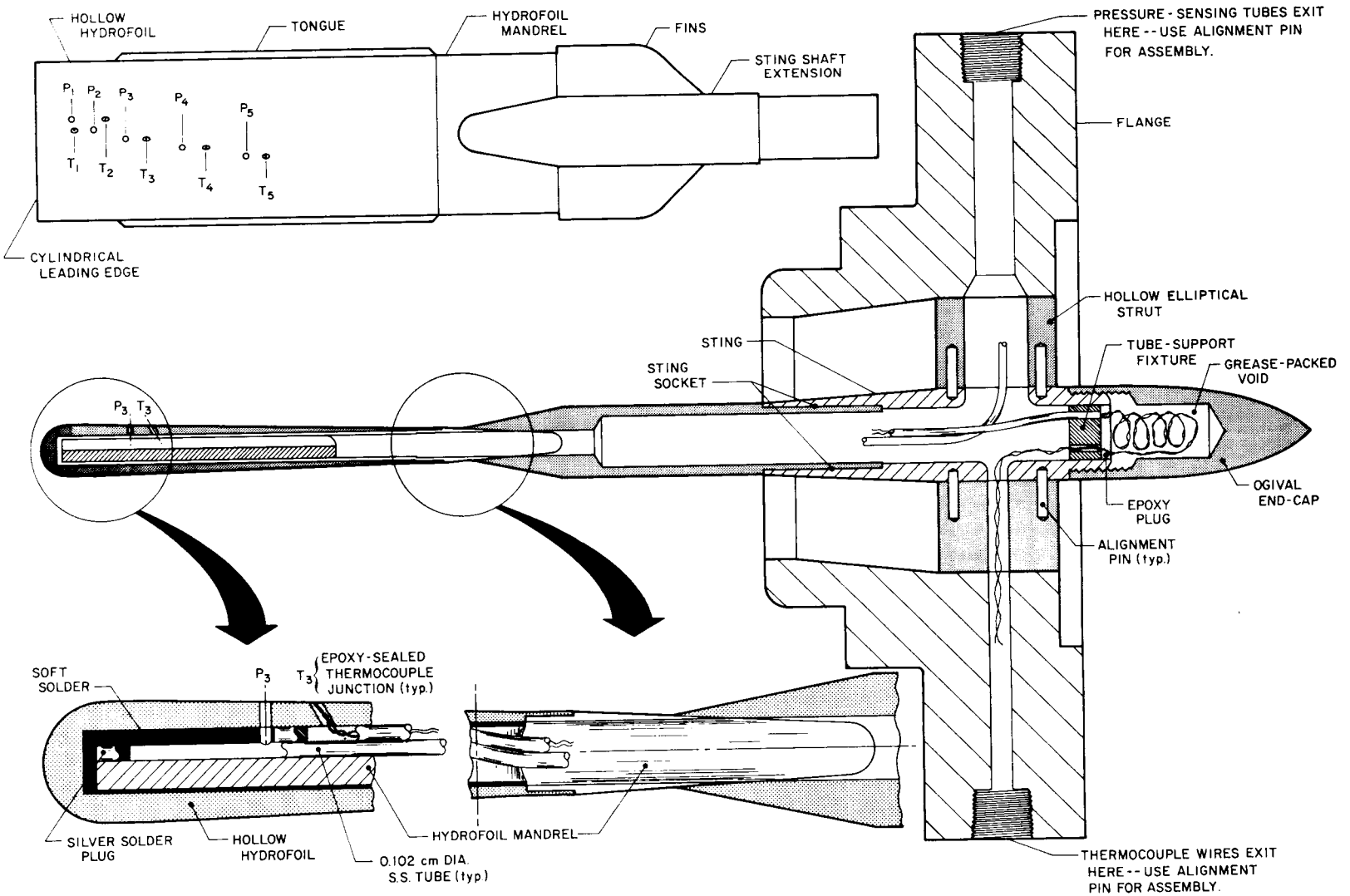

Figure 4.2 Sketch of instrumented hydrofoil and sting assembly.

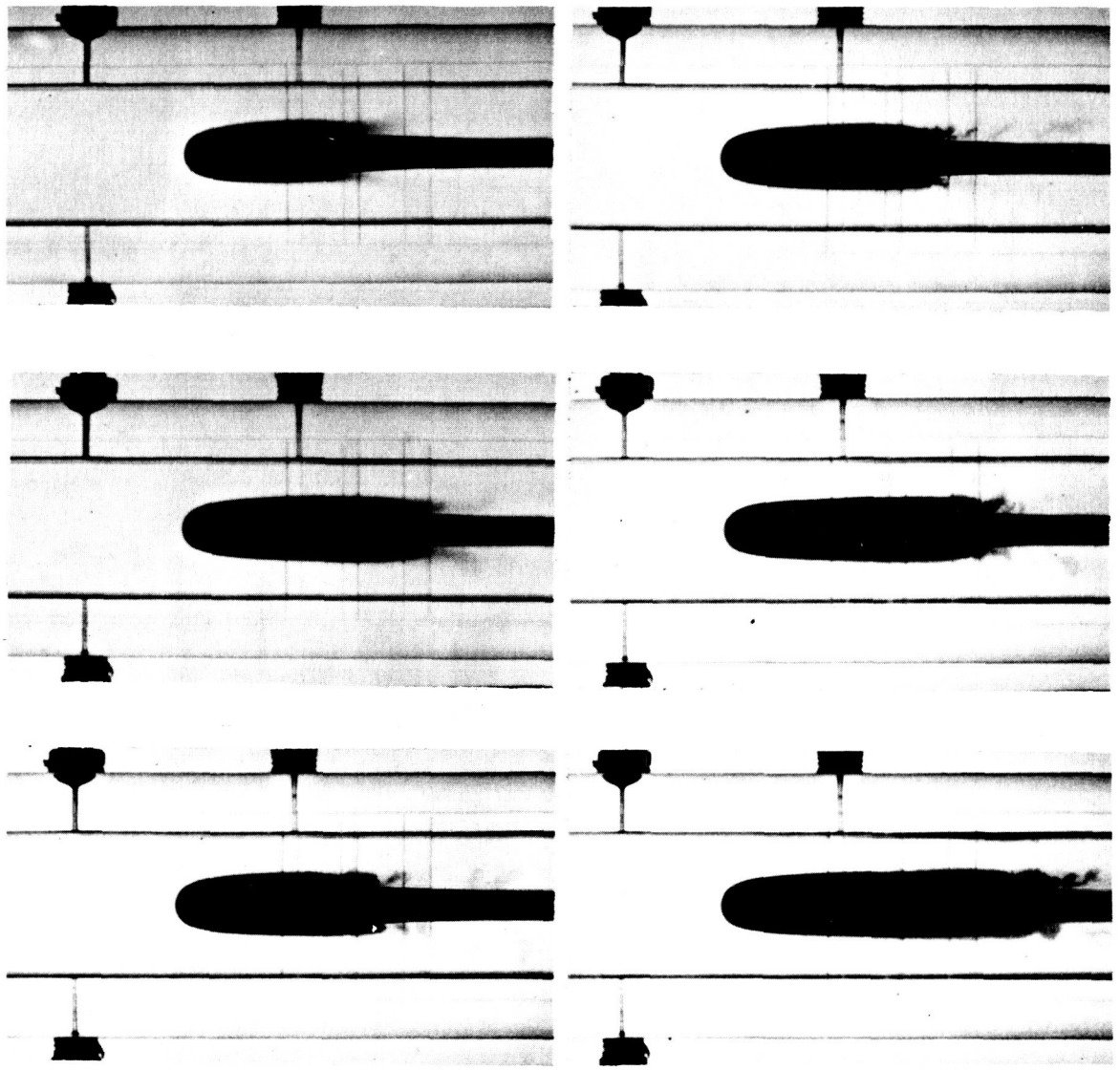

Figure 4. 3 Photographs showing typical appearance of vaporous hydrogen cavities on the tapered hydrofoil.

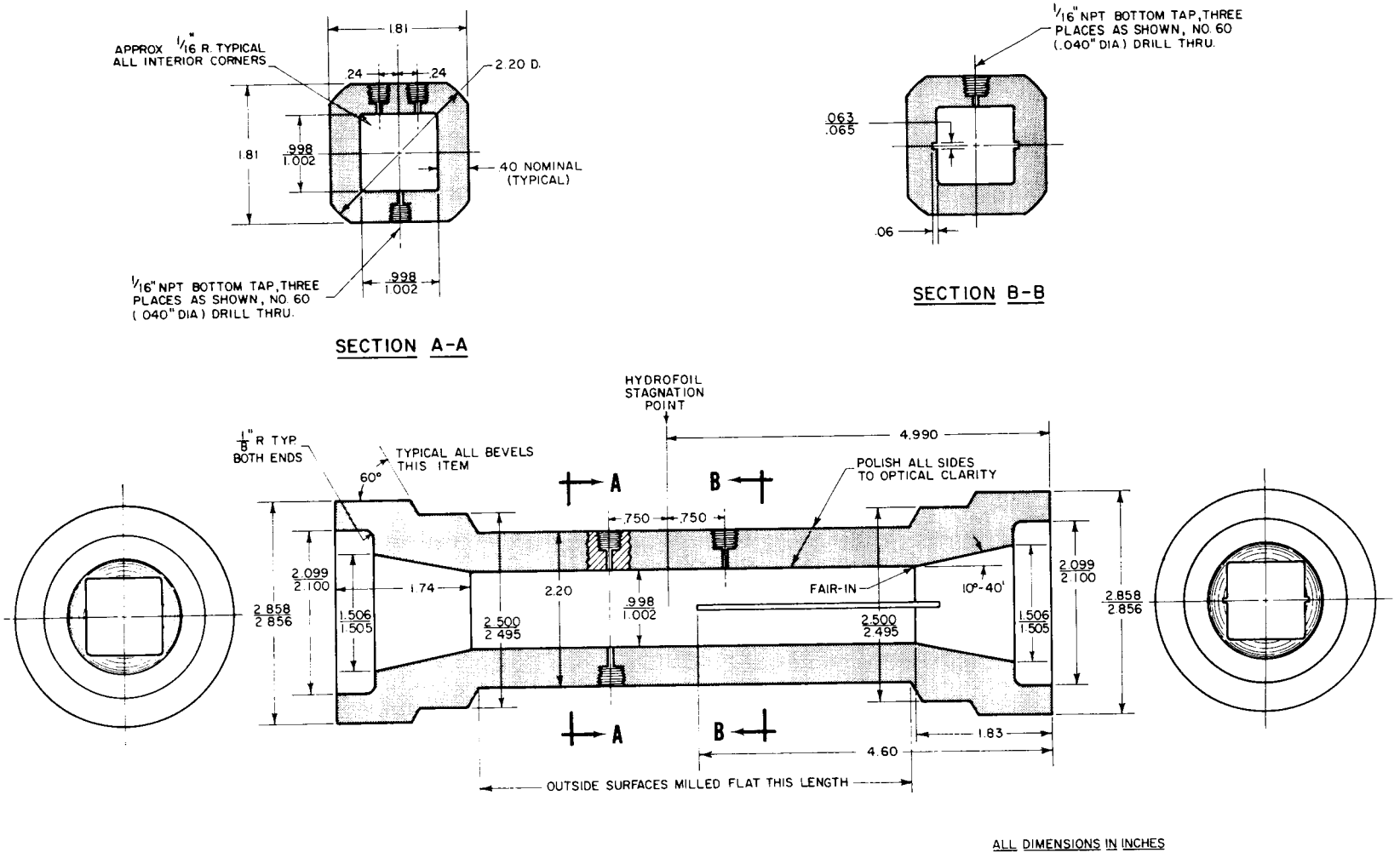

Figure 4.4 Details of plastic tunnel.

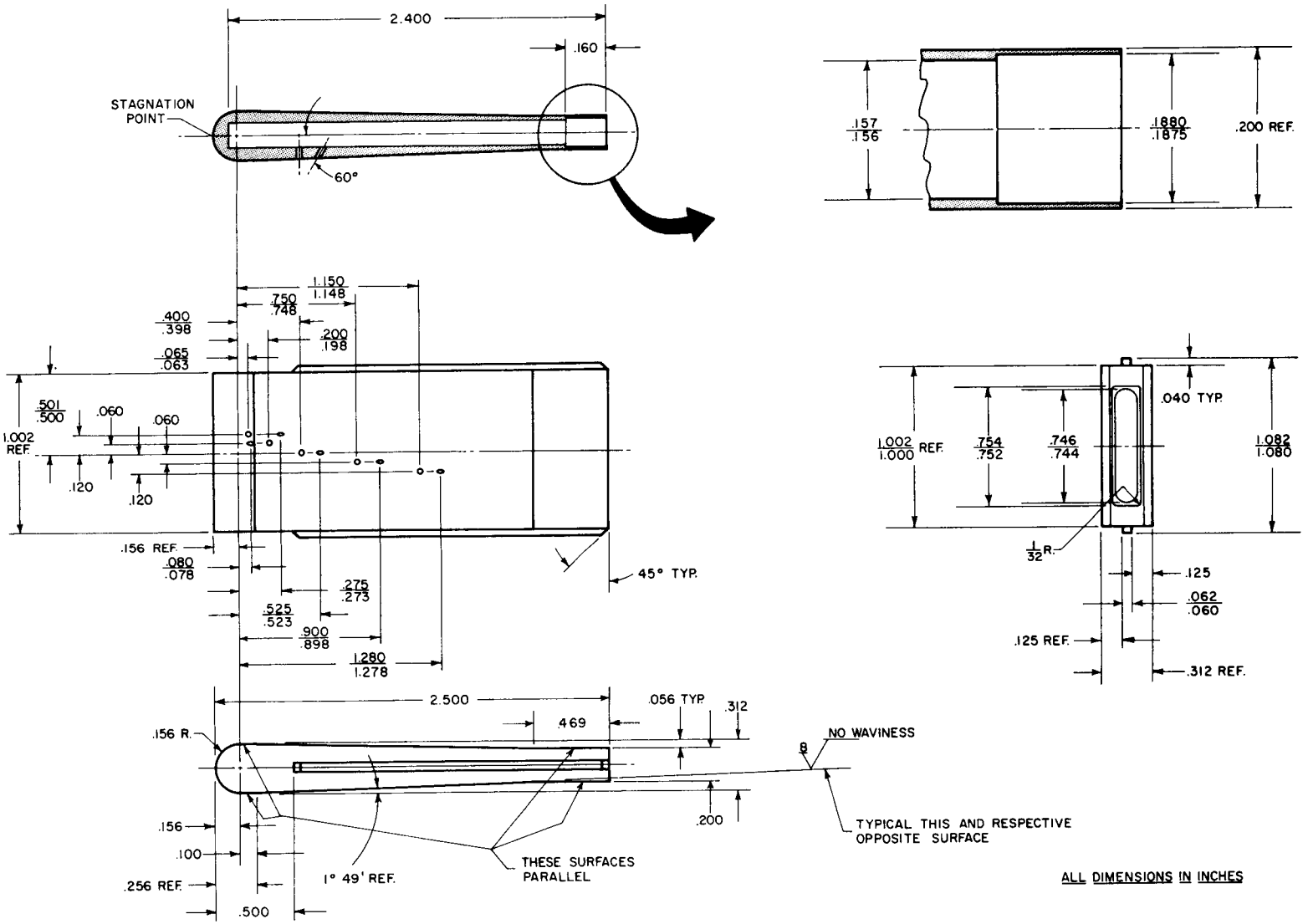

Figure 4.5 Details of hollow hydrofoil.

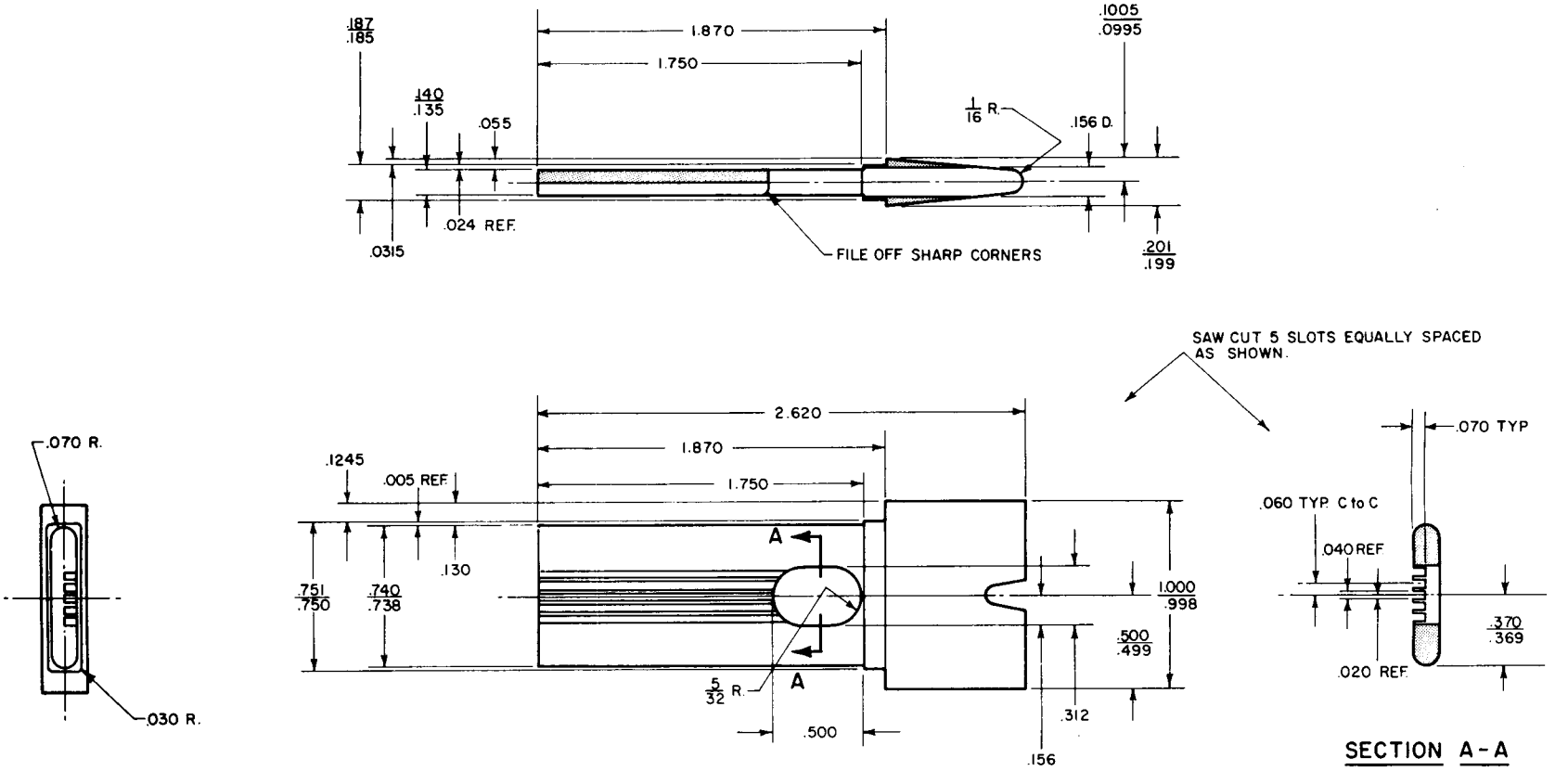

Figure 4.6 Details of hydrofoil mandrel.

ALL DIMENSIONS IN INCHES

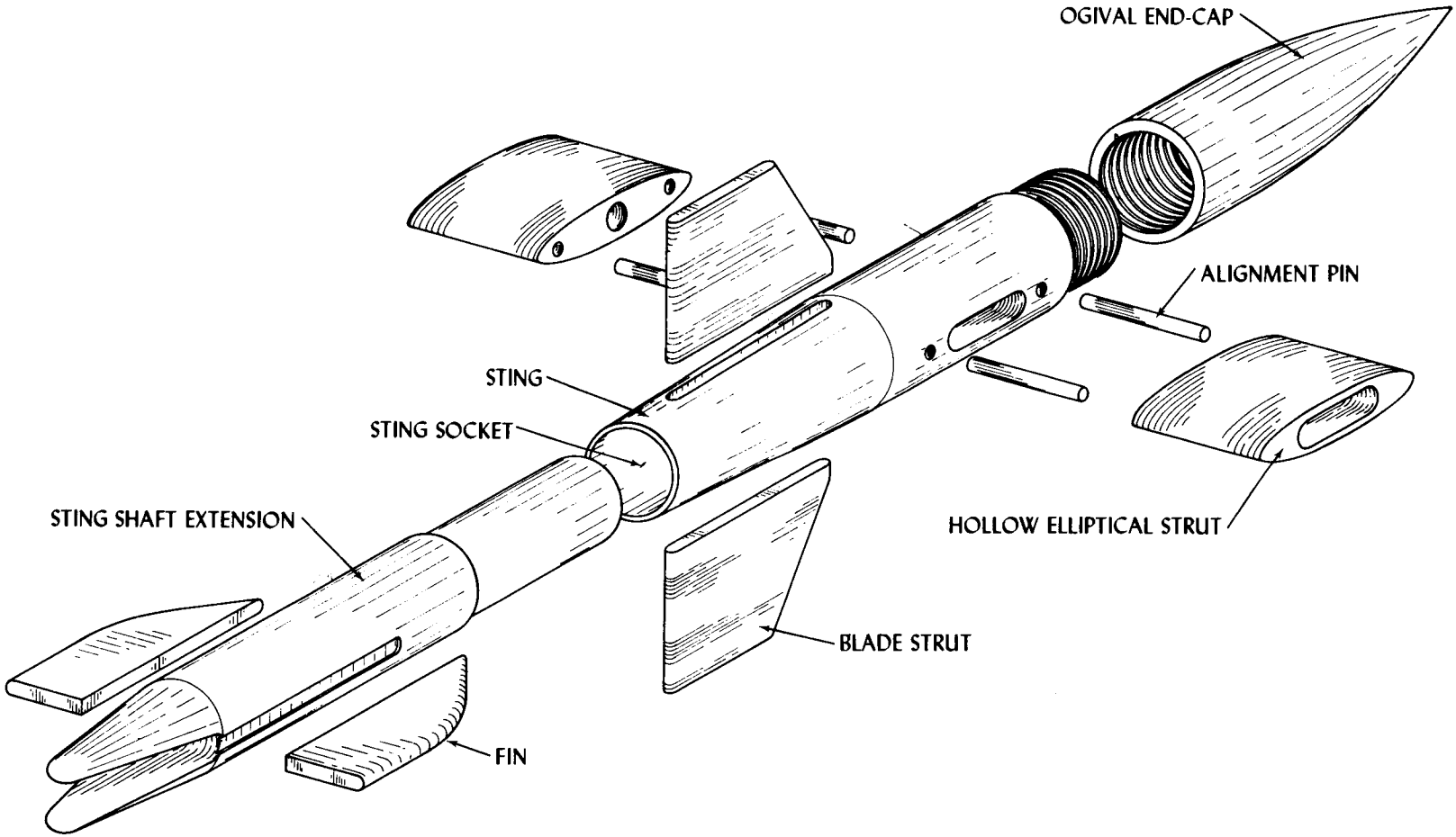

Figure 4.7 Exploded view of sting assembly.

The slight taper required to eliminate tunnel cavitation could have been provided by tapering the sidewalls of the tunnel; however, this approach was rejected because of the difficulties in machining a smooth, non-wavy, divergent passage (diffuser) in a square cross section acrylic tunnel. This plastic tunnel was designed with a square flow passage to enhance two-dimensional flow and to promote smooth transition to circular cross sections--inlet and outlet ducts were cylindrical. This square tunnel permits direct observation of cavity shape and thickness with minimum optical distortion--a primary objective of this study. Consistent with this objective was the necessity to design a snug fit between the edges of the hydrofoil and the tunnel, so that cavitation would not occur prematurely at the hydrofoil-tunnel interface. This was easily accomplished by taking advantage of the differential thermal contraction between the acrylic tunnel and the brass hydrofoil. A snug fit at room temperature assures a tight fit at cryogenic temperatures; however, the fit must not be sufficiently tight to fracture the plastic tunnel when cooled to cryogenic temperatures. The square corners of the tunnel flow passage were rounded, to reduce stress concentrations, and to discourage cavitation along these corners. This rounding facilitates cleaning and polishing of the tunnel. The square-to-circular transitions, at the inlet and outlet of the tunnel, were designed to eliminate cavitation at these locations. Also, the inlet transition was designed to promote uniform two-dimensional flow at the hydrofoil. Uniformity of flow in the tunnel inlet was experimentally verified by static pressure measurements at different locations in the tunnel inlet, see figure 4. 4.

The sting-mount assembly was designed to 1) eliminate cavitation in the vicinity of the sting-mount and 2) provide a rigid support for the hydrofoil (and subsequently for scaled ogives). The latter criterion

was satisfied by providing a close-tolerance tongue-and-groove joint between tunnel and hydrofoil, see figures 4. 4 and 4. 5. This tongue-and-groove also provided assurance that the hydrofoil was properly positioned in the tunnel. The hydrofoil-sting-tunnel assembly was designed so that the hydrofoil-tunnel interface completely shields the tongue-and-groove joint, thus avoiding premature cavitation along this joint. The aft (downstream) end of the sting was fitted with a hollow 4. 33-caliber ogive, see figure 4. 7. This ogive was attached by threads to permit ready access to the instrument wires and tubes, inside the cylindrical sting, and to facilitate installation of this instrumentation. This ogive-shaped cap was hollowed out to allow room for thermally anchoring the thermocouple wires.

The thermocouple junctions and pressure-sensing ports, used to measure temperatures and pressures within the cavities developed on the hydrofoil, were located as shown in figure 4. 5. All of the sensors were located on one side of the hydrofoil--with pressure and temperature sensors at each station closely spaced--to ensure a fair comparison of the pressure profiles obtained from the pressure and temperature measurements within the cavity. Although the cavities developed on the hydrofoil (top and bottom sides) appeared symmetrical, this approach assures that both the pressure and temperature sensors are subjected to the same cavity environment. Also, the sensors were located as near as possible to the central plane of the hydrofoil, to avoid potential 'edge effects,' within the cavity, at the tunnel-hydrofoil interface.

The hydrofoil test assembly was installed in the same space allocated for the plastic venturi [20] in the experimental apparatus; fabrication details follow.

4.1.2 Details of Fabrication

The tunnel was constructed from annealed, cast acrylic rod. A 31/32-inch (2.46 cm) diameter hole was drilled through the axis of this cylindrical rod and reamed to 63/64-inch (2.50 cm). This hole served as a pilot for a square-shaped broaching tool; thus, the square-hole passage was broached using a three-pass broaching operation. The first broaching tool rough-cut the square hole. The second broaching tool finish-cut the square hole, and the third broaching tool burnished the passage. The broaching tools were specially designed, by an industrial tool manufacturing firm, to broach plastic with minimum waviness and maximum smoothness. Broaching an acceptable square hole required a special technique. It was necessary to complete each broaching operation with a single thrust, i.e., the broaching tool had to be shoved all of the way through the plastic without stopping. The rate at which the broach was shoved through the plastic was not critical. Satisfactory broaching operations were performed using a vertical drill press, hydraulic press, and an ordinary machine lathe. The only requirements were that the machine provide smooth, continuous feed, and sufficient travel to complete the broaching operatipn in one stroke. Several tool lubricants were tried (e.g. kerosene and light machine oil), and we learned that a commercial additive for automotive engine oils worked best.

Following the broaching operation, the square tunnel was slotted, on two opposing sides, to provide the groove for the tongue-and-groove hydrofoil-tunnel joint. This slotting was accomplished with an anchor-shaped tool, and an axial scraping motion, on a milling machine. The square-to-circular transitions, on the ends of the tunnel, were then made by making a taper-cut with a machine lathe. This machining operation leaves tapered gullies at each corner of the square passage, see figure 4.4. The edges of these tapered gullies were then very carefully

rounded, by hand, using appropriate Swiss pattern files and polishing compounds. The entire internal passage was then carefully polished to a high lustre, using plastic polishing compound. To ensure uniform polishing on each sidewall, a square-shaped wooden bar was machined. This bar, when covered with a thin cotton cloth, was designed to extend through, and fit comfortably inside of, the tunnel. Polishing compound was applied to the cloth, and polishing was accomplished by grasping the wooden bar on each end and sliding it back and forth in the tunnel.

With the critical machining and polishing completed, the tunnel exterior was machined and polished. Internal tunnel dimensions were easily measured by conventional means. Tunnel dimensions are given on figure 4. 4. The locations of pressure taps, upstream and downstream of the hydrofoil leading edge, are also shown. Note that the exterior surfaces of the tunnel walls are machined flat and parallel to the interior surfaces, so that cavities may be observed with minimum optical distortion. Scribe marks on the tunnel were used to estimate developed cavity lengths, see figure 4. 3.

The sting assembly consisted of a hollow coaxial cylinder, supported by four radial struts, see figure 4. 7. Two of these struts were hollow ellipsoids, and two were very thin solid blade-struts with rounded edges. The hollow struts served as conduits, for pressure transmitting tubes and thermocouple wires, as did the hollow cylindrical sting. These sting mount features are shown on figures 4. 1, 4. 2, and 4. 7. The sting was soldered into place, in the mounting flange, as shown on figures 4. 1 and 4. 2. Coaxial alignment of the sting was maintained, through the soldering operation, by alignment pins and the slot-inserted blade-struts, see figures 4. 1 and 4. 2. Alignment of the hydrofoil, when soldered to the sting socket, was guaranteed by using a specially devised assembly fixture.

Five pressure transmitting tubes[7] were routed from the hydrofoil, through the hollow sting, and up through one of the hollow elliptical struts. Then, the tubes pass through a slot in the flange and extend through a short length of 0.25-inch (0.64 cm) diameter tube that is located outside of the flange. The smaller tubes are collectively soldered inside this larger tube, to form a seal, and then the larger tube is sealed to the flange with a commercial compression fitting. Similar fittings are provided for the pressure sensing stations on the plastic tunnel. The small pressure transmitting tubes terminate, outside of the flange, in the vacuum insulation space. These tubes are then solder-connected to larger tubes, which penetrate the vacuum barrier, and are attached to pressure transducers.

The other hollow elliptical strut is used to guide thermocouple wires into the vacuum space. Details of the thermocouple fabrication, seals, etc., are given in appendix B.

Construction of the hydrofoil is quite intricate; therefore, one must carefully study figures 4.2 and 4.5-4.7 to fully appreciate the finer details. The hollow hydrofoil is easily manufactured by conventional means. The 1.817 degree taper was easily attained with a sine-plate attachment for a milling machine, and the cylindrical leading edge was obtained by scraping the hydrofoil with a concave-radius wheel-cutter; the hydrofoil was held in a vise, and the wheel-cutter was mounted in a milling head and drawn across the hydrofoil--without rotation of the cutter.

The transition from cylindrical sting to hydrofoil is accomplished with two diametrically opposed fins and a conically tapered cylindrical

---

[7] Stainless steel tubes, 0.040-inch (0.102 cm) diameter, with 0.005-inch (0.013 cm) wall thickness.

shaft extension, see figure 4. 7. The conically tapered hollow shaft is soldered onto the male portion (mandrel) of the two-piece hydrofoil. The fins are extensions of the tongue machined into the sides of the hydrofoil, and help to gradually decelerate the liquid at the aft end of the hydrofoil.

The mandrel portion of the hydrofoil was designed to accommodate ten of the 0. 040-inch (0. 102 cm) tubes, see figure 4. 6. The ten tubes were installed in five tube tracks--two tubes to the track, i. e. , one tube on top of another. Each tube was plugged with silver solder on the end nearest the leading edge of the hydrofoil. The top tube is slightly shorter than the bottom tube--after the hydrofoil is assembled, sensor ports are drilled through the hydrofoil, into each tube, penetrating only one tube. With the tubes in place, the mandrel and tubes were tinned with soft solder. The hollow hydrofoil, as shown on figure 4. 5, was puddled full of soft solder. The mandrel and hollow hydrofoil were then carefully assembled, while the solder was liquid.

Upon completion of this assembly, holes were drilled through the hydrofoil into each of the ten small tubes as indicated on figure 4. 5. Care must be taken to avoid drilling through the top tube into the tube which lies below. Each of the holes, so drilled, are isolated from the others by the soft solder that fills all voids between the mandrel and hollow hydrofoil. Five of these holes become pressure sensing stations, while the other five are used for thermocouples. This entire assembly is then attached, by soldering, to the sting socket using a special alignment fixture, see figure 4. 2. The small tubes must be threaded through the sting, hollow strut, etc. , to mate the hydrofoil and sting. Also, the five tubes used as thermocouple conduits are extended through a tube

support, at the rear of the sting, and soft soldered to this support. Later, during thermocouple fabrication, this support is epoxied to the sting.

The thermocouples were installed as described in appendix B; following this installation the thermocouple sensors extend through small mounds of epoxy. These epoxy bumps must be removed so that 1) the bare thermocouple junction is flush with the surface of the hydrofoil and 2) the thermocouple junction is surrounded by epoxy that electrically and thermally isolates the thermocouple while sealing it to the hydrofoil. This installation technique assures rapid response of the thermocouples, while electrically and thermally isolating the junctions from the metal hydrofoil. The epoxy bumps were finished flush with the hydrofoil, by using Swiss files and then fine-grit sandpaper; during this hand-finishing operation, the entire hydrofoil was tape-masked, exposing only the epoxy bumps. Following this finishing operation, the entire hydrofoil was carefully polished, measured, and installed in the test apparatus.

4.2 Hydrofoil Contour and Pressure Distribution

The actual and theoretical contours of the 0.5-caliber hydrofoil are shown on figure 4.8. The actual contour was verified by using an optical comparator (shadowgraph), with 31.25 X magnification. The theoretical noncavitating pressure profiles for this tapered hydrofoil, and a non-tapered hydrofoil, are shown on figure 4.9; experimental data from this study are also plotted for comparison. The theoretical pressure profiles were computed using existing computer programs [35, 36]. Figure 4.9 indicates good agreement between experimental and calculated data, in the regions where experimental data are available. Also, note that there is little difference in the calculated data

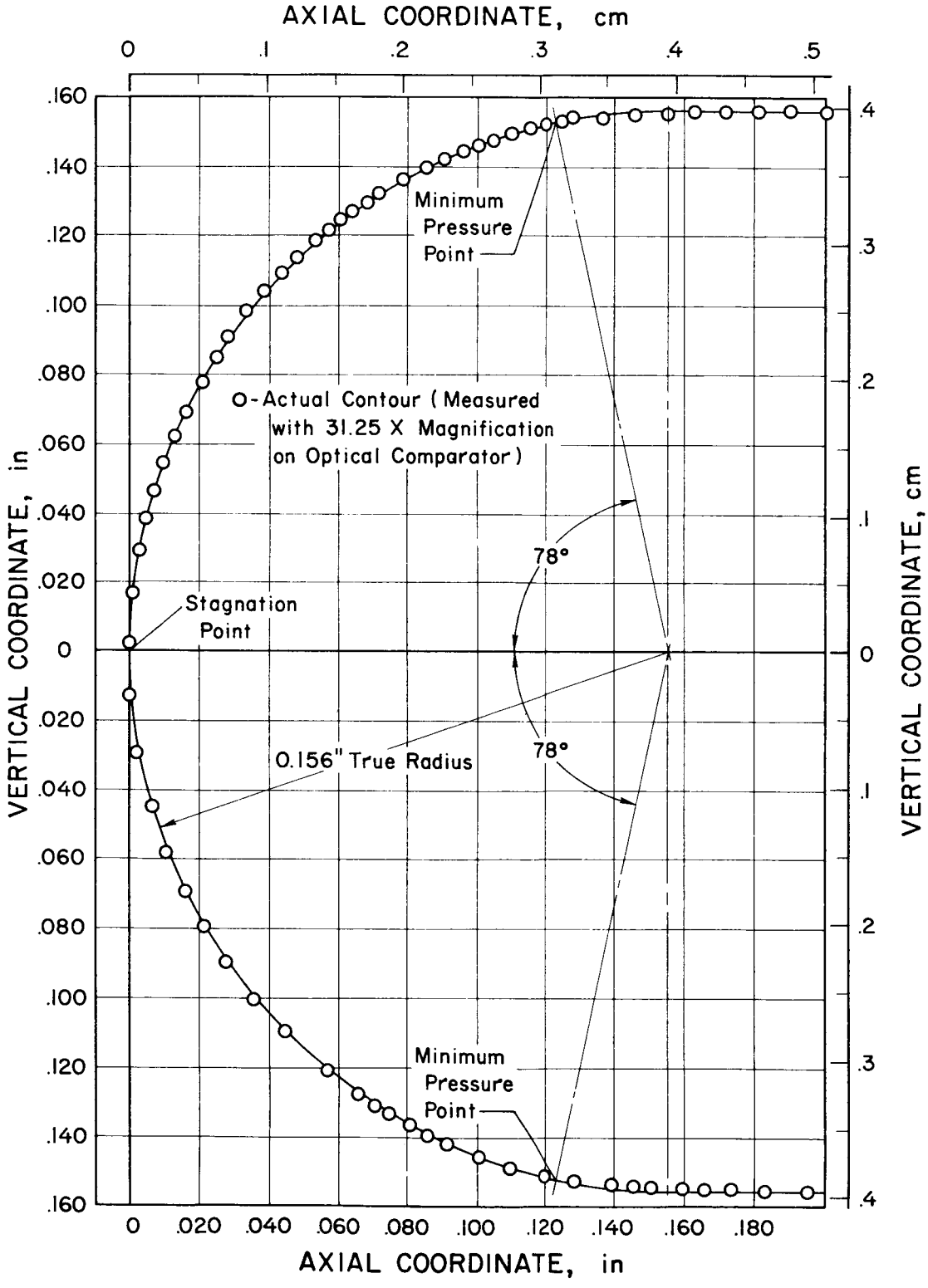

Figure 4.8 Contour of the cylindrical leading edge of the 0.5-caliber hydrofoil.

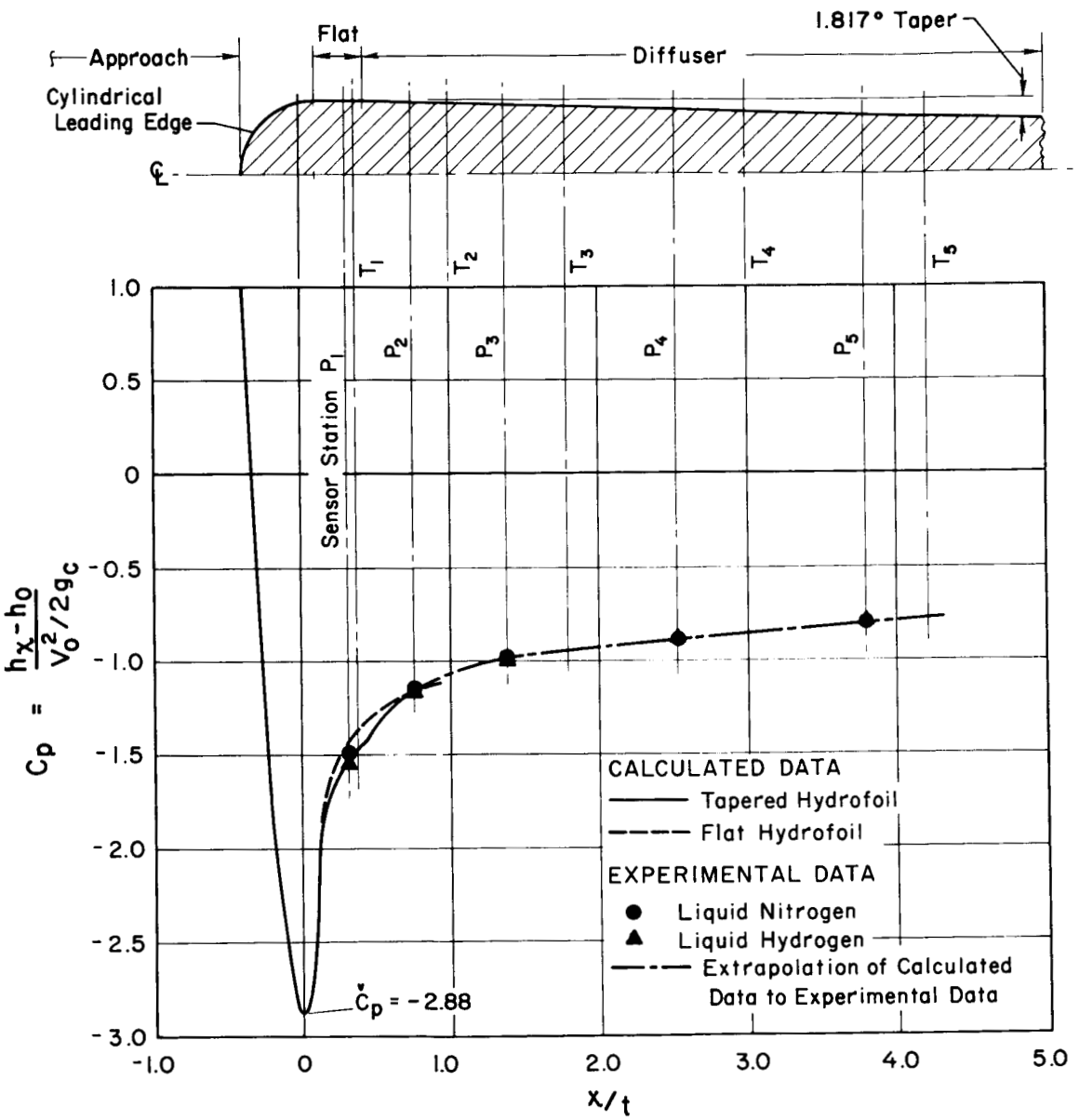

Figure 4.9 Pressure distribution on the 0.5-caliber hydrofoil, for non-cavitating flow. (Calculated data supplied by Werner R. Britsch.)

for the flat and tapered hydrofoils. The slight wiggle, in the calculated C_p for the tapered hydrofoil, occurs at the flat-to-diffuser transition. Figure 4.9 indicates that the minimum pressure point occurs at about 78 degrees of arc, measured from the stagnation point of the hydrofoil. This minimum pressure location is indicated on the contour shown on figure 4.8. The value of 78 degrees corresponds favorably with the pressure coefficient data for a cylindrical body with a hemispherical head [28].

5. DATA ANALYSIS

The desinent (incipient) and developed cavitation data, for liquid hydrogen and liquid nitrogen, are given in complete detail in appendix A. These tabulated data are given in English and metric units. No attempt has been made to separate the desinent and developed cavity data; however, the desinent (or incipient) cavity data are clearly marked by the attachment of asterisks to the run numbers. The desinent and developed cavity data are correlated, and discussed separately in this section.

5.1 Correlation of Desinent Cavitation Data

With the blow-down facility used in this experimental study, it was impossible to maintain a constant fluid temperature, while varying the inlet velocities and pressures to obtain desinent cavities. Consequently, it was necessary to develop a mathematical technique for correlating the desinent data. This was accomplished by using a least-squares surface-fitting computer program. Once an equation is obtained, to fit the experimental surface (P_o, V_o, T_o coordinates), the conventional isotherm data for desinence are readily calculated. Complete details concerning this correlating technique, and the computer program, are given in appendix C. Also, the polynomial

expressions, derived to correlate the desinent hydrogen and nitrogen data, are given in appendix C. These expressions were used to compute the desinent data presented in tables 5.1 and 5.2. These same data are plotted on figures 5.1 to 5.4.

The experimental values of K_{iv} are tabulated under the heading, K_v, in appendix A, along with the experimental values of K_v for developed cavities. The K_{iv} parameter, as given in appendix A, in tables 5.1 and 5.2, and on figures 5.2 and 5.4, is not corrected for tunnel blockage. Multiplying K_{iv} by the square of the appropriate area ratio, A_1/A_2, corrects for tunnel blockage, i.e.,

$$\text{Corrected } K_{iv} = (\text{Experimental } K_{iv})\,(A_1/A_2)^2, \qquad (5\text{-}1)$$

where A_1 = blocked cross sectional flow area and A_2 = unblocked (inlet) cross sectional flow area. This correction factor evolves from consideration of steady volumetric flow, C_p^v, and Bernoulli's equation, and is derived in detail elsewhere [37, 38]. This correction factor assures that the minimum static pressure is the same for blocked and unblocked flows, when the freestream static pressures are identical. Thus, tunnel constraint is easily accounted for, so that the results of this study may be readily compared with other experimental data. In this study, the correction factor has a numerical value of 0.47.

5.2 Discussion of Desinent Cavitation Data

Figure 5.1 indicates that P_o varies almost linearly with V_o, at constant T_o, for hydrogen test fluid; also, P_o increases with T_o, at constant V_o, in a conventional manner. The incipient (desinent) cavitation parameter, K_{iv}, for hydrogen also behaves in a conventional manner, see figure 5.2. On both of these figures, the

Table 5.1. Temperature-compensated desinent data

(Hydrogen: 0.312-inch (0.792-cm) hydrofoil)

T_o (R)	V_o (ft/s)	P_o (psia)	K_{iv}	P_o (N/cm^2)	V_o (m/s)	T_o (K)
37.00	100.0	22.08	1.28	15.22	30.5	20.56
37.00	120.0	29.93	2.04	20.64	36.6	20.56
37.00	140.0	37.78	2.34	26.05	42.7	20.56
37.00	160.0	45.62	2.43	31.46	48.8	20.56
37.00	180.0	53.47	2.42	36.87	54.9	20.56
37.00	200.0	61.32	2.37	42.28	61.0	20.56
38.50	100.0	25.31	1.10	17.45	30.5	21.39
38.50	120.0	33.01	1.90	22.76	36.6	21.39
38.50	140.0	40.71	2.23	28.07	42.7	21.39
38.50	160.0	48.41	2.35	33.38	48.8	21.39
38.50	180.0	56.11	2.36	38.69	54.9	21.39
38.50	200.0	63.82	2.32	44.00	61.0	21.39
40.00	100.0	28.90	0.83	19.93	30.5	22.22
40.00	120.0	36.46	1.71	25.14	36.6	22.22
40.00	140.0	44.01	2.09	30.34	42.7	22.22
40.00	160.0	51.57	2.23	35.55	48.8	22.22
40.00	180.0	59.12	2.27	40.76	54.9	22.22
40.00	200.0	66.67	2.24	45.97	61.0	22.22
41.50	100.0	32.86	0.45	22.65	30.5	23.06
41.50	120.0	40.27	1.44	27.76	36.6	23.06
41.50	140.0	47.67	1.89	32.87	42.7	23.06
41.50	160.0	55.08	2.08	37.98	48.8	23.06
41.50	180.0	62.49	2.14	43.08	54.9	23.06
41.50	200.0	69.90	2.14	48.19	61.0	23.06

Table 5.2. Temperature-compensated desinent data

(Nitrogen: 0.312-inch (0.792-cm) hydrofoil)

T_o (R)	V_o (ft/s)	P_o (psia)	K_{iv}	P_o (N/cm^2)	V_o (m/s)	T_o (K)
140.00	25.0	23.76	2.46	16.38	7.6	77.78
140.00	35.0	30.51	2.27	21.03	10.7	77.78
140.00	45.0	41.03	2.33	28.29	13.7	77.78
140.00	55.0	55.32	2.43	38.14	16.8	77.78
140.00	65.0	73.39	2.53	50.60	19.8	77.78
140.00	75.0	95.23	2.61	65.66	22.9	77.78
150.00	25.0	39.38	3.43	27.15	7.6	83.33
150.00	35.0	45.22	2.66	31.18	10.7	83.33
150.00	45.0	54.83	2.51	37.81	13.7	83.33
150.00	55.0	68.22	2.52	47.03	16.8	83.33
150.00	65.0	85.37	2.58	58.86	19.8	83.33
150.00	75.0	106.30	2.64	73.29	22.9	83.33
160.00	25.0	57.18	3.09	39.42	7.6	88.89
160.00	35.0	62.10	2.37	42.82	10.7	88.89
160.00	45.0	70.80	2.28	48.82	13.7	88.89
160.00	55.0	83.27	2.34	57.42	16.8	88.89
160.00	65.0	99.52	2.43	68.62	19.8	88.89
160.00	75.0	119.54	2.53	82.42	22.9	88.89

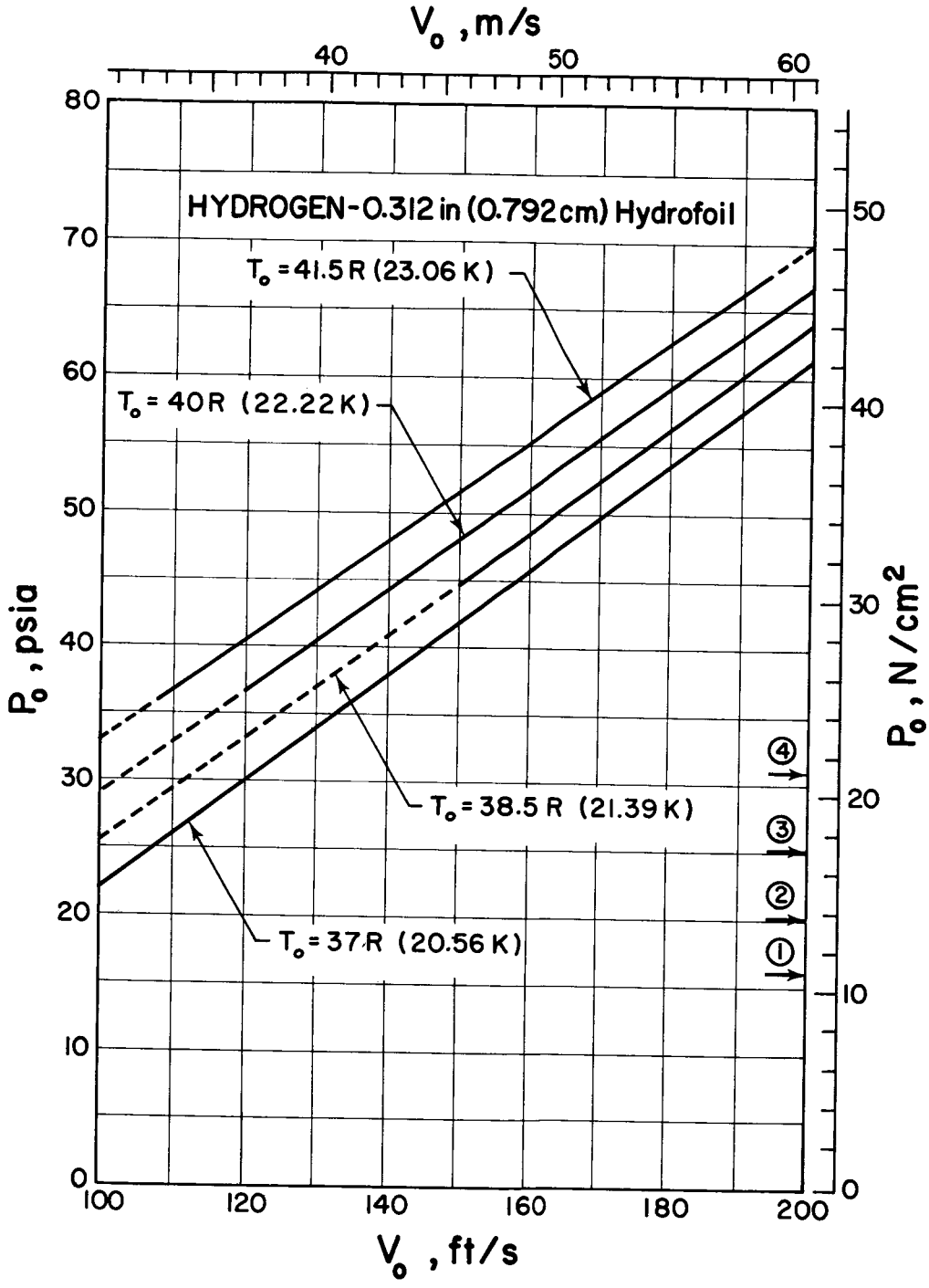

Figure 5.1 Effects of tunnel inlet velocity and liquid temperature on required inlet pressure for desinent cavitation in liquid hydrogen: ① = P_v @ 37R; ② = P_v @ 38.5R; ③ = P_v @ 40R; ④ = P_v @ 41.5R.

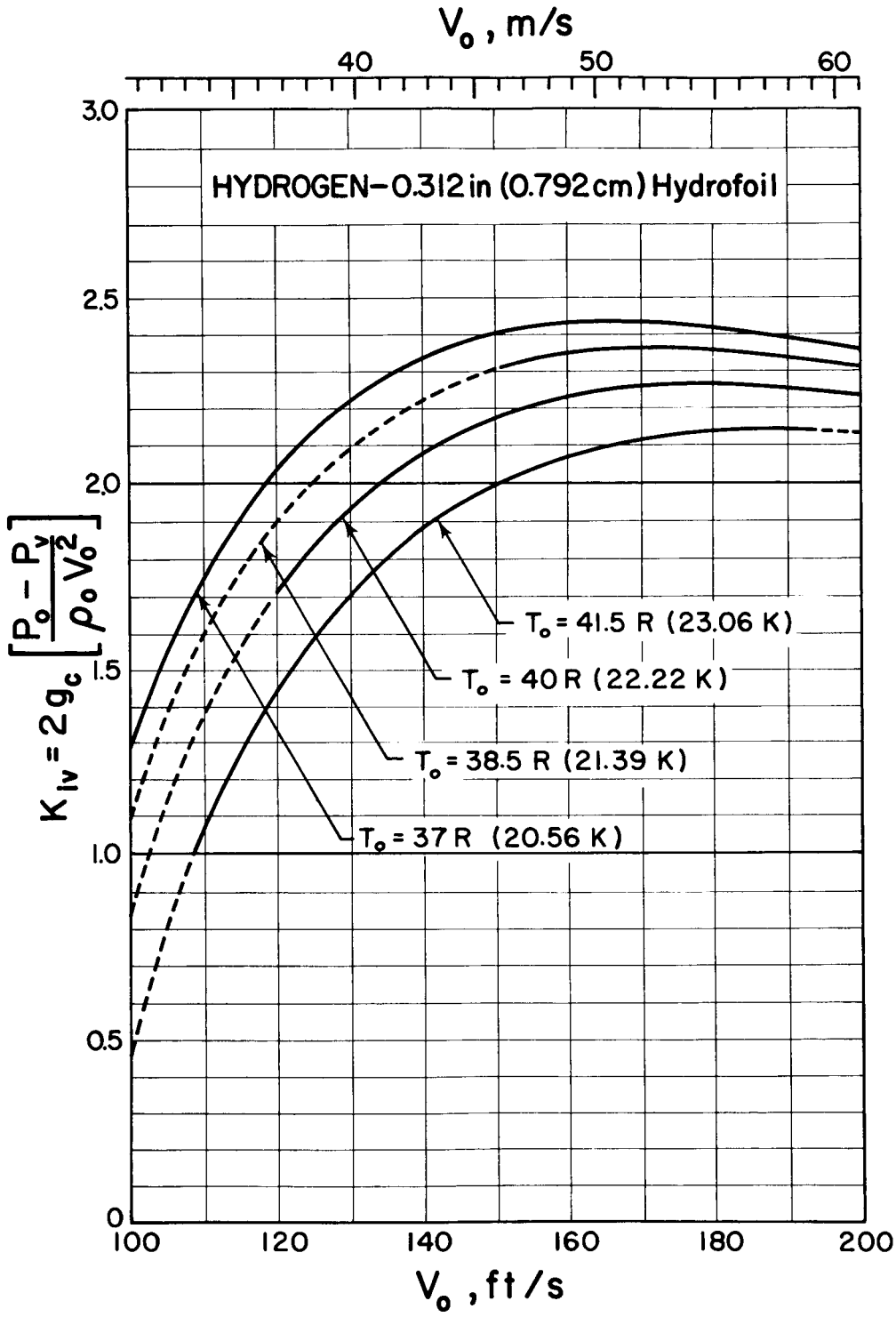

Figure 5.2 Desinent cavitation parameter for liquid hydrogen as a function of tunnel inlet velocity and liquid temperature.

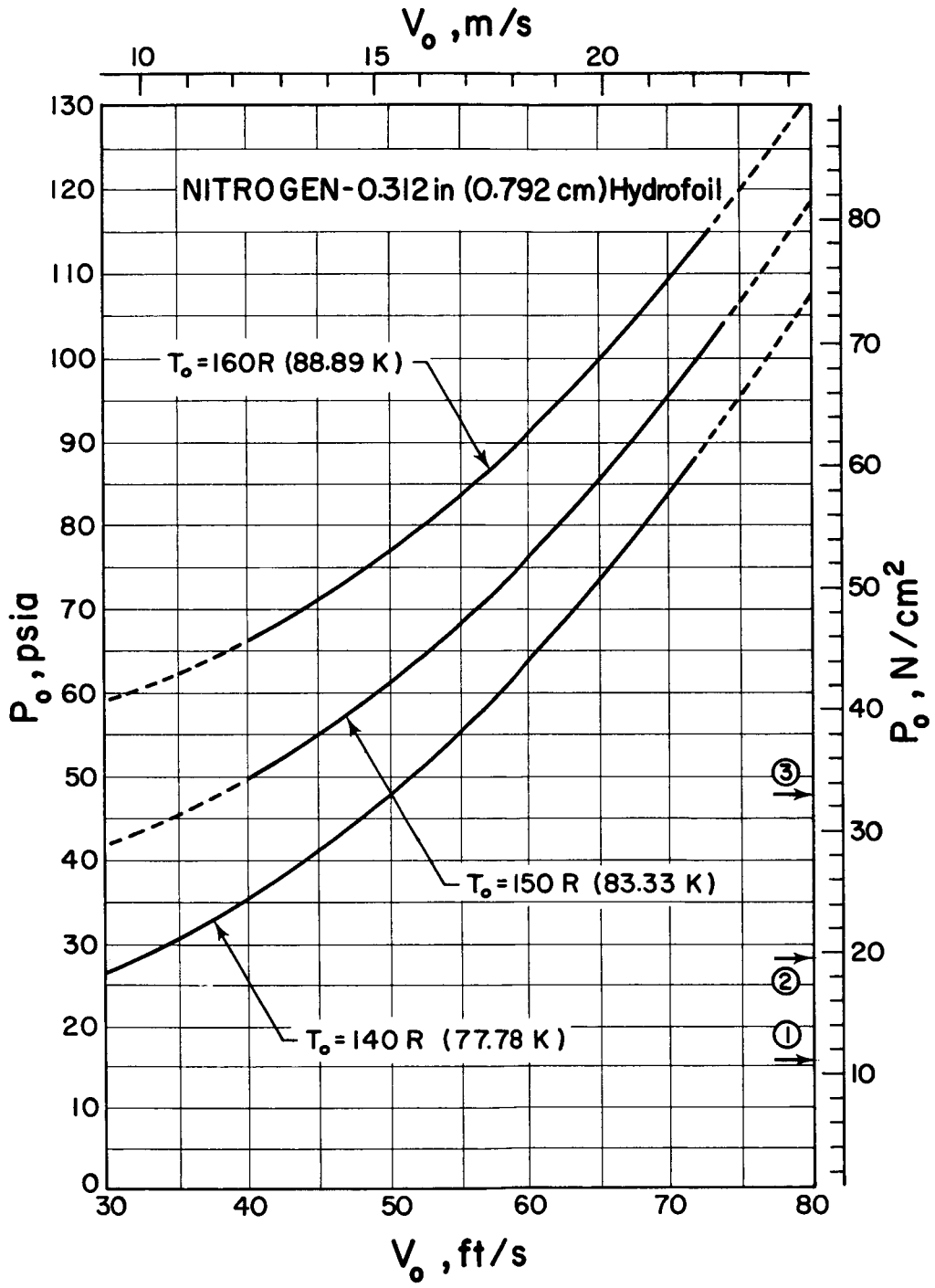

Figure 5.3 Effects of tunnel inlet velocity and liquid temperature on required inlet pressure for desinent cavitation in liquid nitrogen: ① = P_v @ 140R; ② = P_v @ 150R; ③ = P_v @ 160R.

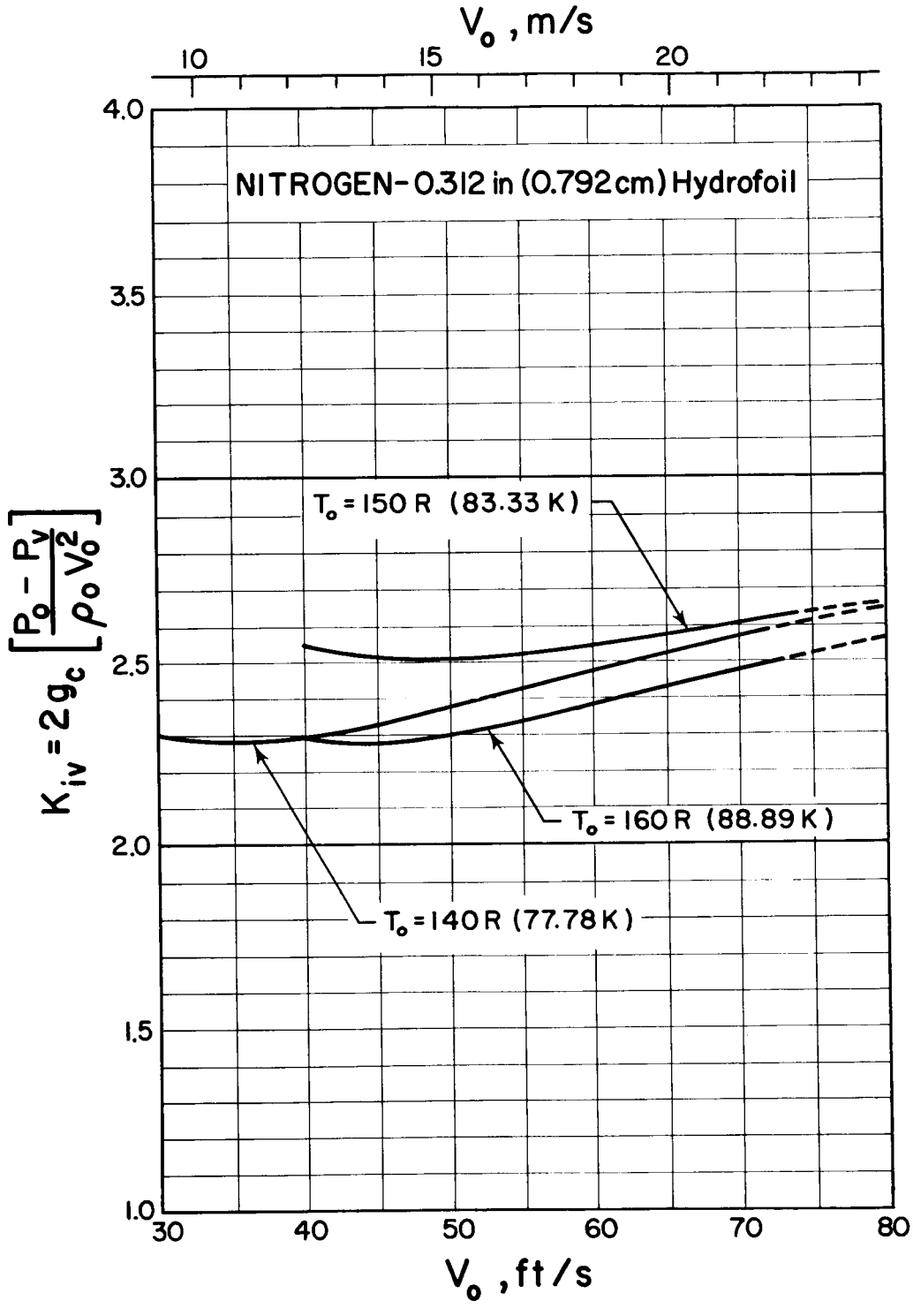

Figure 5.4 Desinent cavitation parameter for liquid nitrogen as a function of tunnel inlet velocity and liquid temperature.

boundaries of the experimental data are indicated by the solid lines, i.e., the broken-line curves are extrapolations of the experimental data. Mathematical extrapolation, by correlative expressions, of experimentally-determined surfaces is rather risky; therefore, the broken-line extrapolations must be used with great caution. Only within the boundaries of the experimental data are the mathematically derived data--as presented in tables 5.1 and 5.2 and on figures 5.1 to 5.4--considered totally valid.

Similar comments may be made about the nitrogen test data shown on figures 5.3 and 5.4; however, the P_o, V_o, T_o curves--figure 5.3--are non-linear and figure 5.4 requires additional discussion. Although the P_o, V_o, T_o curves, on figure 5.3, show the appropriate temperature dependency, the K_{iv} curves, on figure 5.4, do not. This inconsistency in the K_{iv} curves is believed to be mainly due to instrument error, even though this error is very small. In reference [20], it was estimated that the maximum experimental uncertainty in P_o, for hydrogen, is ± 1.0 psi (± 0.69 N/cm^2); for nitrogen, the maximum uncertainty of the pressure measurements, including calibration and read-out errors, is estimated to be within ± 1.5 psi (± 1.04 N/cm^2), with an allowance of ± 0.3 psi (± 0.21 N/cm^2) for systematic error and ± 1.2 psi (± 0.83 N/cm^2) for imprecision. For very low values of V_o (and P_o), the maximum uncertainty in P_o, for hydrogen, did not exceed ± 0.5 psi (± 0.35 N/cm^2). At similar conditions, for nitrogen, the maximum uncertainty in P_o did not exceed ± 1.0 psi (± 0.69 N/cm^2). Then, the pressure measurement error, for the nitrogen data, is considerably larger than that of the hydrogen data--twice as large at the minimum values of V_o and P_o for each fluid, and fifty percent larger at the maximum values of V_o and P_o

for each fluid. The instrument error, for the hydrogen data, was smaller because the tests were performed at lower pressures, permitting the use of lower range pressure transducers--these transducers (and data recording system) have an uncertainty of about ± 0.5 percent of full range, irrespective of the range used.

In reference [21], it was shown that the K_{iv} parameter can easily magnify instrument error. This amplification of instrument error results because K_{iv} is computed from a small pressure difference $(P_o - P_v)$, between two relatively large numbers. Because P_v is constant, for a given T_o, the difference $(P_o - P_v)$ is minimum at the lowest V_o, see figure 5.3. Consequently, the maximum error in K_{iv} will always occur at the minimum velocity, for any specified fluid temperature. Thus, the unusual behavior of the K_{iv} curves, on figure 5.4, at the lower velocities, is not too surprising. To emphasize this point, we extract the following data for run number 294J, as tabulated in appendix A-1a: $T_o \approx 140$ R, $V_o \approx 30$ ft/s and $P_o - P_v \approx 12$ psi. Now, if we assume that there is no error in ρ_o, V_o, or P_v, and that the error in P_o is ± 1.0 psi, K_{iv} will be in error by ≈8.3 percent; therefore, the 140 R isotherm, on figure 5.4, could easily be in error by 8.3 percent at the minimum velocity. Obviously, such a displacement could drastically alter the shape of the curve. Similar computations, at the maximum velocities, where $P_o - P_v$ is maximum, indicate that instrument error should be almost negligible. Then, we must conclude that the K_{iv} curves, at the maximum velocities, are very near their true positions; thus, it appears that the K_{iv}, for nitrogen, is only weakly temperature dependent, and K_{iv} approaches the value of 2.6 at the maximum velocities, irrespective of fluid temperature. The unusual shapes, and positions, of the K_{iv} curves on figure 5.4 are attributed to this weak

temperature dependence, amplification of instrument error, and mathematical correlation of the experimental data. Because of the uncertainties of the extrapolated P_o, V_o, T_o data, at low velocities, on figure 5.3, this data is not plotted on figure 5.4. The data shown on figure 5.4 are considered of real significance only at velocities greater than ~ 45 ft/s (~ 14 m/s).

Similar difficulties were not encountered with the hydrogen data, because of a stronger temperature dependence and lower instrument error. The strong temperature dependence, of hydrogen, is apparent in figure 5.2, even though the temperature variation is small in comparison with the nitrogen data shown on figure 5.4.

The hydrofoil desinent cavity data are quite similar to the data obtained for the quarter-round venturi [21]. For both bodies, the nitrogen and hydrogen data tend toward a single-valued K_{iv}, for each fluid, at the maximum velocities.

The hydrofoil data, presented herein, may also be compared with data for a similar hydrofoil (untapered), tested in water [30]. To make this comparison, the K_{iv} data on figures 5.2 and 5.4 must be multiplied by 0.47 to correct for tunnel blockage. Direct comparison of these data indicates that the asymptotic K_{iv} for water is greater than the asymptotic K_{iv} for either nitrogen or hydrogen (by about 20 to 25 percent). Similar results were obtained in the venturi studies [21], where the K_{iv} data for nitrogen and hydrogen were appreciably lower than the K_{iv} data for refrigerant-114 [39], ethylene glycol [40], and water [40]. Because the latter three liquids have higher bulk densities than the cryogens, it is apparent that the cryogens require less subcooling for desinent cavitation to occur, i.e., for K_{iv} to be smaller for the cryogens, at the same V_o, requires smaller values of $P_o - P_v$--see the definition of K_{iv} on figure 5.4.

5.3 Correlation of Developed Cavitation Data

Typical profiles of measured pressure depression, for liquid hydrogen, are given on figures 5.5 to 5.9; similar profiles, for liquid nitrogen, are plotted on figures 5.10 to 5.13. From these figures, it can be observed that, within data accuracy, stable thermodynamic equilibrium exists throughout the cavity. This topic is discussed in considerable detail in section 5.4 of this report.

The correlative expressions, given by equations (3-12) and (3-27), were used to correlate the developed cavity data from this experiment. These expressions, along with the correlative technique developed by Gelder, et al. [19], the isentropic BFLASH theory [23], and two least-squares data-fitting computer programs [20], were used to correlate these hydrofoil data. For convenience, we will refer to these correlative expressions as 'similarity' equations. The similarity equations are used to correlate developed cavitation data, in similar test items, and to predict the cavitation performance of a test item from fluid-to-fluid, and from one temperature to another, when limited test data from a single fluid are available.

Complete and detailed descriptions of the correlative technique, computational steps, and computer programs are given in reference [20]. The correlative procedure, as previously described [20], can be followed directly when using eq (3-12). To use eq (3-27), simply substitute MTWO for V_o in the computer program. Briefly, this correlative procedure ensures that the B values calculated from eq (3-12), or eq (3-27), and the BFLASH values [23] for each data point, are as nearly identical as possible; because both B values, at each data point, are evaluated from experimental data, this correlative procedure produces the best possible agreement between experiment, the isentropic flashing theory [23], and the correlative expression--eq (3-12)

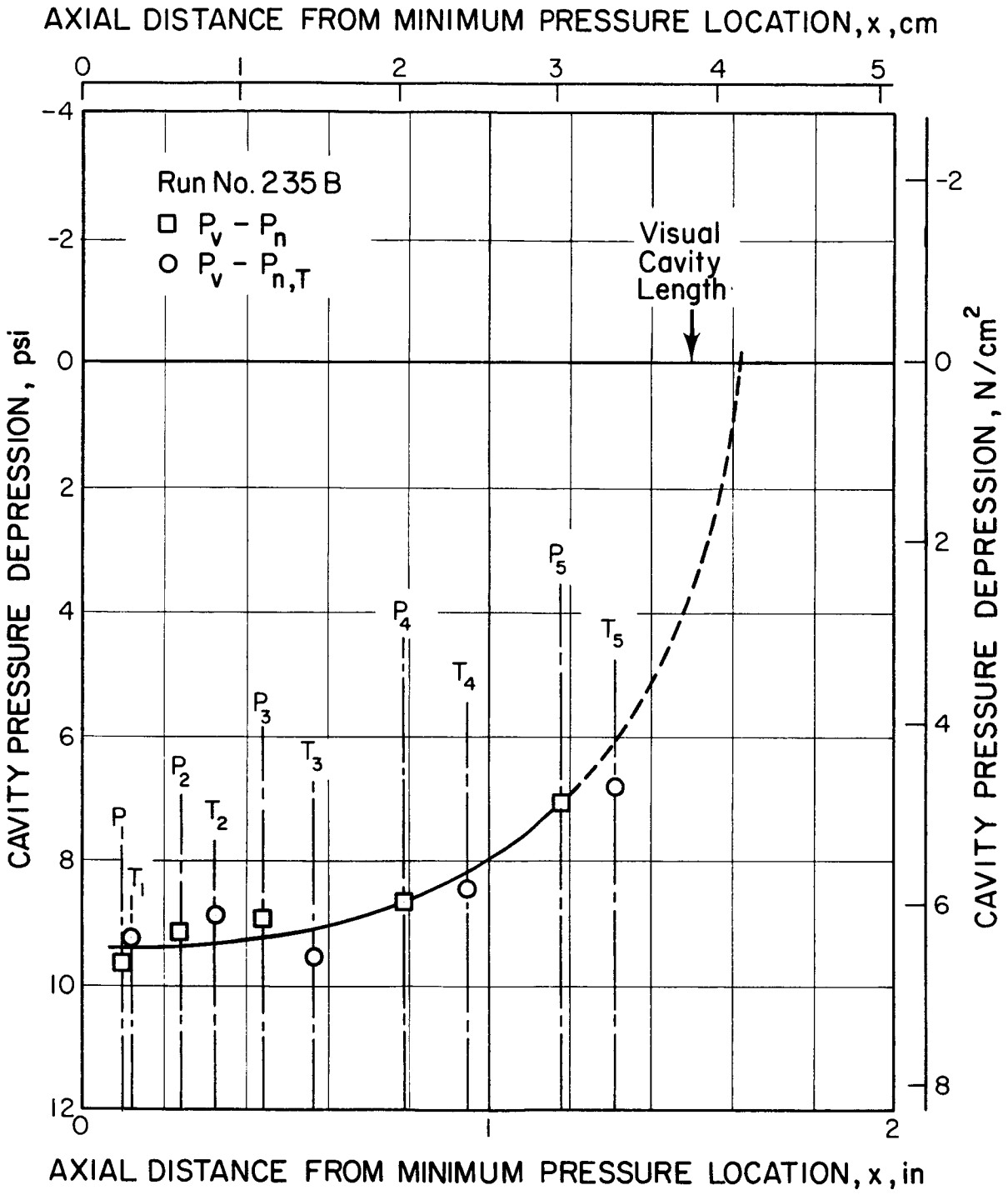

Figure 5.5 Pressure and temperature depressions within cavity in liquid hydrogen.

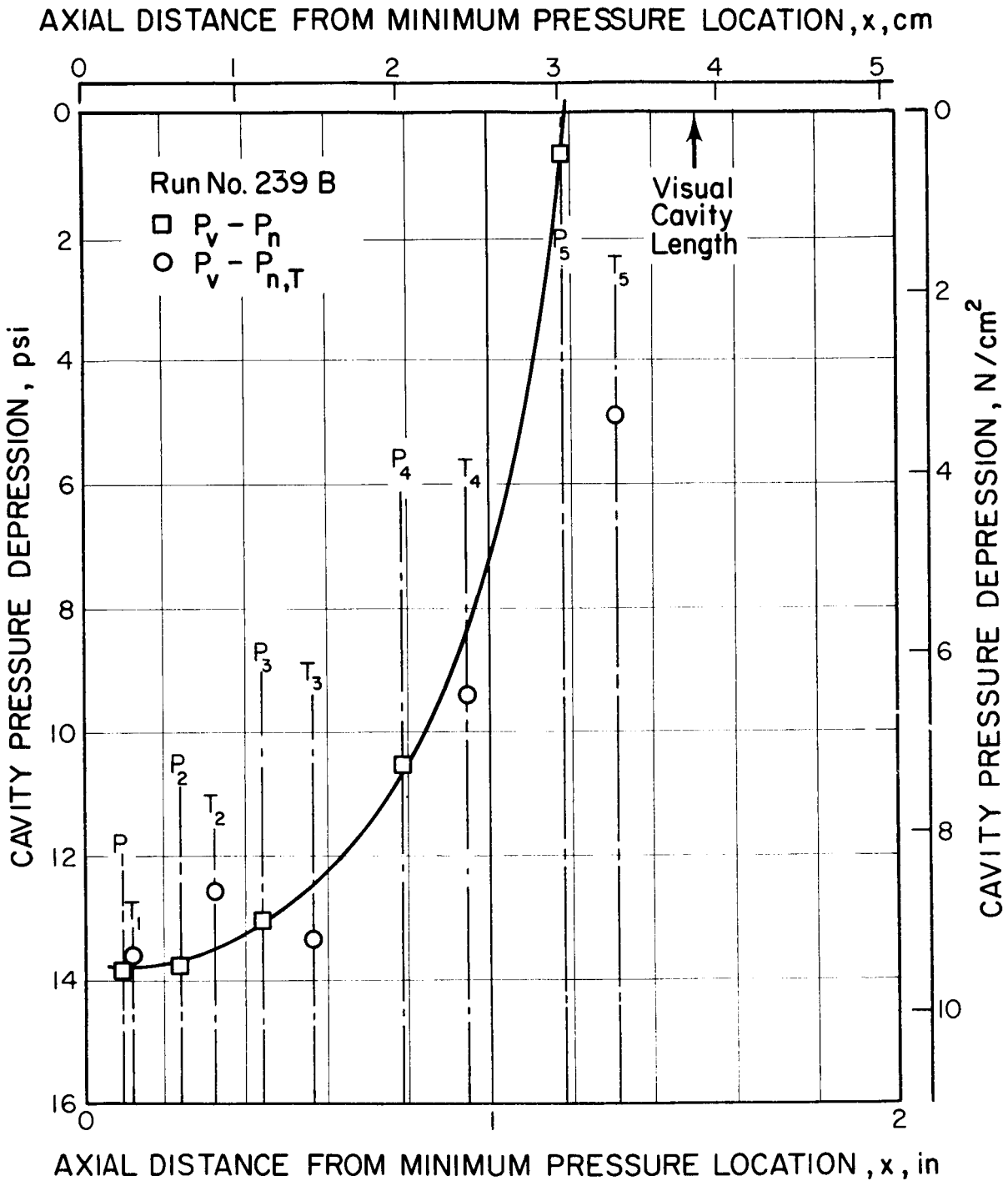

Figure 5.6 Pressure and temperature depressions within cavity in liquid hydrogen.

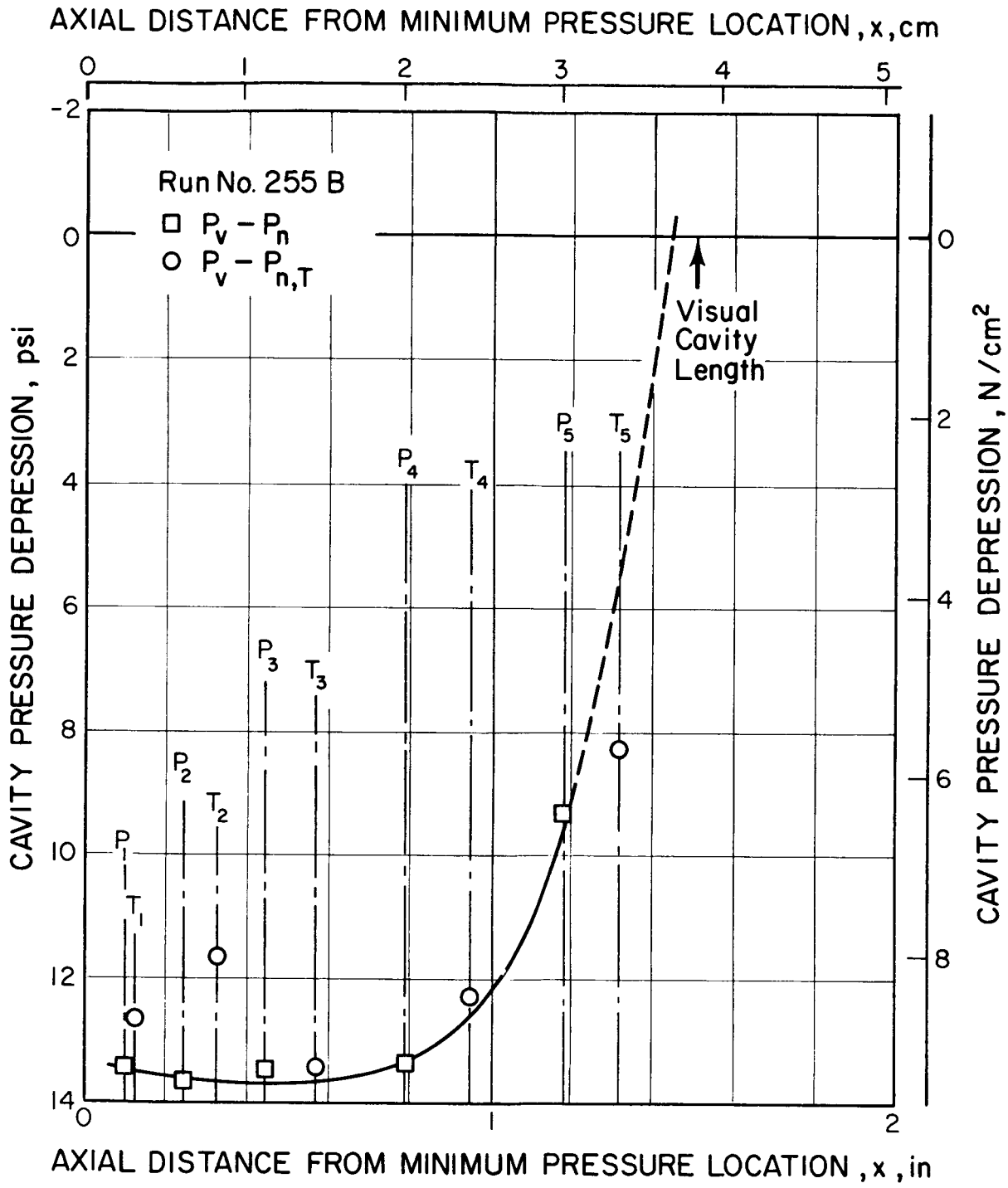

Figure 5.7 Pressure and temperature depressions within cavity in liquid hydrogen.

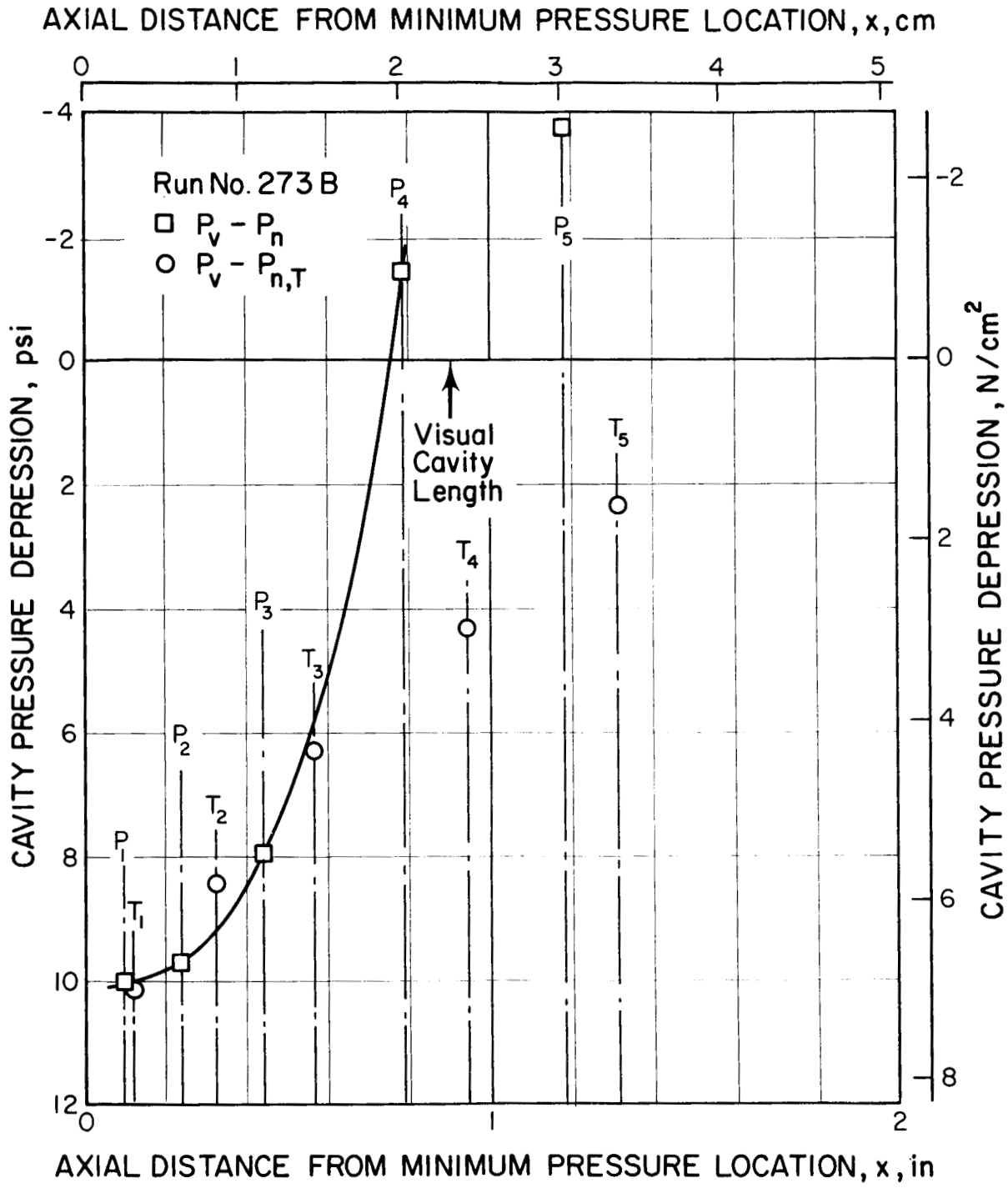

Figure 5.8 Pressure and temperature depressions within cavity in liquid hydrogen.

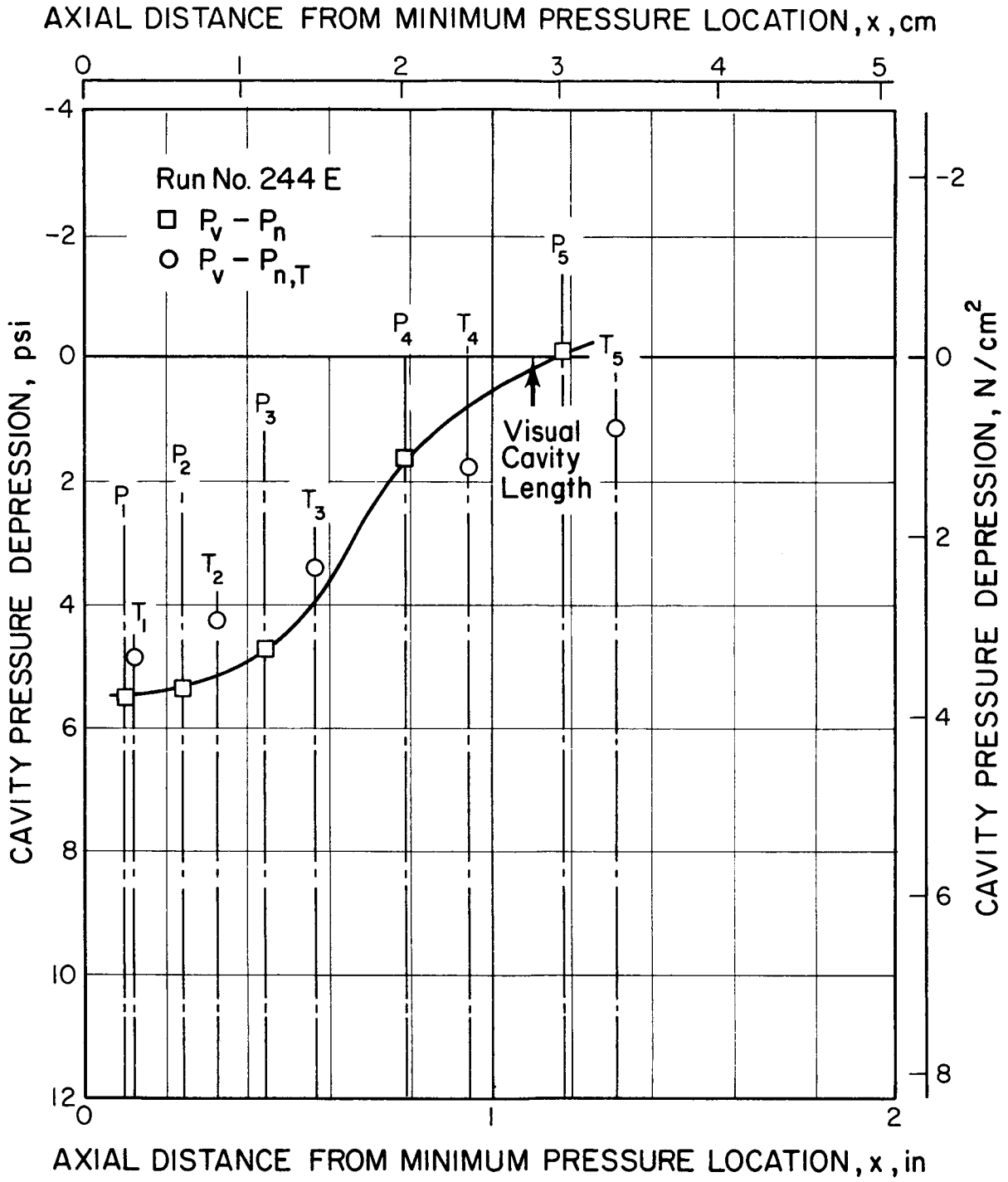

Figure 5.9 Pressure and temperature depressions within cavity in liquid hydrogen.

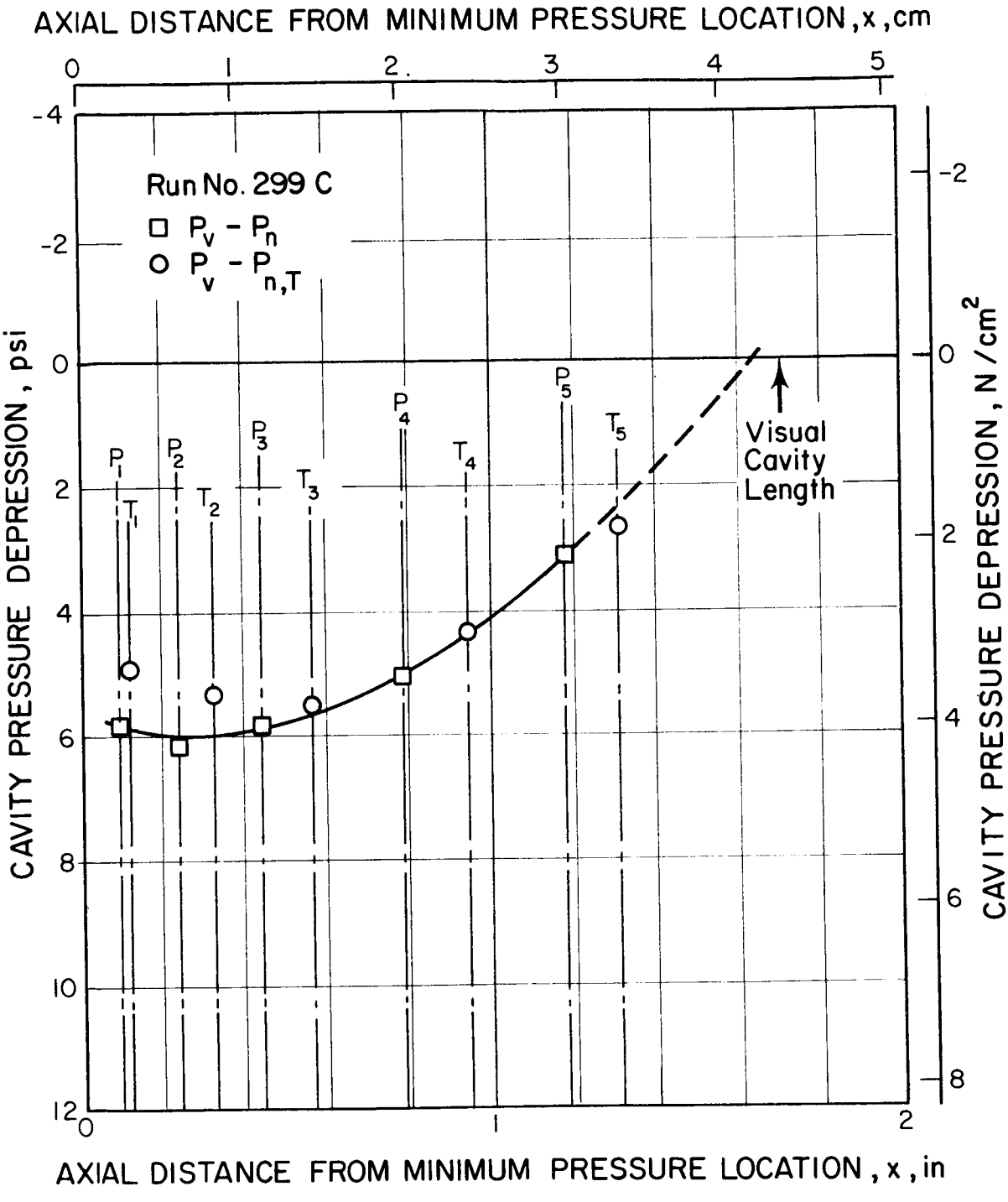

Figure 5.10 Pressure and temperature depressions within cavity in liquid nitrogen.

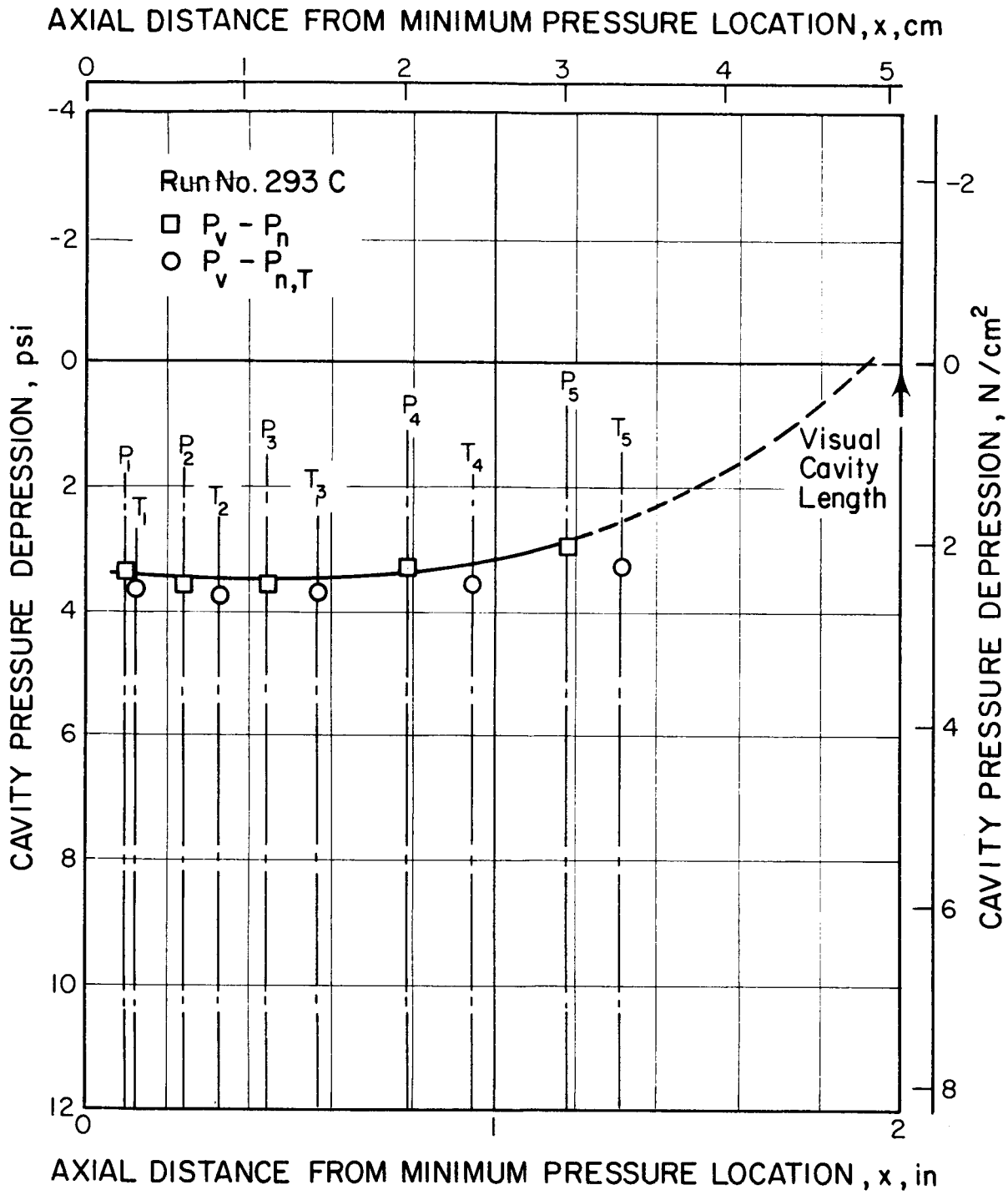

Figure 5.11 Pressure and temperature depressions within cavity in liquid nitrogen.

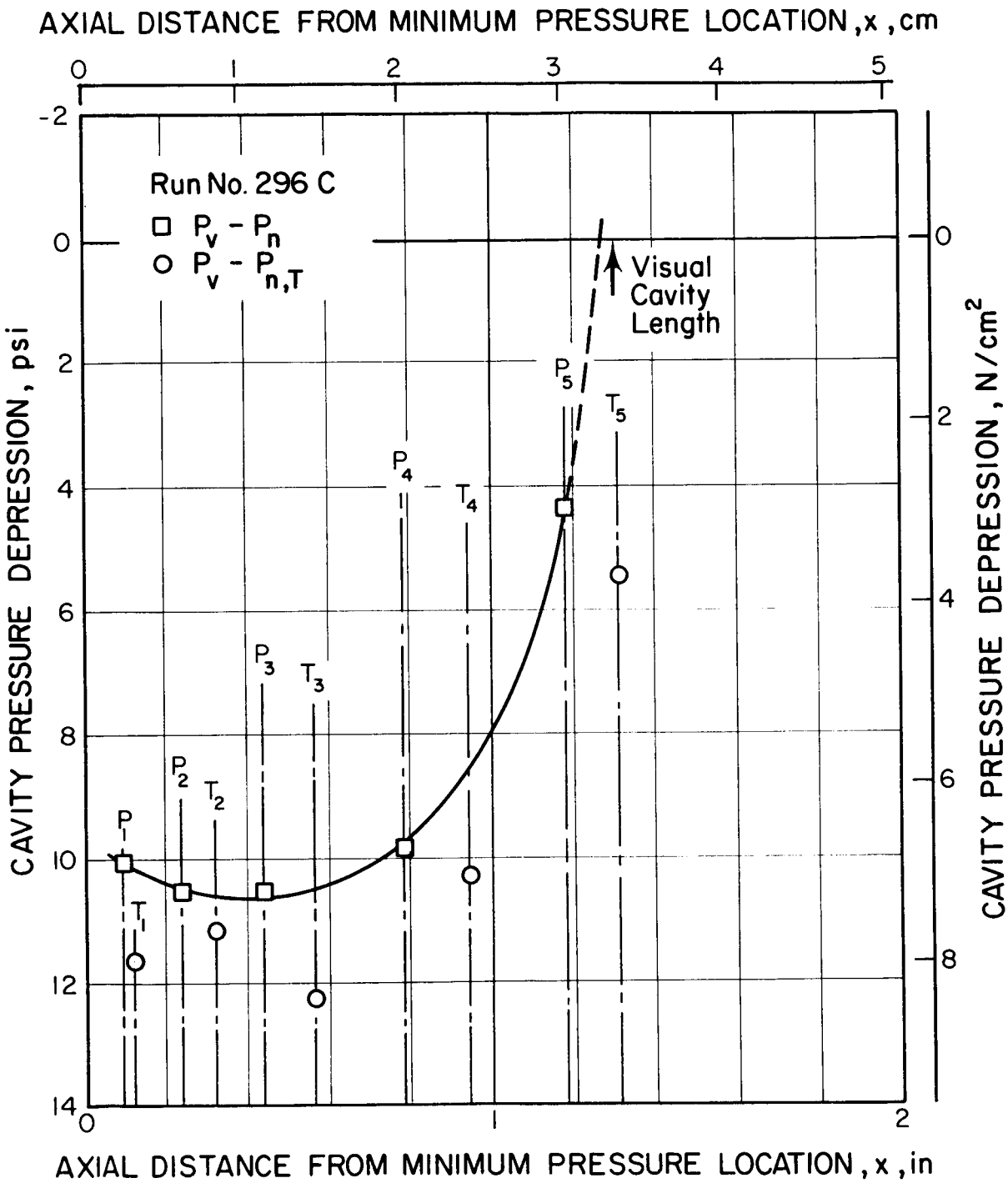

Figure 5.12 Pressure and temperature depressions within cavity in liquid nitrogen.

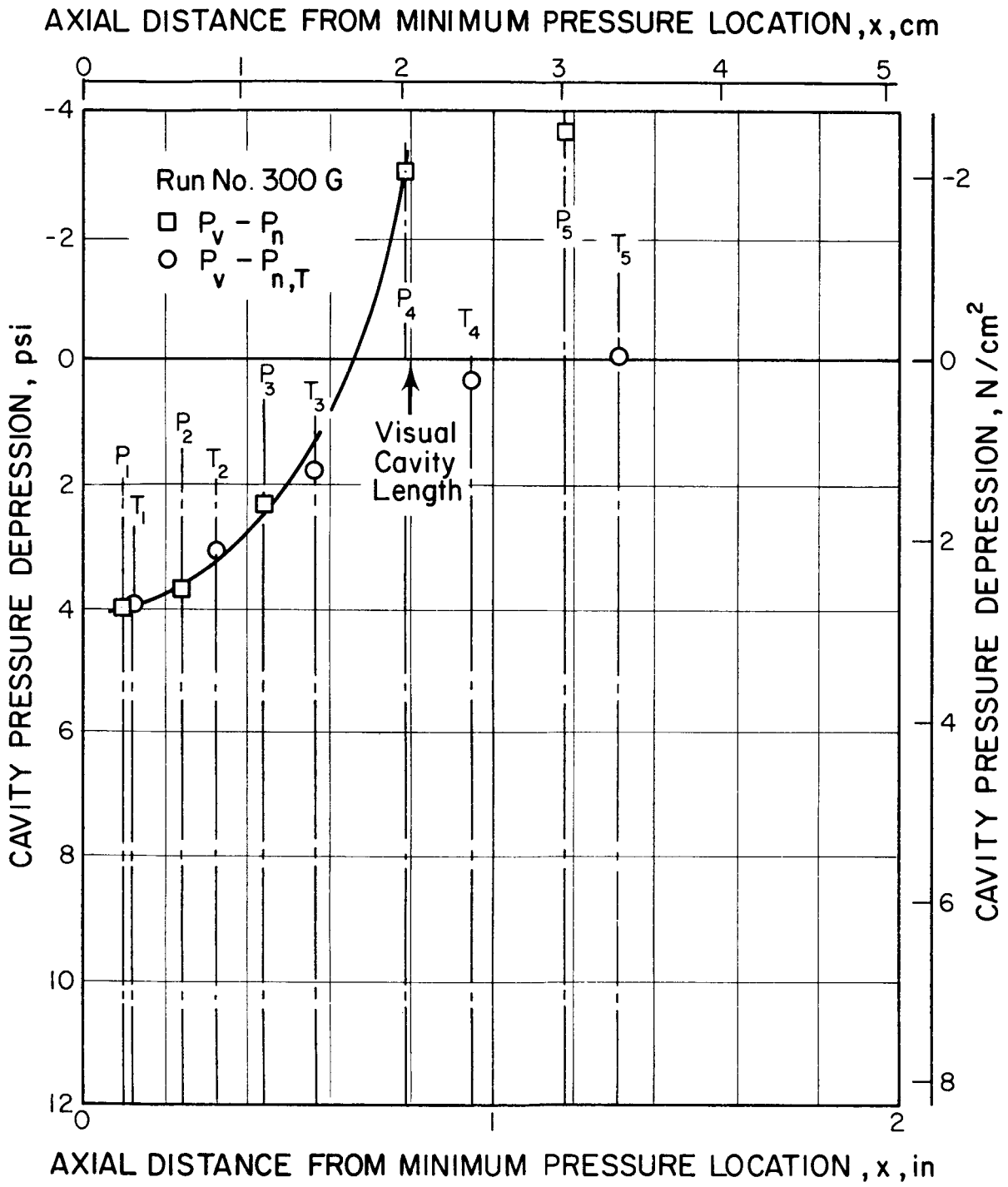

Figure 5.13 Pressure and temperature depressions within cavity in liquid nitrogen.

or eq (3-27). This 'best-fit,' of the experimental data, is obtained by selecting appropriate exponents for each of the correlative parameters in the correlative expression--eq (3-12) or eq (3-27). The exponent selecting process is quite complex and is treated in appropriate detail in reference [20]. Exponents for eq (3-12) and eq (3-27) were derived to evaluate the suitability of MTWO as a correlating parameter. Attempts to correlate the experimental data, using eq (3-20), were abortive, as will be explained in section 5.4 of this report.

In eq (3-12) and eq (3-27), the cavity lengths were evaluated at the visually observed lengths. BFLASH was obtained, for each experimental data point, using the average measured cavity pressure depression $(P_v - \overline{P}_l)$, T_o, and the calculation method outlined in reference [23]. The average minimum cavity pressure, $\overline{P}_l = (P_l + P_{l,T})/2$, was used because the temperature measurements are considered just as accurate as the pressure measurements.

In eq (3-12) and eq (3-27), the fluid physical properties are evaluated at P_o and T_o, with the exception that MTWO is evaluated at the minimum measured cavity pressure, P_l. The standard deviation in B is computed for each set of exponents; the individual exponents may be held constant or chosen by the computer. The standard deviation in B factor is minimized in the computer programs when one or more of the exponents is selected by the computer; the absolute minimum standard deviation is obtained when all of the exponents are selected by the computer--as in this report. The standard deviation is simply computed in those cases where the exponents are held constant. The set of exponents that produces minimum standard deviation in B is selected as the best correlative solution for any particular batch of data; i.e., the standard deviation is a measure of the validity

of the similarity and isentropic-flashing theories, as both are evaluated from experimental data. Because MTWO proved to be a valuable correlating parameter for the hydrofoil data, and it had not been used to correlate the venturi data [20], both the hydrofoil and venturi data were separately correlated using the approach described herein. The results of this effort are given in table 5. 3 and are discussed in the following section of this report.

5. 4 Discussion of Developed Cavitation Data

Photographs of fully developed vaporous cavities, in liquid hydrogen, are shown on figure 4. 3. Inlet velocity and liquid temperature were observed to have very little effect on the appearance of cavitating hydrogen; i. e. , the cavities were generally well defined and uniformly developed. Only at the highest temperature, and lowest velocities, did the hydrogen cavities exhibit a slightly porous, non-uniform character. Similar, though more pronounced, features were observed in the nitrogen cavities. If a cavity is sufficiently porous, i. e. , if it visually resembles vapor streams, erratic developed cavity data may result. This occurs, because the pressure and temperature sensing ports are not continuously covered with vapor during a test, but may be intermittently covered with vapor and then liquid. This effect is believed to be negligible for all of the hydrofoil data acquired and reported herein.

In figures 5. 5 to 5. 13, the data points representing cavity pressure measurements have been connected with a smooth curve to facilitate comparison with the data points obtained from the cavity temperature measurements. The pressure depressions obtained from the cavity temperature measurements are, for the most part, in good agreement with those derived from the measured pressures, i. e. , within the

Table 5.3: Correlative results for liquid hydrogen and liquid nitrogen developed cavity data.

Model	Fluids	Correlative Equation	Source of Data	Exponents E1 α term	E2 V_o term	E3 x term	E4 ν term	Reference Run No.	Standard † Deviation in B-Factor	$\overline{K}_{c,min}$
Hydrofoil	H_2	(3-12)*	This Study	-0.22	0.35	0.52	---	255B	0.3693	1.899
Hydrofoil	N_2	(3-12)	This Study	-3.14	0.88	0.37	---	299C	0.2989	1.766
Hydrofoil	H_2&N_2	(3-12)	This Study	0.80	0.64	0.45	-1.00	255B	0.3717	1.833
Venturi	H_2	(3-12)	Reference [20]	-1.92	0.74	0.31	---	071C	0.3466	2.459
Venturi	H_2&F-114	(3-12)	Reference [3]	1.0	0.8	0.3	---	---	---	2.47
				E1 α term	E2 MTWO term	E3 x term				
Hydrofoil	H_2	(3-27)**	This Study	0.48	0.42	0.35		255B	0.2794	1.899
Hydrofoil	N_2	(3-27)	This Study	1.47	0.63	0.25		299C	0.1999	1.766
Hydrofoil	H_2&N_2	(3-27)	This Study	-0.13	0.59	0.27		255B	0.2565	1.833
Venturi	H_2	(3-27)	Reference [20]	0.10	0.59	0.18		071C	0.2234	2.459

* $$B = B_{ref}\left(\frac{\alpha_{ref}}{\alpha}\right)^{E1}\left(\frac{V_o}{V_{o,ref}}\right)^{E2}\left(\frac{x}{x_{ref}}\right)^{E3}\left(\frac{\nu_{ref}}{\nu}\right)^{E4}\left(\frac{\sigma_{ref}}{\sigma}\right)^{E5}\left(\frac{D}{D_{ref}}\right)^{E6}.$$

** $$B = B_{ref}\left(\frac{\alpha_{ref}}{\alpha}\right)^{E1}\left(\frac{MTWO}{MTWO_{ref}}\right)^{E2}\left(\frac{x}{x_{ref}}\right)^{E3}\left(\frac{\nu}{\nu_{ref}}\right)^{E4}\left(\frac{\sigma_{ref}}{\sigma}\right)^{E5}\left(\frac{D_{ref}}{D}\right)^{E6}.$$

† Standard Deviation $\sqrt{\left[\sum(B-B_t)^2\right]/(NPTS-1)}$, where NPTS = number of data points (including "ref" data point), B_t = BFLASH and is computed from isentropic-flashing theory [23], and B is computed from eq (3-12) or eq (3-27).

allowances of instrument error, the cavity vapor is in stable thermodynamic equilibrium. Evidence of metastable vapor was presented in the venturi study [20]. In figures 5.5 to 5.13, the only significant differences, in the measured pressure and temperature profiles, occur near the trailing edges of the cavities. Similar characteristics were observed in the venturi studies. The trailing edges of a cavity are normally irregular and are characterized by randomly-spaced clouds of condensing vapor. Hence, it is inadvisable to attempt to interpret the cavity data in this ill-defined region; however, the following discussion will shed some light on this topic.

The data on figures 5.5 to 5.13 indicate that some of the cavities were shorter than their visual (as observed on film) length. Because the pressure depression should be near zero at the trailing edge of the cavity, the actual length of the cavity may be estimated by extrapolating the data to zero pressure depression. The actual length of the cavity, and the observed length, differ because of the irregular trailing edges of the cavity and the difficulty in judging the visual length. Both actual and visual cavity lengths were used to correlate the data, and they produced essentially the same results. The visual cavity lengths, as tabulated in appendix A, were used in the final correlative data fits reported in table 5.3.

Now, referring to figure 5.8, we will attempt to explain the apparent discrepancy, in pressure and temperature measurements, near the aft end of the cavity. Note that both the actual and visual cavity lengths indicate that the T_4 and T_5 sensor stations are downstream of the cavity; however, T_4 and T_5 may well be in a region where small clouds of vapor are continuously or intermittently condensing. If these temperature sensors were exposed to liquid only, downstream

of the cavity, we would anticipate that they would indicate near-zero pressure depression, i.e., the liquid temperature should be very near T_o, so that $P_v - P_{n,T}$ is very small. Then figure 5.8, and T_4 and T_5, indicate exactly what we would expect--a gradual transition from aft-end cavity vapor temperature, T_3, to bulkstream liquid temperature, T_o (represented by zero pressure depression on figure 5.8). The presence of vapor, in any quantity, would tend to cool these downstream temperature sensors to a temperature intermediate to T_3 and T_o. Similar comments apply to the other pressure depression plots. Referring to figures 5.5 to 5.13, we note that the agreement, between the pressure and temperature measurements, is exceptionally good in those cases where the cavity covered all sensors, e.g., see figures 5.5, 5.7, 5.10, and 5.11. Plots similar to figures 5.5 to 5.13, of all the data, reveal that stable thermodynamic equilibrium exists within the cavity vapor--within data accuracy.

'Similarity' equations, used to correlate cavitation performance of a particular flow device from fluid-to-fluid, were fitted with numerical exponents derived from the experimental data (hydrofoil and venturi) of this study. These equations were derived herein and represent extensions of the work of Gelder, et al. [19]. The numerical exponents for hydrogen-refrigerant 114 test fluids in a venturi were obtained from the literature [3]; these exponents are compared, in table 5.3, with those obtained in our venturi studies [20], and with those deduced from our hydrofoil experiments. The exponents given in table 5.3 were obtained with a least-squares fitting technique and a digital computer; the suitability of the various exponents to the experimental data is indicated by the standard deviation in B-factor as explained previously. In the hydrogen venturi study, the value of B ranges from two to five;

in the hydrofoil experiments, the value of B ranges from one to five, for both hydrogen and nitrogen test fluids.

The expressions used to correlate the experimental data are given at the bottom of table 5. 3. As indicated in table 5. 3, there is little difference in the exponents obtained for the venturi data, using different test fluids, i. e. , the exponents in lines 4 and 5 are in good agreement, excluding the diffusivity term. The lack of variation in α (< 10 percent) explains why E1 tends to a negative number (line 4) when correlating with liquid hydrogen alone. Gelder, et al. [19], obtained a value of 0. 5 for E1 when correlating refrigerant 114 data with 25 percent variation in α. There was over 400 percent change in α in the hydrogen-refrigerant 114 data correlated by Moore and Ruggeri [3], and thus the value for E1 reported in line 5 of table 5. 3 is to be preferred when correlating with eq (3-12). The mathematical technique, used to derive the exponents, can easily pick an extraneous value for any of the exponents if there does not exist significant variation in the corresponding physical parameter.

Use of the viscosity and surface tension terms in eq (3-12) did not significantly improve the venturi hydrogen data correlation, and consequently exponents for these terms are not included in table 5. 3; however, we shall demonstrate that viscosity is an important correlating parameter when attempting to correlate data from fluid-to-fluid. It is anticipated that both of these parameters may improve data correlation where sufficient variation in the fluid properties occurs. In the venturi hydrogen data, the viscosity varied less than 20 percent and the surface tension varied less than 40 percent.

Exponents on the hydrofoil data, using eq (3-12), are given in the first three lines of table 5. 3. Again, the viscosity and surface tension terms had little influence on the data correlation for single

fluids (lines 1 and 2) and were not used; however, the viscosity term significantly improved the combined fluid correlation (line 3), and the corresponding exponent, E4, was determined. For the combined fluids (line 3), inclusion of the viscosity term reduced the standard deviation by 15 percent--a substantial reduction. In all of our venturi and hydrofoil data, use of the ν and σ terms improved the correlation; however, it is felt that use of these additional correlating parameters is not justified, unless they substantially improve the correlative fit. Therefore, it is apparent that only the combined fluid hydrofoil data (line 3) benefited from the use of ν. Correlation of the hydrogen-refrigerant 114 data (line 5) would most likely be improved by using one or both of these terms. In the nitrogen data (line 2), α varied by only 12 percent, ν varied by 35 percent, and σ varied by 30 percent. In the hydrogen data (line 1) α varied by 12 percent, ν varied by 16 percent, and σ varied by 20 percent. Thus, it is not surprising that the ν and σ terms were of little benefit in the single fluid correlations, nor that the exponent on the α term seeks a negative value. In the combined fluid data (line 3) α varied by almost 100 percent, ν varied by 35 percent, and σ varied by 300 percent. Then the α exponent, E1, should be quite meaningful, the ν exponent, E4, (though beneficial) is suspect, and the σ exponent, E5, should be beneficial. Because the σ term was of negligible value in the correlative fit, even though it varied by a factor of three, we must conclude that σ is not an important correlating parameter for the cryogens tested; however, it may yet prove to be a valuable correlating parameter for other fluid combinations--with smaller or larger variations in σ. Although the ν term improved the combined fluid correlation, the numerical value of E4 is suspect because of the relatively small variation in ν for these data. Again, ν may be an excellent correlating parameter for other fluid combinations and is of considerable value for the hydrogen-nitrogen combination.

It is interesting to note that the combined fluid correlations (lines 3 and 5) produced exponents, E1, E2, and E3, of nearly the same value. Certainly, it is not expected that the exponents, for different bodies, should be the same. Recent tests [24], on zero-caliber ogives, indicate that these exponents may vary widely from one hydrodynamic body to another.

Comparison of the best experimental exponents (lines 3 and 5 of table 5.3), with the exponents predicted from heat transfer considerations (table 3.1), is not too gratifying. It appears that the predicted values of E2 and E3 bracketed the experimental data, but the predicted values of E1 and E4 did not. These tests do not reveal that a particular flow mode, and technique for evaluating the thermal boundary layer thickness, are to be preferred; however, lines 2 and 4 of table 3.1 are in the best general agreement with the experimental data (lines 3 and 5 of table 5.3). Actually, this agreement between experiment and heat transfer theory is not too bad, when we consider the numerous assumptions involved in the analysis--particularly the neglect of mass transfer across the liquid-vapor interface. The following discussion indicates that mass transfer must be considered.

The venturi and hydrofoil data were also correlated using eq (3-27); this was accomplished by substituting MTWO for V_o in the computer program. These results are shown on lines 6 through 9 in table 5.3. It is apparent from the foregoing discussion, and the results shown in table 5.3, that the ν and σ terms did not materially improve the correlation. That eq (3-27) is quite superior to eq (3-12), as a correlative expression, is readily shown by direct comparison of the results given on lines 1 and 6, lines 2 and 7, lines 3 and 8, and lines 4 and 9. A marked reduction ($\sim 1/3$) in standard deviation of B-factor is achieved, in each case, by substituting MTWO for V_o. A line-by-line

comparison of these same data will also show that the importance of the α, and x terms is generally lessened when eq (3-27) is used, i.e., the numerical values of E1 and E3 are reduced. The numerical value of E1 is sometimes so small (lines 8 and 9) that the α term could, in these cases, be neglected. The α term is undoubtedly diluted somewhat, because of the many thermophysical and thermodynamic fluid properties embodied in the MTWO parameter. It is believed that the slight correlative improvement offered by the ν and σ terms, when using eq (3-27), can be attributed to the very strong influence of the MTWO parameter. While the ν term was of considerable benefit (line 3), when using eq (3-12), it has little effect when the standard deviation is reduced to a much lower value (line 8), by use of the MTWO parameter. The predominant influence of the MTWO term may also be responsible for the slight reductions in E3, when using eq (3-27). The importance of MTWO, as a correlating parameter, emphasizes that mass transfer plays an important role in the cavitation process.

An attempt was made to correlate the experimental data using both V_o and V_ℓ (or $V_{2\varphi}$) as separate correlating parameters, i.e., an expression of the form given in eq (3-20) was used. This attempt failed because $V_\ell \propto (1/\text{BFLASH})^{0.5}$, see eq (3-30). Now BFLASH will appear on the right-hand side of eq (3-20) because V_ℓ is a function of BFLASH; also, the exponents on all of the terms are computed by minimizing the differences in calculated B (left side of eq (3-20)) and BFLASH at each data point. Then the computer merely selects an exponent, for the V_ℓ term, that causes B (left side) to nearly match BFLASH (right side) at each data point--the minimum standard deviation in B is automatically and simultaneously assured. Thus, the exponents on all of the terms, other than V_ℓ, are made negligibly small, and the results

are trivial, i.e., the exponents on eq (3-20) are chosen so that eq (3-20) is reduced to $B \approx BFLASH$. Combining the V_o and V_ℓ terms, to form the MTWO parameter, avoids this difficulty. Recall that $MTWO \propto V_o (BFLASH)^{0.5}$, see eq (3-29). Because V_o is a strong correlating parameter, the computer cannot simply match B and BFLASH on either side of eq (3-20); to do so would result in large standard deviations of B, because the V_o component of MTWO would not be properly exponentiated. To achieve a minimum standard deviation, as demanded in the computer program, the exponent selected for MTWO must be compatible with the V_o and V_ℓ components of MTWO.

To substantiate this argument, we refer again to table 5.3--note that E2 does not vary much when MTWO is substituted for V_o (lines 1 and 6, 2 and 7, etc.). This result indicates that V_o is the dominant component in the MTWO parameter. Also, the mean value of E2, on the MTWO term, is ~ 0.55 (lines 6 to 9)--then the functional dependency of B, upon BFLASH, is estimated by combining eq (3-29) and eq (3-27) to obtain $B \propto (BFLASH)^{0.28}$. This functional dependency is well removed from the trival relationship, $B \approx (BFLASH)^{1.0}$.

It is remarkable that the variation in the exponent on MTWO is so small (lines 6 to 9). Also, the agreement of all of the exponents for the hydrofoil and venturi data (specifically lines 8 and 9) is quite good. It appears that the α term could be eliminated in lines 8 and 9.

The diameter (size) terms in eq (3-12) and eq (3-27) were not included in table 5.3, because our tests were conducted with only one hydrofoil and only one venturi size. Moore and Ruggeri [3] obtained an exponent value of -0.1 for the diameter term--E6 = -0.1 in eq (3-12)--based on tests using refrigerant 114 in two different venturi sizes. Those tests were performed with a venturi identical to the one used in our study [20], and with a larger (1.414:1) geometrically similar venturi.

The arithmetic mean value of the developed cavitation parameter, $\overline{K}_{c,min}$, does not vary appreciably for the venturi data presented in table 5.3. This parameter is also relatively constant for the hydrofoil data; this is an important result, because constant $\overline{K}_{c,min}$, eq (3-12), and the isentropic flashing theory [23] are used to predict [4, 5] the cavitating performance of a particular piece of equipment. The fact that $\overline{K}_{c,min}$ is different, for different models, limits the current predictive techniques [4, 5] to a particular piece of equipment, i.e., the geometry (shape) of the cavitating equipment must be identical or similar. Actually, it was anticipated [20] that $\overline{K}_{c,min}$, for many cavitating bodies, would not remain constant--as with the venturi--for all fluids, cavity lengths, velocities, temperatures, etc. Then, it was no surprise that $\overline{K}_{c,min}$ for the hydrofoil varied slightly, see table 5.3.

Also, $K_{c,min}$ varied more for the hydrofoil than for the venturi; $K_{c,min}$ was within 7 percent of $\overline{K}_{c,min}$ for the venturi, but a similar comparison for the hydrofoil shows 15 percent deviation. An attempt was made to mathematically determine the functional dependency of $K_{c,min}$, upon x, V_o, and T_o; however, the variation in $K_{c,min}$ was sufficiently small, and data scatter was sufficiently large--recall that instrument error is amplified in this type of parameter--to discourage this effort. It was determined that the hydrofoil $K_{c,min}$ is independent of cavity length, and increases very slightly with increasing temperature and velocity, for both hydrogen and nitrogen; the temperature effect is stronger than the velocity effect. Because $K_{c,min}$ varies somewhat with flow conditions, for each body, it is convenient to use $\overline{K}_{c,min}$ for predictive purposes. $\overline{K}_{c,min}$, of course, varies widely with body or equipment geometry, as does the pressure coefficient, C_p. Thus, it is quite obvious that prediction of cavitation performance, from one piece of equipment to another, will require significant advances in the 'state-of-the art.'

The conventional cavitation parameter for developed cavitation, K_v, also varies with flow conditions for any particular geometry, e.g., see table A-1a and Rouse and McNown [28].

The results obtained herein indicate that eq (3-27), rather than eq (3-12), should be used for predictive calculations [4, 5].

The pressure depression in the cavitated region is determined by subtracting the measured cavity pressure, in one case, and the saturation pressure associated with the measured cavity temperature, in the other case, from the vapor pressure of the liquid entering the test section. In the hydrogen data reported here, the measured cavity pressure, P_l, was less than bulkstream vapor pressure by as much as 15.76 psi (10.87 N/cm^2); these pressure-depressions are obtained by subtracting P_l from P_v in the tabulated data of appendix A. For the nitrogen data, P_v exceeded P_l by as much as 10.08 psi (6.96 N/cm^2).

Cavity pressure depression increases with increasing cavity length, fluid temperature, and velocity for these tests. The data in appendix A readily disclose these trends if we permit only one of the three parameters (x, V_o, and T_o) to vary at a time and note the value of $P_v - P_l$ for two different values of the parameter being varied. As an example, T_o and V_o are relatively constant in Runs 244 D and 244E, but the cavity length differs by a factor of three; $P_v - P_l$ for the longer cavity (Run 244 E) is about 1.2 times the $P_v - P_l$ for the shorter cavity (Run 244 D). Similar comparisons may be made for variations in V_o and T_o, or portions of the data may be plotted collectively on single graphs, etc., to demonstrate these trends. These functional dependencies are also shown by simply observing the characteristics of the experimentally derived exponents in table 5.3. In reference [23], it is shown that the pressure depression increases with increasing T_o and B. Referring to line 3 of table 5.3, we observe that B increases with

increasing V_o, x, and ν. Then, for the combined fluid hydrofoil data, $P_v - P_l$ must increase with increasing T_o, V_o, x, and ν. From lines 8 and 9, we observe that $P_v - P_l$ also increases with increasing values of MTWO. Similar deductions may be drawn for any body-fluid combination.

5.5 Developed Cavity Shapes

One of the main objectives of the hydrofoil experiment was to obtain cavity volume-thickness data, in an effort to improve the correlative theory. The hydrofoil-tunnel configuration was designed to provide optimum photographs of the developed cavities. Enlarged photographs of the cavities, for each experimental data point recorded in appendix A, were carefully studied to determine cavity shape, thickness, and volume. All of the cavities were elliptically shaped, and the photographed cavities were easily fit with a transparent-plastic elliptical-template. By recording appropriate data from the template, e.g., major and minor axes dimensions, maximum cavity thickness, and angle of projection, it was possible to compute cavity volumes, shapes, etc. We found that cavity thickness and volume increased with increasing cavity length, and were nearly independent of V_o and T_o. Because we are primarily interested in the shape of cavities near their leading edge, we restricted our attention to cavity volumes in the front-half of the cavity; in this way, the ill-defined trailing regions of the cavity are avoided. The shapes, of all of the cavities, were adequately represented by a simple algebraic expression of parabolic form. For hydrogen, we obtained $\delta_v = 0.77x^{0.37}$ and for nitrogen $\delta_v = 0.44x^{0.63}$, where both δ_v and x are in millimeters, and x cannot exceed the cavity half-length.

Interestingly enough, the cavities formed on a wide variety of ogival-shaped bodies [28] can also be fit with similar algebraic expressions of the form $\delta_v = C_o x^p$. These cavity data, and our hydrofoil data

and shape analyses, provided the basis for assuming the existence of parabolic shaped cavities in the general analysis of section 3. These data also permitted the selection of a mean value for p ($\approx$ 0.65) in section 3.1 of this report.

Because of its application in the pumping machinery field, pressure-head has been included in the data tabulated in appendix A. Mathematical conversion of pressure to pressure-head merely requires evaluation of the liquid density at the point of measurement; however, selection of the appropriate liquid density can be a bit perplexing. Figures 5.5 to 5.13 indicate that the measured pressures and temperatures, within the cavities, are not in perfect agreement. Also, due to the thermal expansivity of liquid hydrogen, the bulkstream temperature does not remain perfectly constant as the liquid flows over the hydrofoil. The following methods were used to calculate pressure-head from the cavity measurements: (1) Head (h_n) was calculated from measured cavity pressure by using the saturation density at the measured pressure. (2) Head ($h_{n,T}$) was calculated from measured cavity temperature by using the saturation density at the measured temperature. Both values of head are given in the tabulated data in appendix A.

6. CONCLUDING REMARKS

Desinent cavity data, for a 0.5-caliber hydrofoil, were acquired for vaporous hydrogen and nitrogen cavities; the results are given in appendix A and on figures 5.1 to 5.4. Correlation of the desinent data is treated in appendix C. The desinent data tend toward a single-valued K_{iv}, at the maximum velocities, irrespective of temperature. The hydrogen data are more temperature-dependent than the nitrogen data. Also, these cryogenic liquids require less subcooling--relative to higher boiling-point liquids--for desinent cavitation to occur.

Pressure and temperature profiles were measured within fully developed, vaporous hydrogen and nitrogen cavities; these results, for the hydrofoil, are given in appendix A and on figures 5.5 to 5.13. Within data accuracy, these pressure and temperature depressions were in stable thermodynamic equilibrium. These data were correlated using a previously described [20] technique, and the extended theory developed herein. Using the conventional correlating technique [20], it was found that α, V_o, x, and ν were valuable correlating parameters for combined fluids. Using the new MTWO parameter, only α, MTWO, and x were of value--it seems quite likely that α may be negligible for combined fluid correlations. Thus, only MTWO and x may be required for future correlations. If the MTWO correlation is not used, the results may be degraded by $\sim$ 50 percent (as based on standard deviation in B). Because MTWO is such an influential parameter, its use is highly recommended in future work, for both correlative and predictive purposes.

Correlative expressions, predicted from convective heat transfer theory, and evaluated from experimental data, are in reasonable agreement; however, more analysis is required to explain the intricacies of the mass transfer phenomena--an important physical effect, as evidenced by the influence of the MTWO parameter.

$K_{c,min}$ was found to vary by about 15 percent, about a mean value, $\overline{K}_{c,min}$, for the hydrofoil. This was about double the deviation experienced with the venturi tests [20]. Variations, in $K_{c,min}$, of 1.65:1 were found in tests on zero-caliber ogives [24] in water. It is quite apparent that $K_{c,min}$ will vary with equipment geometry, fluid, velocities, temperatures, etc. Then, the current predictive technique [4, 5], that relies on constant $K_{c,min}$ (or $\overline{K}_{c,min}$), must be used with appropriate caution.

The cavity-shape data, acquired during this study, indicates that the cavities can be described by a simple expression of the form $\delta_v = C_o x^p$; this expression is valid only in the frontal regions of the cavity.

7. NOMENCLATURE

a_ℓ = acoustic velocity of liquid, evaluated at the minimum cavity pressure, P_1

a_v = acoustic velocity of vapor, evaluated at the minimum cavity pressure, P_1

B = ratio of vapor to liquid volume associated with the sustenance of a fixed cavity in a liquid

BFLASH = B derived from isentropic flashing theory (Ref. [23])

$B_t \equiv$ BFLASH

C_n = (n = 0, 1, 2, 3 . . . etc.): constants or numerical coefficients in various algebraic expressions

C_p = pressure coefficient $[\equiv (h_x - h_o)/(V_o^2/2g_c)]$

C_p^v = minimum pressure coefficient $[\equiv (h^v - h_o)/(V_o^2/2g_c)]$

$C_{p,\ell}$ = specific heat of liquid at constant pressure, evaluated at the tunnel inlet (P_o and T_o)

$C_{p,v}$ = specific heat of vapor at constant pressure, evaluated at the minimum cavity pressure, P_1

$C_{v,\ell}$ = specific heat of liquid at constant volume, evaluated at P_1

$C_{v,v}$ = specific heat of vapor at constant volume, evaluated at P_1

D = characteristic dimension of cavitating body, e. g. diameter of an axisymmetric body, or thickness (t) of a hydrofoil

g_c = conversion factor in Newton's law of motion (gravitational acceleration)

G_c = choking two-phase liquid-vapor mass-flow flux, see eq (3-21)

h_n = (n = 1, 2, 3, 4, or 5): head corresponding to cavity pressure, measured at a particular instrument port on the hydrofoil

$h_{n,T}$ = (n = 1, 2, 3, 4, or 5): head corresponding to the saturation pressure at the cavity temperature, measured at a particular instrument port on the hydrofoil

h_o = tunnel inlet head corresponding to absolute inlet pressure

h_v = head corresponding to saturation or vapor pressure at the tunnel inlet temperature

h_x = convective heat transfer coefficient at axial distance x

h_x = head corresponding to absolute pressure, measured on the hydrofoil at distance x, downstream of the minimum pressure point--for non-cavitating flow

h_v = head corresponding to the minimum absolute pressure on the leading edge of the hydrofoil, computed from expression for C_p^v

k = thermal conductivity of liquid, evaluated at tunnel inlet

$K_{c,min}$ = developed cavitation parameter, based on minimum measured cavity pressure [$\equiv (P_o - P_l)/(\rho_o V_o^2/2 g_c)$]

$\overline{K}_{c,min}$ = arithmetic mean value of $K_{c,min}$ for a complete set of data points for a particular hydrodynamic body-fluid combination

K_{iv} = cavitation parameter, K_v, evaluated at incipient (desinent) conditions [$\equiv (P_o - P_v)/(\rho_o V_o^2/2 g_c)$]

K_v = developed cavitation parameter [$\equiv (P_o - P_v)/(\rho_o V_o^2/2 g_c)$]

$M_{2\varphi}$ = two-phase Mach number [$\equiv V_o/V_{2\varphi}$]

MTWO = liquid phase velocity ratio [$\equiv V_o/V_\ell$]

Nu_x = length Nusselt number [$\equiv h_x x/k$]

Pe = Peclet number [$\equiv V_o x/\alpha$]

P_n = (n = 1, 2, 3, 4, or 5): absolute cavity pressure, measured at a particular station or instrument port on the hydrofoil

$P_{n,T}$ = (n = 1, 2, 3, 4, or 5): saturation pressure corresponding to the measured cavity temperature at a particular station or instrument port on the hydrofoil

P_o = tunnel absolute inlet pressure

Pr	=	Prandtl number [$\equiv C_{p,\ell}\mu/k$]
P_v	=	saturation or vapor pressure at tunnel inlet temperature
R	=	radius of axisymmetric body, see figure 3.1b
Re_x	=	Reynolds number [$\equiv \rho V_o x/\mu$]
t	=	maximum thickness of hydrofoil
T_n	=	(n = 1, 2, 3, 4, or 5): measured cavity temperature at a particular station or instrument port on the hydrofoil
T_o	=	bulkstream temperature in degrees Rankine (Kelvin), of liquid entering the tunnel
V_ℓ	=	characteristic liquid velocity component, normal to cavity wall
V_o	=	velocity of test liquid at inlet to tunnel
$V_{2\varphi}$	=	velocity of two-phase liquid-vapor mixture across cavity wall
$\mathcal{V}_\ell$	=	volume of liquid associated with the sustenance of a developed cavity
$\mathcal{V}_v$	=	volume of vapor associated with the sustenance of a developed cavity
We_x	=	Weber number [$\equiv \rho V_o^2 x/\sigma$]
x	=	axial distance measured from minimum pressure point on hydrofoil, used to measure cavity length, and as an axial coordinate in analyses

X = fluid quality, mass fraction of vapor per unit mass of fluid

Z = evaluated by eq (3-23)

Greek

α = thermal diffusivity of liquid, evaluated at tunnel inlet

δ_ℓ = characteristic thickness of the thermal boundary layer in the liquid

δ_v = thickness of the developed vaporous cavity

μ = absolute viscosity of liquid, evaluated at tunnel inlet

ν = kinematic viscosity of liquid, evaluated at tunnel inlet [$\equiv \mu/\rho$]

ρ = density of liquid, evaluated at tunnel inlet [$\equiv \rho_o$]

ρ_ℓ = density of liquid, evaluated at minimum cavity pressure, P_1

ρ_v = density of vapor, evaluated at minimum cavity pressure, P_1

$\rho_{2\varphi}$ = density of two-phase liquid-vapor mixture at the liquid-vapor interface, evaluated at P_1

σ = surface tension of liquid in contact with its vapor, evaluated at tunnel inlet

Subscripts

ℓ = denotes liquid phase

o = denotes tunnel inlet location

ref = reference run (data point), or test conditions, to which a computation is being referenced when attempting to correlate cavitation performace via eq (3-12) or eq (3-27)

v = denotes vapor phase

2φ = denotes two-phase liquid-vapor

Superscripts

E1 = exponent on thermal diffusivity ratio in eq (3-12) and eq (3-27)

E2 = exponent on tunnel inlet velocity ratio in eq (3-12) and also used as an exponent on the MTWO ratio in eq (3-27)

E3 = exponent on cavity length ratio in eq (3-12) and eq (3-27)

E4 = exponent on kinematic viscosity ratio in eq (3-12) and eq (3-27)

E5 = exponent on surface tension ratio in eq (3-12) and eq (3-27)

E6 = exponent on (characteristic dimension) cavitating body diameter (or thickness) ratio in eq (3-12) and eq (3-27)

E7 = exponent on $V_{2\varphi}$ ratio in eq (3-20)

m1 = exponent on Reynolds number in Nusselt relationship, see eq (3-1)

m2 = exponent on Reynolds number in thermal boundary layer expressions, see eq (3-2)

n1 = exponent on Prandtl number in Nusselt relationship, see eq (3-1)

n2 = exponent on Prandtl number in thermal boundary layer expressions, see eq (3-2)

p = exponent in algebraic expression for cavity shape ($\delta_v = C_2 x^p$)

8. REFERENCES

1. Pinkel, I., Hartmann, M. J., Hauser, C. H., Miller, M. J., Ruggeri, R. S., and Soltis, R. F., Pump technology, Chap. VI, pp. 81-101, taken from Conference on Selected Technology for the Petroleum Industry, NASA SP-5053 (1966).
2. Erosion by Cavitation or Impingement, STP-408, 288 pages (1967), available from ASTM, 1916 Race Street, Philadelphia, Pa., 19103.
3. Moore, R. D., and Ruggeri, R. S., Prediction of thermodynamic effects of developed cavitation based on liquid hydrogen and freon-114 data in scaled venturis, NASA Tech. Note D-4899 (Nov. 1968).
4. Ruggeri, R. S., and Moore, R. D., Method for prediction of pump cavitation performance for various liquids, liquid temperatures, and rotative speeds, NASA Tech. Note D-5292 (June 1969).
5. Moore, R. D., Prediction of pump cavitation performance, Proc. Int. Symp. on the Fluid Mechanics and Design of Turbomachinery, Pennsylvania State Univ., University Park, Pa., Aug. 30 - Sept. 3, 1970.
6. Moore, R. D., and Meng, P. R., Comparison of noncavitation and cavitation performance for 78°, 80.6°, and 84° helical inducers operated in hydrogen, NASA Tech. Note D-6361 (May 1971).
7. Spraker, W. A., Two-phase compressibility effects on pump cavitation, Symposion on Cavitation in Fluid Machinery, presented at winter meeting, Chicago, Ill., Nov. 7-11, 1965, pp. 162-171 (ASME, New York, N. Y.).

8. Jakobsen, J. K., On the mechanism of head breakdown in cavitating inducers, Trans. ASME, Ser. D, 86, No. 2, 291-305 (June 1964).

9. Chivers, T. C., Cavitation in centrifugal pumps, first and second papers, Proc. Inst. Mech. Engrs. 184, Part 1, No. 2, 37-68 (1969-70).

10. Fisher, R. C., Discussion of "A survey of modern centrifugal pump practice for oilfield and oil refining services" by N. Tetlow, Proc. Inst. Mech. Engrs. 152, 305-306 (Jan. - Dec. 1945).

11. Stahl, H. A., and Stepanoff, A. J., Thermodynamic aspects of cavitation in centrifugal pumps, Trans. ASME 78, No. 8, 1691-1693 (Nov. 1956).

12. Jacobs, R. B., Prediction of symptoms of cavitation, J. Res. Nat. Bur. Stand. (U. S.), 65C (Eng. and Instr.), No. 3, 147-156 (July - Sept. 1961).

13. Hollander, A., Thermodynamic aspects of cavitation in centrifugal pumps, ARS J. 32, 1594-1595 (Oct. 1962).

14. Stepanoff, A. J., Centrifugal and Axial Flow Pumps, pp. 256-265 (John Wiley and Sons, Inc., New York, N. Y., 1957).

15. Stepanoff, A. J., Cavitation properties of liquids, ASME J. of Engr. for Power 86, No. 2, 195-200 (Apr. 1964).

16. Saleman, Victor, Cavitation and NPSH requirements of various liquids, ASME J. of Basic Engr. 81, No. 2, 167-180 (June 1959).

17. Wilcox, W. W., Meng, P. R., and Davis, R. L., Performance of an inducer-impeller combination at or near boiling conditions for liquid hydrogen, Book, Advances in Cryogenic Engineering 8, Ed. K. D. Timmerhaus, pp. 446-455 (Plenum Press, Inc., New York, N. Y. 1963).

18. Spraker, W. A., The effects of fluid properties on cavitation in centrifugal pumps, ASME J. of Engr. for Power 87, No. 3, 309-318 (July 1965).

19. Gelder, T. F., Ruggeri, R. S., and Moore, R. D., Cavitation similarity considerations based on measured pressure and temperature depressions in cavitated regions of freon-114, NASA Tech. Note D-3509 (July 1966).

20. Hord, J., Anderson, L. M., and Hall, W. J., Cavitation in liquid cryogens, Volume I: Venturi, NASA Rept. CR-2054 (May 1972).

21. Hord, J., Edmonds, D. K., and Millhiser, D. R., Thermodynamic depressions within cavities and cavitation inception in liquid hydrogen and liquid nitrogen, NASA Rept. CR-72286 (March 1968). Available from NASA, Office of Scientific and Technical Information, AFSS-A, Washington, D. C.

22. Ruggeri, R. S., Experimental studies on thermodynamic effects of developed cavitation, Proc. Int. Symp. on the Fluid Mechanics and Design of Turbomachinery, Pennsylvania State Univ., University Park, Pa., Aug. 30-Sept. 3, 1970.

23. Hord, J., and Voth, R. O., Tabulated values of cavitation B-factor for helium, H_2, N_2, F_2, O_2, refrigerant 114, and H_2O, Nat. Bur. Stand. (U. S.), Tech. Note 397 (Feb. 1971).

24. Billet, M. L., Thermodynamic effects on developed cavitation in water and freon-113 (M. S. Thesis, Pennsylvania State Univ., Dept. of Aerospace Engr., University Park, Pa., Mar. 1970).

25. Eisenberg, P., and Pond, H. L., Water tunnel investigations of steady state cavities, Report No. 668, David W. Taylor Model Basin (Oct. 1948).

26. Edmonds, D. K., and Hord, J., Incipient and developed cavitation in liquid cryogens, Nat. Bur. Stand. (U. S.), Tech. Note 374 (Feb. 1969).

27. Kays, W. M., Convective Heat and Mass Transfer (McGraw-Hill, Book Co., New York, N. Y., 1966).

28. Rouse, H., and McNown, J. S., Cavitation and pressure distribution on head forms at zero angle of yaw, State Univ. of Iowa, Bulletin 32 (Aug. 1948).

29. Brentari, E. G., Giarratano, P. J., and Smith, R. V., Boiling heat transfer for oxygen, nitrogen, hydrogen, and helium, Nat. Bur. Stand. (U. S.), Tech. Note 317, p. 36 (Sept. 1965).

30. Holl, J. W., and Wislicenus, G. F., Scale effects on cavitation, ASME J. of Basic Engr., 385-398 (Sept. 1961).

31. Moore, R. D., and Ruggeri, R. S., Venturi scaling studies on thermodynamic effects of developed cavitation of freon-114, NASA Tech. Note D-4387 (Feb. 1968).

32. Cooper, P., Analysis of single and two-phase flows in turbopump inducers, ASME J. of Engr. for Power, 577-588 (Oct. 1967).

33. Smith, R. V., Choking two-phase flow literature summary and idealized design solutions for hydrogen, nitrogen, oxygen, and refrigerants 12 and 11, Nat. Bur. Stand. (U. S.), Tech. Note 179 (Aug. 1963).

34. Brennan, J. A., Edmonds, D. K., and Smith, R. V., Two-phase (liquid-vapor), mass-limiting flow with hydrogen and nitrogen, Nat. Bur. Stand. (U. S.), Tech. Note 359 (Jan. 1968).

35. Katsanis, T., and McNally, W. D., Fortran program for calculating velocities and streamlines on a blade-to-blade stream surface of a tandem blade turbomachine, NASA Tech. Note D-5044 (Mar. 1969).

36. Katsanis, T., and McNally, W. D., Fortran program for calculating velocities in a magnified region on a blade-to-blade stream surface of a tandem blade turbomachine, NASA Tech. Note D-5091 (April 1969).

37. Parkin, B. R., and Holl, J. W., Incipient cavitation scaling experiments for hemispherical and 1.5-caliber ogive-nosed bodies, Report No. NOrd 7958-264, Ordnance Research Laboratory, Pennsylvania State Univ., (May 1953).

38. Parkin, B. R., Scale effects in cavitating flow--a preliminary report, Report No. 21-7, Hydrodynamics Laboratory, California Inst. of Tech., (Dec. 1951).

39. Gelder, T. F., Moore, R. D., and Ruggeri, R. S., Incipient cavitation of freon-114 in a tunnel venturi, NASA Tech Note D-2662 (Feb. 1965).

40. Ruggeri, R. S., Moore, R. D., and Gelder, T. F., Incipient cavitation of ethylene glycol in a tunnel venturi, NASA Tech. Note D-2722 (Mar. 1965).

APPENDIX A: Experimental cavitation data--nitrogen and hydrogen--for hydrofoil.

Table A-1a. Experimental cavitation data for 0.312-inch hydrofoil using liquid nitrogen (English Units).

RUN NO.	CAVITY INCHES	T0 DEG R	V0 FT/SEC	P0 PSIA	PV PSIA	H0 FT	HV FT	KV	T 1 DEG R	T 2 DEG R	T 3 DEG R	T 4 DEG R	T 5 DEG R
282A**		137.45	25.4	20.18	13.04	57.3	37.0	2.02					
282B	1.60	137.41	27.0	18.78	13.00	53.3	36.9	1.44	136.35	136.19	136.21	136.33	136.64
282E	1.30	137.43	26.7	18.75	13.02	53.3	37.0	1.47	136.46	136.37	136.44	136.84	137.29
282G**		137.48	24.2	20.18	13.07	57.3	37.1	2.21					
282H**		137.54	24.3	20.33	13.11	57.8	37.3	2.23					
283A**		139.79	44.2	42.23	15.21	120.8	43.5	2.54					
283B	1.30	139.77	48.3	37.16	15.20	106.3	43.5	1.73	137.68	137.77	137.74	138.38	139.09
283C	0.70	139.88	47.7	37.55	15.30	107.4	43.8	1.80	138.33	138.89	139.39	140.00	140.08
283D**		139.79	44.6	41.88	15.21	119.8	43.5	2.47					
284A*		139.63	71.9	82.81	15.06	236.5	43.1	2.41					
284B	1.10	139.61	77.6	69.68	15.04	199.1	43.0	1.67	137.29	137.50	137.56	139.01	139.72
284C	1.30	139.70	77.4	69.48	15.13	198.6	43.3	1.67	137.03	137.30	137.38	138.76	139.63
284D	0.80	139.68	77.2	69.90	15.11	199.7	43.2	1.69	137.38	138.08	138.94	139.91	139.77
284E	0.50	139.91	77.3	70.98	15.34	203.0	43.9	1.71	138.04	138.85	139.79	140.17	140.09
284F**		139.84	71.0	84.38	15.27	241.2	43.7	2.52					
285B	1.50	148.99	57.9	52.55	26.56	154.9	78.4	1.47	144.86	144.59	144.22	145.71	146.32
285C	0.80	149.45	57.1	53.38	27.27	157.6	80.6	1.52	146.23	146.47	147.51	148.91	148.73
285D	1.30	149.87	56.9	53.18	27.91	157.3	82.6	1.48	145.58	145.48	145.22	146.70	147.73
285E	1.00	150.43	56.3	53.75	28.79	159.2	85.4	1.50	146.77	146.93	147.04	148.90	149.78
285F**		150.98	50.6	62.58	29.70	185.7	88.2	2.45					
285G	0.80	151.33	54.8	53.88	30.26	160.1	90.0	1.50	148.39	148.88	149.62	151.15	151.49
285H**		151.15	50.3	62.88	29.96	186.7	89.0	2.49					
286A**		159.03	49.4	74.18	45.18	226.7	138.2	2.34					
286B	1.50	159.44	55.1	64.73	46.11	198.2	141.2	1.20	155.56	156.40	157.45	159.25	159.66
286C	0.50	159.64	54.2	66.08	46.56	202.4	142.7	1.31	156.46	157.93	159.26	159.89	160.00
287G**		159.61	38.4	64.33	46.48	197.1	142.5	2.39					
288A	0.60	150.82	40.4	41.96	29.43	124.5	87.4	1.47	148.72	149.80	150.52	150.75	150.84
288B	1.00	150.62	40.8	41.08	29.11	121.8	86.4	1.37	148.00	148.52	149.36	150.26	150.48
288C	1.30	150.68	41.4	40.66	29.20	120.6	86.6	1.27	147.65	147.92	148.18	149.67	150.39

* DENOTES AN INCIPIENT RUN
** DENOTES A DESINENT RUN

Table A-1a. (cont'd)

RUN NO.	CAVITY INCHES	T0 DEG R	V0 FT/SEC	P0 PSIA	PV PSIA	H0 FT	HV FT	KV	T 1 DEG R	T 2 DEG R	T 3 DEG R	T 4 DEG R	T 5 DEG R
288D	1.00	150.82	41.0	41.13	29.43	122.1	87.4	1.33	148.36	148.88	149.80	150.82	151.00
288E*		150.89	37.3	44.63	29.55	132.5	87.7	2.07					
289A	1.20	159.44	77.7	92.46	46.11	282.8	141.2	1.51	154.08	154.53	154.26	156.10	158.24
289B	0.90	159.53	77.4	93.00	46.31	284.5	141.9	1.53	154.37	155.02	155.16	157.59	158.83
289C	0.90	159.55	77.2	93.36	46.36	285.7	142.1	1.55	154.71	155.47	156.04	158.36	159.14
289D**		159.61	70.1	107.90	46.48	330.1	142.5	2.46					
290A*		149.49	72.7	97.24	27.33	286.8	80.8	2.51					
290C	0.75	149.51	78.5	82.43	27.36	243.3	80.8	1.70	146.03	146.75	147.64	149.09	149.20
290D	1.50	149.69	78.7	81.26	27.63	240.0	81.7	1.65	145.08	145.22	145.13	145.78	146.77
290E	0.45	149.80	78.1	82.46	27.80	243.6	82.2	1.70	146.36	147.38	148.90	149.44	149.47
290F**		149.80	69.8	96.56	27.80	285.1	82.2	2.68					
291A	1.70	140.26	32.5	24.98	15.68	71.6	44.9	1.62	138.56	138.37	138.38	138.62	138.96
292A**		137.81	30.5	22.96	13.35	65.3	38.0	1.89					
292B**		137.79	30.3	22.86	13.34	65.0	37.9	1.90					
292C	1.60	137.66	32.2	20.66	13.23	58.7	37.6	1.31	136.21	136.06	136.06	136.30	136.62
292D	0.70	137.70	31.9	20.86	13.26	59.3	37.7	1.36	136.73	136.84	137.03	137.59	137.68
292E	0.90	137.70	32.2	20.76	13.26	59.0	37.7	1.33	136.57	136.53	136.69	137.25	137.50
292F	0.50	137.75	31.6	20.96	13.31	59.6	37.8	1.40	136.91	137.11	137.50	137.75	137.75
292G**		137.75	30.5	22.56	13.31	64.1	37.8	1.82					
292H	1.50	137.83	31.5	20.58	13.37	58.5	38.0	1.33	136.55	136.31	136.30	136.49	136.82
292J	0.90	137.75	32.2	20.76	13.31	59.0	37.8	1.32	136.62	136.55	136.71	137.21	137.61
292L**		137.86	30.2	22.60	13.40	64.3	38.1	1.85					
293A	0.60	139.75	78.9	74.51	15.18	213.0	43.4	1.75	137.43	137.92	138.69	139.48	139.46
293B	0.90	139.81	78.4	73.60	15.23	210.4	43.6	1.75	136.66	136.96	137.39	138.46	139.18
293C	2.00	139.88	78.4	72.46	15.30	207.2	43.8	1.71	135.83	135.68	135.74	135.94	136.30
293D	0.90	140.02	77.8	72.69	15.45	207.9	44.2	1.74	137.16	137.52	138.49	139.18	139.63
293E**		140.09	71.3	87.58	15.52	250.5	44.5	2.61					
293F	1.30	140.22	78.3	72.23	15.65	206.8	44.8	1.70	137.75	137.90	137.93	138.71	139.77

* DENOTES AN INCIPIENT RUN
** DENOTES A DESINENT RUN

Table A-1a. (cont'd)

RUN NO.	CAVITY INCHES	T0 DEG R	V0 FT/SEC	P0 PSIA	PV PSIA	H0 FT	HV FT	KV	T 1 DEG R	T 2 DEG R	T 3 DEG R	T 4 DEG R	T 5 DEG R
294C	1.30	140.29	35.0	25.96	15.72	74.4	45.1	1.55	138.58	138.58	138.58	139.10	139.73
294D	1.50	140.31	34.3	25.93	15.74	74.3	45.1	1.60	138.56	138.47	138.46	138.83	139.32
294E	0.90	140.31	32.5	25.76	15.74	73.8	45.1	1.75	138.82	138.92	139.05	139.73	140.17
294F	0.60	140.29	32.1	25.66	15.72	73.5	45.1	1.78	138.91	139.25	139.61	140.08	140.17
294G**		140.35	29.5	27.96	15.77	80.1	45.2	2.58					
294H	0.90	140.67	32.8	25.46	16.10	73.1	46.2	1.61	139.25	139.25	139.32	140.00	140.45
294J**		140.67	29.9	28.06	16.10	80.5	46.2	2.46					
295A**		149.53	74.1	102.11	27.38	301.2	80.9	2.58					
295B	1.30	149.69	80.2	83.14	27.63	245.5	81.7	1.64	145.67	145.87	145.71	146.83	148.16
295C	0.90	149.80	80.1	83.00	27.80	245.2	82.2	1.64	146.00	146.38	146.57	148.05	149.29
295D	0.60	149.76	79.6	83.66	27.74	247.1	82.1	1.68	146.59	147.26	148.32	149.63	149.63
295E	1.40	149.74	80.0	82.58	27.72	243.9	82.0	1.63	145.17	145.30	145.17	145.91	147.11
295F	0.90	149.81	80.1	83.04	27.83	245.3	82.3	1.64	145.87	146.38	146.63	148.43	149.35
295G	0.60	149.76	79.6	83.84	27.74	247.6	82.1	1.68	146.43	147.11	148.16	149.31	149.33
295H**		149.98	72.1	99.78	28.08	294.8	83.1	2.62					
296A*		159.50	73.1	110.13	46.23	336.7	141.7	2.35					
296B	0.50	159.37	77.7	95.36	45.95	291.6	140.7	1.61	155.83	157.00	158.54	159.25	159.17
296C	1.30	159.44	77.8	91.60	46.11	280.2	141.2	1.48	153.72	154.01	153.40	154.48	156.92
296D	0.75	159.52	76.9	92.50	46.27	283.0	141.8	1.54	154.93	155.75	156.56	158.80	159.10
296E	0.90	159.55	76.9	91.56	46.36	280.2	142.1	1.50	154.33	154.93	155.11	157.52	158.85
296F	0.50	159.48	76.3	92.52	46.19	283.0	141.5	1.56	155.21	156.38	158.11	159.03	159.21
296G**		159.70	69.0	109.39	46.68	334.7	143.1	2.59					
297D**		159.44	39.2	65.46	46.11	200.4	141.2	2.48					
297H**		159.53	39.3	65.46	46.31	200.5	141.9	2.45					
298A*		159.46	51.0	73.83	46.15	226.0	141.4	2.09					
298C	1.30	159.52	56.5	64.42	46.27	197.3	141.8	1.12	155.02	155.95	156.98	158.71	159.25
298D	0.90	159.53	56.2	65.21	46.31	199.7	141.9	1.18	155.47	156.85	158.35	159.23	159.39
298E**		159.52	49.4	73.86	46.27	226.1	141.8	2.22					
298F	1.25	159.64	56.0	64.76	46.56	198.4	142.7	1.14	155.43	156.64	158.04	159.10	159.43
298G	0.90	159.61	54.3	65.16	46.48	199.6	142.5	1.25	155.77	157.34	158.65	159.19	159.39
298H	1.15	159.79	54.9	64.63	46.89	198.1	143.8	1.16	155.32	156.62	158.11	159.12	159.43

* DENOTES AN INCIPIENT RUN
** DENOTES A DESINENT RUN

Table A-1a. (cont'd)

RUN NO.	CAVITY INCHES	T0 DEG R	V0 FT/SEC	P0 PSIA	PV PSIA	H0 FT	HV FT	KV	T 1 DEG R	T 2 DEG R	T 3 DEG R	T 4 DEG R	T 5 DEG R
298J**		160.06	48.6	73.32	47.51	224.9	145.9	2.15					
299A*		149.99	52.5	63.06	28.11	186.5	83.2	2.41					
299B	0.75	150.05	58.4	53.29	28.19	157.7	83.5	1.40	147.26	147.55	148.21	149.83	150.34
299C	1.70	150.12	57.8	52.48	28.31	155.3	83.8	1.38	146.79	146.47	146.32	147.19	148.36
299D	1.15	150.01	57.7	52.62	28.14	155.7	83.3	1.40	146.61	146.65	146.63	148.16	149.44
299E	0.50	149.90	57.0	53.21	27.97	157.4	82.8	1.48	147.11	147.87	149.29	149.83	149.81
299F	0.90	149.98	57.0	52.66	28.08	155.8	83.1	1.44	146.88	146.95	147.64	149.20	149.74
299G**		150.12	51.2	61.62	28.31	182.3	83.8	2.41					
299H	1.50	150.07	57.7	51.96	28.22	153.8	83.6	1.36	146.23	146.02	145.73	146.65	148.01
299J**		150.08	51.6	61.43	28.25	181.7	83.7	2.37					
300A	0.60	150.57	42.1	41.41	29.02	122.8	86.1	1.33	148.32	149.20	150.07	150.46	150.46
300B	1.30	150.59	42.8	40.46	29.05	120.0	86.2	1.19	147.47	147.60	147.62	148.84	149.76
300C	0.90	150.71	42.4	40.92	29.26	121.4	86.8	1.24	148.01	148.52	149.31	150.44	150.66
300D	0.60	150.68	41.8	41.58	29.20	123.3	86.6	1.35	148.39	149.44	150.19	150.52	150.53
300E	0.90	150.77	42.1	40.83	29.34	121.2	87.1	1.23	148.14	148.46	149.09	150.35	150.70
300F	1.15	150.75	42.7	40.57	29.32	120.4	87.0	1.18	147.74	147.91	148.19	149.65	150.39
300G	0.80	150.89	41.7	40.86	29.55	121.3	87.7	1.24	148.34	148.95	149.78	150.70	150.91
301A**		140.15	45.7	42.63	15.57	122.1	44.6	2.38					
301B	0.60	140.13	49.2	37.46	15.56	107.3	44.6	1.67	138.83	139.30	140.00	140.49	140.54
301C	1.15	140.15	48.9	36.88	15.57	105.6	44.6	1.64	138.51	138.67	138.91	139.50	140.27
301D**		140.26	44.5	41.36	15.68	118.5	44.9	2.39					

* DENOTES AN INCIPIENT RUN
** DENOTES A DESINENT RUN

Table A-1a. (cont'd)

RUN NO.	P 1 PSIA	P 2 PSIA	P 3 PSIA	P 4 PSIA	P 5 PSIA	P 1,T PSIA	P 2,T PSIA	P 3,T PSIA	P 4,T PSIA	P 5,T PSIA
282B	12.18	11.98	12.08	12.08	12.23	12.10	11.97	11.98	12.09	12.34
282E	12.35	12.22	12.23	12.38	14.08	12.19	12.11	12.17	12.51	12.89
283B	13.46	13.41	13.61	13.96	16.68	13.24	13.32	13.29	13.88	14.53
283C	13.82	14.08	16.45	25.45	26.49	13.83	14.35	14.83	15.43	15.50
284B	12.12	11.98	12.08	13.98	25.25	12.89	13.08	13.13	14.47	15.14
284C	11.86	11.53	12.01	13.23	25.98	12.68	12.91	12.97	14.23	15.06
284D	12.20	12.15	13.05	41.20	42.10	12.97	13.60	14.40	15.34	15.20
284E	12.78	12.83	15.03	43.18	43.63	13.56	14.31	15.21	15.59	15.52
285B	21.05	21.05	21.45	22.15	24.15	20.89	20.55	20.09	21.97	22.78
285C	22.58	23.18	26.63	35.11	38.08	22.66	22.97	24.41	26.45	26.18
285D	22.26	22.11	22.45	23.78	27.18	21.80	21.66	21.34	23.29	24.72
285E	23.35	23.55	24.65	32.05	37.19	23.39	23.61	23.76	26.43	27.77
285G	24.66	24.88	26.68	35.38	39.73	25.68	26.40	27.52	29.96	30.53
286B	36.38	36.83	39.76	47.03	49.71	37.90	39.59	41.74	45.66	46.60
286C	37.83	40.68	48.61	52.33	53.38	39.70	42.78	45.70	47.14	47.39
288A	25.94	26.76	31.71	34.04	34.71	26.16	27.80	28.94	29.32	29.46
288B	25.23	25.56	27.06	32.55	33.46	25.10	25.87	27.13	28.54	28.88
288C	24.81	25.01	25.36	28.93	32.19	24.61	25.00	25.36	27.61	28.74
288D	25.26	25.63	27.10	32.35	33.56	25.63	26.40	27.80	29.43	29.73
289A	36.16	36.06	36.23	38.94	53.86	35.09	35.93	35.42	38.97	43.44
289B	37.00	37.20	37.70	48.68	64.72	35.62	36.85	37.13	42.05	44.74
289C	37.31	37.56	38.46	53.46	67.16	36.27	37.72	38.86	43.71	45.42
290C	24.10	24.51	25.68	50.27	55.67	22.39	23.36	24.59	26.72	26.89
290D	22.86	22.96	23.06	23.56	25.01	21.16	21.34	21.23	22.06	23.39
290E	24.21	25.21	29.06	56.46	55.51	22.83	24.23	26.43	27.24	27.30
291A	14.58	14.65	14.75	14.83	15.11	14.04	13.86	13.88	14.09	14.41
292C	11.79	12.26	12.16	12.19	12.66	11.98	11.86	11.86	12.06	12.33
292D	12.16	12.54	12.66	14.66	16.73	12.42	12.51	12.68	13.16	13.24
292E	12.04	12.34	12.46	13.14	15.46	12.28	12.25	12.39	12.86	13.08

Table A-1a. (cont'd)

RUN NO.	P 1 PSIA	P 2 PSIA	P 3 PSIA	P 4 PSIA	P 5 PSIA	P 1,T PSIA	P 2,T PSIA	P 3,T PSIA	P 4,T PSIA	P 5,T PSIA
292F	12.23	12.66	14.01	16.71	16.86	12.57	12.74	13.08	13.31	13.31
292H	11.68	12.18	12.21	12.18	12.48	12.26	12.07	12.06	12.22	12.49
292J	12.11	12.46	12.53	13.66	15.86	12.33	12.26	12.40	12.83	13.18
293A	12.96	13.06	14.31	34.91	47.71	13.02	13.45	14.16	14.92	14.90
293B	12.50	12.45	12.70	15.00	36.13	12.36	12.62	12.99	13.94	14.62
293C	11.94	11.71	11.74	12.01	12.36	11.67	11.56	11.60	11.76	12.06
293D	12.79	12.74	13.24	17.89	38.24	12.79	13.10	13.98	14.62	15.06
293F	12.98	12.33	13.93	13.23	15.48	13.31	13.44	13.47	14.18	15.20
294C	14.93	14.46	14.46	14.96	16.56	14.06	14.06	14.06	14.55	15.16
294D	14.83	14.43	14.46	14.78	15.18	14.04	13.96	13.94	14.30	14.76
294E	15.13	14.74	14.76	16.53	19.43	14.28	14.38	14.50	15.16	15.59
294F	15.24	14.96	15.86	19.81	22.03	14.36	14.69	15.04	15.50	15.59
294H	15.06	14.76	14.76	16.16	18.21	14.69	14.69	14.76	15.43	15.88
295B	22.91	23.04	23.01	23.84	29.81	21.92	22.18	21.97	23.46	25.34
295C	23.35	23.45	23.65	26.60	49.05	22.35	22.85	23.12	25.18	27.02
295D	24.38	24.51	25.86	41.36	55.43	23.14	24.06	25.57	27.55	27.55
295E	22.78	22.71	22.88	23.63	26.28	21.27	21.43	21.27	22.23	23.86
295F	23.37	23.37	24.24	27.44	53.11	22.18	22.85	23.19	25.73	27.11
295G	24.34	24.49	26.02	48.44	56.34	22.92	23.86	25.34	27.05	27.08
296B	39.13	39.99	47.56	68.46	69.80	38.43	40.80	44.10	45.66	45.50
296C	36.03	35.60	35.60	36.27	41.77	34.43	34.95	33.84	35.83	40.65
296D	37.65	37.93	39.70	57.44	66.57	36.68	38.29	39.92	44.66	45.34
296E	36.81	36.49	37.36	44.11	60.66	35.56	36.68	37.03	41.89	44.78
296F	38.57	39.32	47.67	66.42	67.77	37.23	39.55	43.16	45.18	45.58
298C	36.02	36.62	39.40	47.08	50.10	36.85	38.68	40.77	44.46	45.66
298D	36.66	38.11	43.91	50.31	52.01	37.72	40.51	43.67	45.62	45.99
298F	36.76	38.03	43.06	49.91	51.46	37.65	40.06	43.01	45.34	46.07
298G	37.66	40.31	48.71	51.66	53.16	38.33	41.52	44.34	45.54	45.99
298H	37.03	38.43	43.23	50.15	51.55	37.44	40.03	43.16	45.38	46.07

Table A-1a. (cont'd)

RUN NO.	P 1 PSIA	P 2 PSIA	P 3 PSIA	P 4 PSIA	P 5 PSIA	P 1,T PSIA	P 2,T PSIA	P 3,T PSIA	P 4,T PSIA	P 5,T PSIA
299B	23.26	23.24	24.42	32.92	37.82	24.06	24.46	25.42	27.86	28.65
299C	22.45	22.18	22.48	23.26	25.20	23.41	22.97	22.78	23.96	25.63
299D	22.75	22.59	23.22	25.35	33.35	23.17	23.21	23.19	25.34	27.24
299E	23.66	24.21	30.56	37.26	38.86	23.86	24.92	27.02	27.86	27.83
299F	23.06	23.21	24.51	30.86	36.96	23.53	23.63	24.59	26.89	27.72
299H	22.51	22.41	22.66	23.61	26.71	22.66	22.37	21.99	23.21	25.13
300A	25.91	26.36	31.21	33.51	34.31	25.57	26.89	28.22	28.85	28.85
300B	24.66	24.56	24.90	26.66	30.23	24.36	24.54	24.56	26.35	27.74
300C	25.27	25.37	26.52	31.72	33.16	25.13	25.87	27.05	28.82	29.17
300D	26.05	26.63	32.13	33.73	34.38	25.68	27.24	28.42	28.94	28.97
300E	25.23	25.18	26.36	31.01	32.83	25.31	25.79	26.72	28.68	29.23
300F	24.97	24.95	25.34	28.72	31.87	24.74	24.97	25.39	27.58	28.74
300G	25.56	25.86	27.26	32.61	33.26	25.60	26.51	27.77	29.23	29.58
301B	14.36	14.41	15.29	23.83	26.19	14.30	14.74	15.43	15.92	15.97
301C	14.10	13.98	14.03	15.16	19.56	13.99	14.14	14.36	14.93	15.70

Table A-1a. (cont'd)

RUN NO.	H 1 FT	H 2 FT	H 3 FT	H 4 FT	H 5 FT	H 1,T FT	H 2,T FT	H 3,T FT	H 4,T FT	H 5,T FT
282B	34.5	33.9	34.2	34.2	34.6	34.3	33.9	33.9	34.2	35.0
282E	35.0	34.6	34.6	35.1	40.1	34.5	34.3	34.5	35.5	36.6
283B	38.3	38.1	38.7	39.8	48.0	37.6	37.9	37.8	39.5	41.5
283C	39.4	40.1	47.3	74.9	78.1	39.4	40.9	42.4	44.2	44.4
284B	34.3	33.9	34.2	39.8	74.3	36.6	37.2	37.3	41.3	43.3
284C	33.5	32.6	34.0	37.6	76.5	36.0	36.7	36.8	40.6	43.1
284D	34.6	34.4	37.1	125.1	128.1	36.8	38.7	41.1	43.9	43.5
284E	36.3	36.4	43.0	131.6	133.1	38.6	40.8	43.5	44.7	44.5
285B	61.3	61.3	62.5	64.7	70.8	60.8	59.7	58.3	64.1	66.6
285C	66.0	67.8	78.6	105.4	115.0	66.2	67.2	71.6	78.0	77.2
285D	65.0	64.5	65.6	69.7	80.3	63.6	63.2	62.2	68.2	72.6
285E	66.4	69.0	72.4	95.7	112.1	68.5	69.2	69.6	77.9	82.2
285G	72.4	73.1	78.7	106.3	120.4	75.6	77.8	81.4	89.0	90.8
286B	109.5	111.0	120.5	144.3	153.2	114.4	119.9	126.9	139.8	142.9
286C	114.2	123.4	149.5	161.9	165.4	120.2	130.3	139.9	144.6	145.5
288A	76.4	79.0	94.6	102.0	104.2	77.1	82.2	85.8	87.0	87.5
288B	74.2	75.2	79.9	97.3	100.2	73.8	76.2	80.2	84.6	85.6
288C	72.9	73.5	74.6	85.8	96.1	72.3	73.5	74.6	81.6	85.2
288D	74.3	75.4	80.0	96.6	100.5	75.4	77.8	82.2	87.4	88.3
289A	108.8	108.5	109.0	117.8	167.0	105.4	108.1	106.4	117.9	132.4
289B	111.5	112.2	113.8	149.8	204.0	107.1	111.1	111.9	127.9	136.7
289C	112.5	113.3	116.2	165.7	212.4	109.2	113.9	117.5	133.3	139.0
290C	70.7	72.0	75.6	155.0	173.1	65.4	68.4	72.2	78.9	79.4
290D	66.8	67.2	67.5	69.0	73.5	61.6	62.2	61.8	64.4	68.5
290E	71.0	74.1	86.2	175.8	172.6	66.7	71.1	77.9	80.5	80.7
291A	41.6	41.8	42.1	42.4	43.2	40.0	39.5	39.5	40.2	41.1
292C	33.3	34.7	34.4	34.5	35.9	33.9	33.6	33.6	34.1	34.9
292D	34.4	35.6	35.9	41.9	48.1	35.2	35.5	36.0	37.4	37.6
292E	34.1	35.0	35.3	37.3	44.3	34.8	34.7	35.1	36.5	37.2

Table A-1a. (cont'd)

RUN NO.	H 1 FT	H 2 FT	H 3 FT	H 4 FT	H 5 FT	H 1,T FT	H 2,T FT	H 3,T FT	H 4,T FT	H 5,T FT
292F	34.6	35.9	39.9	48.0	48.5	35.6	36.1	37.2	37.8	37.8
292H	33.0	34.5	34.6	34.5	35.4	34.7	34.2	34.1	34.6	35.4
292J	34.3	35.3	35.5	38.9	45.5	34.9	34.7	35.1	36.4	37.5
293A	36.8	37.1	40.8	104.8	146.5	37.0	38.3	40.4	42.6	42.6
293B	35.4	35.3	36.0	42.9	108.7	35.0	35.8	36.9	39.7	41.8
293C	33.8	33.1	33.2	34.0	35.0	33.0	32.7	32.8	33.3	34.1
293D	36.3	36.2	37.6	51.6	115.5	36.3	37.2	39.8	41.8	43.1
293F	36.9	34.9	39.7	37.6	44.3	37.8	38.2	38.3	40.4	43.5
294C	42.7	41.3	41.3	42.8	47.6	40.1	40.1	40.1	41.6	43.4
294D	42.4	41.2	41.3	42.2	43.4	40.0	39.8	39.7	40.8	42.2
294E	43.3	42.1	42.2	47.5	56.3	40.7	41.0	41.4	43.4	44.7
294F	43.6	42.8	45.5	57.5	64.3	41.0	42.0	43.0	44.4	44.7
294H	43.1	42.2	42.2	46.4	52.6	42.0	42.0	42.2	44.2	45.5
295B	67.0	67.4	67.3	69.9	88.6	63.9	64.7	64.1	68.7	74.5
295C	68.4	68.7	69.3	78.5	151.0	65.3	66.8	67.6	74.0	79.8
295D	71.6	72.0	76.2	125.7	172.3	67.7	70.6	75.3	81.5	81.5
295E	66.6	66.4	66.9	69.2	77.5	62.0	62.4	62.0	64.9	69.9
295F	68.4	68.4	71.1	81.1	164.5	64.7	66.8	67.9	75.8	80.1
295G	71.4	71.9	76.7	149.0	175.4	67.0	69.9	74.5	79.9	80.0
296B	118.4	121.2	146.0	216.9	221.5	116.2	123.8	134.6	139.8	139.2
296C	108.4	107.0	107.0	109.2	127.0	103.3	104.9	101.4	107.7	123.4
296D	113.6	114.5	120.3	179.1	210.3	110.5	115.7	121.0	136.5	138.7
296E	110.9	109.9	112.7	134.7	190.1	106.9	110.5	111.6	127.4	136.9
296F	116.6	119.0	146.4	209.8	214.5	112.3	119.8	131.6	138.2	139.5
298C	108.4	110.3	119.3	144.5	154.5	111.1	117.0	123.7	135.8	139.8
298D	110.4	115.1	134.0	155.2	160.8	113.9	122.9	133.2	139.6	140.8
298F	110.8	114.9	131.2	153.8	159.0	113.6	121.4	131.0	138.7	141.1
298G	113.7	122.2	149.9	159.7	164.7	115.8	126.2	135.4	139.4	140.8
298H	111.6	116.1	131.8	154.6	159.3	113.0	121.3	131.6	138.8	141.1

Table A-1a. (cont'd)

RUN NO.	H 1 FT	H 2 FT	H 3 FT	H 4 FT	H 5 FT	H 1,T FT	H 2,T FT	H 3,T FT	H 4,T FT	H 5,T FT
299B	68.1	68.0	71.7	98.4	114.2	70.6	71.8	74.8	82.4	84.9
299C	65.6	64.7	65.7	68.1	74.1	68.5	67.2	66.6	70.2	75.4
299D	66.5	66.0	68.0	74.6	99.8	67.8	67.9	67.9	74.5	80.5
299E	69.3	71.0	90.9	112.4	117.5	69.9	73.2	79.8	82.4	82.3
299F	67.5	67.9	72.0	91.9	111.4	68.9	69.2	72.2	79.4	82.0
299H	65.8	65.5	66.2	69.2	78.8	66.2	65.3	64.2	67.9	73.9
300A	76.3	77.7	93.0	100.3	102.9	75.3	79.4	83.6	85.5	85.5
300B	72.4	72.1	73.2	78.7	89.9	71.5	72.0	72.1	77.7	82.1
300C	74.3	74.6	78.2	94.6	99.2	73.9	76.2	79.9	85.5	86.5
300D	76.8	78.6	95.9	101.0	103.1	75.6	80.5	84.2	85.8	85.9
300E	74.2	74.0	77.7	92.4	98.2	74.5	75.9	78.9	85.0	86.7
300F	73.4	73.3	74.5	85.1	95.1	72.7	73.4	74.7	81.5	85.2
300G	75.2	76.2	80.5	97.5	99.5	75.4	78.2	82.2	86.7	87.8
301B	41.0	41.1	43.8	69.8	77.2	40.8	42.1	44.2	45.7	45.8
301C	40.2	39.8	40.0	43.4	56.7	39.9	40.3	41.0	42.7	45.0

Table A-1b. Experimental cavitation data for 0.312-inch hydrofoil using liquid nitrogen (SI Units).

RUN NO.	CAVITY CM	TO DEG K	VO M/SEC	PO N/CM/CM	PV N/CM/CM	HO M	HV M	KV	T 1 DEG K	T 2 DEG K	T 3 DEG K	T 4 DEG K	T 5 DEG K
282A**		76.36	7.8	13.91	8.99	17.5	11.3	2.02					
282B	4.06	76.34	8.2	12.95	8.97	16.3	11.3	1.44	75.75	75.66	75.67	75.74	75.91
282E	3.30	76.35	8.1	12.93	8.98	16.2	11.3	1.47	75.81	75.76	75.80	76.02	76.27
282G**		76.38	7.4	13.91	9.01	17.5	11.3	2.21					
282H**		76.41	7.4	14.02	9.04	17.6	11.4	2.23					
283A**		77.66	13.5	29.12	10.49	36.8	13.3	2.54					
283B	3.30	77.65	14.7	25.62	10.48	32.4	13.3	1.73	76.49	76.54	76.52	76.88	77.27
283C	1.78	77.71	14.5	25.89	10.55	32.7	13.4	1.80	76.85	77.16	77.44	77.78	77.82
283D**		77.66	13.6	28.88	10.49	36.5	13.3	2.47					
284A*		77.57	21.9	57.10	10.38	72.1	13.1	2.41					
284B	2.79	77.56	23.7	48.04	10.37	60.7	13.1	1.67	76.27	76.39	76.42	77.23	77.62
284C	3.30	77.61	23.6	47.90	10.43	60.5	13.2	1.67	76.13	76.28	76.32	77.09	77.57
284D	2.03	77.60	23.5	48.19	10.42	60.9	13.2	1.69	76.32	76.71	77.19	77.73	77.65
284E	1.27	77.73	23.6	48.94	10.58	61.9	13.4	1.71	76.69	77.14	77.66	77.87	77.83
284F**		77.69	21.7	58.18	10.53	73.5	13.3	2.52					
285B	3.81	82.77	17.7	36.23	18.31	47.2	23.9	1.47	80.48	80.33	80.12	80.95	81.29
285C	2.03	83.03	17.4	36.80	18.80	48.0	24.6	1.52	81.24	81.37	81.95	82.73	82.63
285D	3.30	83.26	17.3	36.67	19.25	47.9	25.2	1.48	80.88	80.82	80.68	81.50	82.07
285E	2.54	83.57	17.2	37.06	19.85	48.5	26.0	1.50	81.54	81.63	81.69	82.72	83.21
285F**		83.88	15.4	43.15	20.47	56.6	26.9	2.45					
285G	2.03	84.07	16.7	37.15	20.86	48.8	27.4	1.50	82.44	82.71	83.12	83.97	84.16
285H**		83.97	15.3	43.35	20.66	56.9	27.1	2.49					
286A**		88.35	15.0	51.15	31.15	69.1	42.1	2.34					
286B	3.81	88.58	16.8	44.63	31.79	60.4	43.1	1.20	86.42	86.89	87.47	88.47	88.70
286C	1.27	88.69	16.5	45.56	32.10	61.7	43.5	1.31	86.92	87.74	88.48	88.83	88.89
287G**		88.67	11.7	44.35	32.05	60.1	43.4	2.39					
288A	1.52	83.79	12.3	28.93	20.29	38.0	26.6	1.47	82.62	83.22	83.62	83.75	83.80
288B	2.54	83.68	12.4	28.32	20.07	37.1	26.3	1.37	82.22	82.51	82.98	83.48	83.60
288C	3.30	83.71	12.6	28.03	20.13	36.8	26.4	1.27	82.03	82.18	82.32	83.15	83.55

* DENOTES AN INCIPIENT RUN
** DENOTES A DESINENT RUN

Table A-1b. (cont'd)

RUN NO.	CAVITY CM	T0 DEG K	V0 M/SEC	P0 N/CM/CM	PV N/CM/CM	H0 M	HV M	KV	T 1 DEG K	T 2 DEG K	T 3 DEG K	T 4 DEG K	T 5 DEG K
288D	2.54	83.79	12.5	28.36	20.29	37.2	26.6	1.33	82.42	82.71	83.22	83.79	83.89
288E*		83.83	11.4	30.77	20.37	40.4	26.7	2.07					
289A	3.05	88.58	23.7	63.75	31.79	86.2	43.1	1.51	85.60	85.85	85.70	86.72	87.91
289B	2.29	88.63	23.6	64.12	31.93	86.7	43.3	1.53	85.76	86.12	86.20	87.55	88.24
289C	2.29	88.64	23.5	64.37	31.96	87.1	43.3	1.55	85.95	86.37	86.69	87.98	88.41
289D**		88.67	21.4	74.39	32.05	100.6	43.4	2.46					
290A*		83.05	22.2	67.04	18.84	87.4	24.6	2.51					
290C	1.90	83.06	23.9	56.83	18.86	74.1	24.6	1.70	81.13	81.53	82.02	82.83	82.89
290D	3.81	83.16	24.0	56.03	19.05	73.1	24.9	1.65	80.60	80.68	80.63	80.99	81.54
290E	1.14	83.22	23.8	56.85	19.17	74.2	25.1	1.70	81.31	81.88	82.72	83.02	83.04
290F**		83.22	21.3	66.58	19.17	86.9	25.1	2.68					
291A	4.32	77.92	9.9	17.22	10.81	21.8	13.7	1.62	76.98	76.87	76.88	77.01	77.20
292A**		76.56	9.3	15.83	9.21	19.9	11.6	1.89					
292B**		76.55	9.2	15.76	9.20	19.8	11.6	1.90					
292C	4.06	76.48	9.8	14.24	9.12	17.9	11.5	1.31	75.67	75.59	75.59	75.72	75.90
292D	1.78	76.50	9.7	14.38	9.14	18.1	11.5	1.36	75.96	76.02	76.13	76.44	76.49
292E	2.29	76.50	9.8	14.31	9.14	18.0	11.5	1.33	75.87	75.85	75.94	76.25	76.39
292F	1.27	76.53	9.6	14.45	9.17	18.2	11.5	1.40	76.06	76.17	76.39	76.53	76.53
292G**		76.53	9.3	15.55	9.17	19.5	11.5	1.82					
292H	3.81	76.57	9.6	14.19	9.22	17.8	11.6	1.33	75.86	75.73	75.72	75.83	76.01
292J	2.29	76.53	9.8	14.31	9.17	18.0	11.5	1.32	75.90	75.86	75.95	76.23	76.45
292L**		76.59	9.2	15.58	9.24	19.6	11.6	1.85					
293A	1.52	77.64	24.0	51.37	10.47	64.9	13.2	1.75	76.35	76.62	77.05	77.49	77.48
293B	2.29	77.67	23.9	50.75	10.50	64.1	13.3	1.75	75.92	76.09	76.33	76.92	77.32
293C	5.08	77.71	23.9	49.96	10.55	63.1	13.4	1.71	75.46	75.38	75.41	75.52	75.72
293D	2.29	77.79	23.7	50.12	10.65	63.4	13.5	1.74	76.20	76.40	76.94	77.32	77.57
293E**		77.83	21.7	60.38	10.70	76.4	13.5	2.61					
293F	3.30	77.90	23.9	49.80	10.79	63.0	13.7	1.70	76.53	76.61	76.63	77.06	77.65

* DENOTES AN INCIPIENT RUN
** DENOTES A DESINENT RUN

Table A-1b. (cont'd)

RUN NO.	CAVITY CM	T0 DEG K	V0 M/SEC	P0 N/CM/CM	PV N/CM/CM	H0 M	HV M	KV	T 1 DEG K	T 2 DEG K	T 3 DEG K	T 4 DEG K	T 5 DEG K
294C	3.30	77.94	10.7	17.90	10.84	22.7	13.7	1.55	76.99	76.99	76.99	77.28	77.63
294D	3.81	77.95	10.5	17.88	10.85	22.7	13.7	1.60	76.98	76.93	76.92	77.13	77.40
294E	2.29	77.95	9.9	17.76	10.85	22.5	13.7	1.75	77.12	77.18	77.25	77.63	77.87
294F	1.52	77.94	9.8	17.69	10.84	22.4	13.7	1.78	77.17	77.36	77.56	77.82	77.87
294G**		77.97	9.0	19.28	10.88	24.4	13.8	2.58					
294H	2.29	78.15	10.0	17.55	11.10	22.3	14.1	1.61	77.36	77.36	77.40	77.78	78.03
294J**		78.15	9.1	19.35	11.10	24.5	14.1	2.46					
295A**		83.07	22.6	70.40	18.88	91.8	24.7	2.58					
295B	3.30	83.16	24.4	57.32	19.05	74.8	24.9	1.64	80.93	81.04	80.95	81.57	82.31
295C	2.29	83.22	24.4	57.23	19.17	74.7	25.1	1.64	81.11	81.32	81.43	82.25	82.94
295D	1.52	83.20	24.3	57.68	19.13	75.3	25.0	1.68	81.44	81.81	82.40	83.13	83.13
295E	3.56	83.19	24.4	56.94	19.11	74.3	25.0	1.63	80.65	80.72	80.65	81.06	81.73
295F	2.29	83.23	24.4	57.25	19.19	74.8	25.1	1.64	81.04	81.32	81.46	82.46	82.97
295G	1.52	83.20	24.3	57.81	19.13	75.5	25.0	1.68	81.35	81.73	82.31	82.95	82.96
295H**		83.32	22.0	68.80	19.36	89.9	25.3	2.62					
296A*		88.61	22.3	75.93	31.88	102.6	43.2	2.35					
296B	1.27	88.54	23.7	65.75	31.68	88.9	42.9	1.61	86.57	87.22	88.08	88.47	88.43
296C	3.30	88.58	23.7	63.16	31.79	85.4	43.1	1.48	85.40	85.56	85.22	85.82	87.18
296D	1.90	88.62	23.4	63.78	31.90	86.3	43.2	1.54	86.07	86.53	86.98	88.22	88.39
296E	2.29	88.64	23.4	63.13	31.96	85.4	43.3	1.50	85.74	86.07	86.17	87.51	88.25
296F	1.27	88.60	23.3	63.79	31.85	86.3	43.1	1.56	86.23	86.88	87.84	88.35	88.45
296G**		88.72	21.0	75.42	32.19	102.0	43.6	2.59					
297D**		88.58	11.9	45.13	31.79	61.1	43.1	2.48					
297H**		88.63	12.0	45.13	31.93	61.1	43.3	2.45					
298A*		88.59	15.5	50.90	31.82	68.9	43.1	2.09					
298C	3.30	88.62	17.2	44.42	31.90	60.1	43.2	1.12	86.12	86.64	87.21	88.17	88.47
298D	2.29	88.63	17.1	44.96	31.93	60.9	43.3	1.18	86.37	87.14	87.97	88.46	88.55
298E**		88.62	15.1	50.92	31.90	68.9	43.2	2.22					
298F	3.17	88.69	17.1	44.65	32.10	60.5	43.5	1.14	86.35	87.02	87.80	88.39	88.57
298G	2.29	88.67	16.5	44.93	32.05	60.8	43.4	1.25	86.54	87.41	88.14	88.44	88.55
298H	2.92	88.77	16.7	44.56	32.33	60.4	43.8	1.16	86.29	87.01	87.84	88.40	88.57

* DENOTES AN INCIPIENT RUN
** DENOTES A DESINENT RUN

Table A-1b. (cont'd)

RUN NO.	CAVITY CM	T0 DEG K	V0 M/SEC	P0 N/CM/CM	PV N/CM/CM	H0 M	HV M	KV	T 1 DEG K	T 2 DEG K	T 3 DEG K	T 4 DEG K	T 5 DEG K
298J**		88.92	14.8	50.55	32.76	68.6	44.5	2.15					
299A*		83.33	16.0	43.48	19.38	56.8	25.4	2.41					
299B	1.90	83.36	17.8	36.74	19.44	48.1	25.4	1.40	81.81	81.97	82.34	83.24	83.52
299C	4.32	83.40	17.6	36.18	19.52	47.3	25.6	1.38	81.55	81.37	81.29	81.77	82.42
299D	2.92	83.34	17.6	36.28	19.40	47.5	25.4	1.40	81.45	81.47	81.46	82.31	83.02
299E	1.27	83.28	17.4	36.69	19.28	48.0	25.2	1.48	81.73	82.15	82.94	83.24	83.23
299F	2.29	83.32	17.4	36.31	19.36	47.5	25.3	1.44	81.60	81.64	82.02	82.89	83.19
299G**		83.40	15.6	42.49	19.52	55.6	25.6	2.41					
299H	3.81	83.37	17.6	35.83	19.46	46.9	25.5	1.36	81.24	81.12	80.96	81.47	82.23
299J**		83.38	15.7	42.35	19.48	55.4	25.5	2.37					
300A	1.52	83.65	12.8	28.55	20.01	37.4	26.2	1.33	82.40	82.89	83.37	83.59	83.59
300B	3.30	83.66	13.1	27.90	20.03	36.6	26.3	1.19	81.93	82.00	82.01	82.69	83.20
300C	2.29	83.73	12.9	28.21	20.17	37.0	26.5	1.24	82.23	82.51	82.95	83.58	83.70
300D	1.52	83.71	12.7	28.67	20.13	37.6	26.4	1.35	82.44	83.02	83.44	83.62	83.63
300E	2.29	83.76	12.8	28.15	20.23	36.9	26.5	1.23	82.30	82.48	82.83	83.53	83.72
300F	2.92	83.75	13.0	27.97	20.21	36.7	26.5	1.18	82.08	82.17	82.33	83.14	83.55
300G	2.03	83.83	12.7	28.17	20.37	37.0	26.7	1.24	82.41	82.75	83.21	83.72	83.84
301A**		77.86	13.9	29.39	10.74	37.2	13.6	2.38					
301B	1.52	77.85	15.0	25.83	10.72	32.7	13.6	1.67	77.13	77.39	77.78	78.05	78.08
301C	2.92	77.86	14.9	25.43	10.74	32.2	13.6	1.64	76.95	77.04	77.17	77.50	77.93
301D**		77.92	13.6	28.52	10.81	36.1	13.7	2.39					

* DENOTES AN INCIPIENT RUN
** DENOTES A DESINENT RUN

Table A-1b. (cont'd)

RUN NO.	P 1 N/CM/CM	P 2 N/CM/CM	P 3 N/CM/CM	P 4 N/CM/CM	P 5 N/CM/CM	P 1,T N/CM/CM	P 2,T N/CM/CM	P 3,T N/CM/CM	P 4,T N/CM/CM	P 5,T N/CM/CM
282B	8.40	8.26	8.33	8.33	8.43	8.34	8.25	8.26	8.33	8.51
282E	8.52	8.43	8.43	8.54	9.71	8.40	8.35	8.39	8.62	8.89
283B	9.28	9.25	9.38	9.63	11.50	9.13	9.19	9.16	9.57	10.02
283C	9.53	9.71	11.34	17.55	18.26	9.53	9.89	10.22	10.64	10.69
284B	8.36	8.26	8.33	9.64	17.41	8.89	9.02	9.05	9.97	10.44
284C	8.18	7.95	8.28	9.12	17.91	8.74	8.90	8.94	9.81	10.38
284D	8.41	8.38	9.00	28.41	29.03	8.94	9.38	9.93	10.58	10.48
284E	8.81	8.85	10.36	29.77	30.08	9.35	9.87	10.49	10.75	10.70
285B	14.51	14.51	14.79	15.27	16.65	14.40	14.17	13.85	15.15	15.70
285C	15.57	15.98	18.36	24.21	26.26	15.62	15.84	16.83	18.24	18.05
285D	15.35	15.24	15.48	16.40	18.74	15.03	14.94	14.71	16.06	17.04
285E	16.10	16.24	17.00	22.10	25.64	16.12	16.28	16.38	18.22	19.15
285G	17.00	17.15	18.40	24.39	27.39	17.71	18.20	18.98	20.66	21.05
286B	25.08	25.39	27.41	32.43	34.27	26.13	27.29	28.78	31.48	32.13
286C	26.08	28.05	33.52	36.08	36.80	27.37	29.49	31.51	32.50	32.67
288A	17.89	18.45	21.86	23.47	23.93	18.04	19.17	19.95	20.21	20.31
288B	17.40	17.62	18.66	22.44	23.07	17.31	17.83	18.71	19.67	19.91
288C	17.11	17.24	17.49	19.95	22.19	16.97	17.24	17.49	19.03	19.81
288D	17.42	17.67	18.68	22.30	23.14	17.67	18.20	19.17	20.29	20.49
289A	24.93	24.86	24.98	26.85	37.14	24.19	24.77	24.42	26.87	29.95
289B	25.51	25.65	25.99	33.56	44.62	24.56	25.41	25.60	28.99	30.85
289C	25.72	25.90	26.52	36.86	46.31	25.01	26.01	26.79	30.14	31.32
290C	16.62	16.90	17.71	34.66	38.38	15.44	16.11	16.95	18.43	18.54
290D	15.76	15.83	15.90	16.24	17.24	14.59	14.71	14.64	15.21	16.12
290E	16.69	17.38	20.04	38.93	38.27	15.74	16.71	18.22	18.78	18.82
291A	10.05	10.10	10.17	10.22	10.42	9.68	9.56	9.57	9.72	9.94
292C	8.13	8.45	8.38	8.40	8.73	8.26	8.18	8.18	8.31	8.50
292D	8.38	8.65	8.73	10.11	11.53	8.56	8.62	8.74	9.08	9.13
292E	8.30	8.51	8.59	9.06	10.66	8.47	8.45	8.54	8.87	9.02

Table A-1b. (cont'd)

RUN NO.	P 1 N/CM/CM	P 2 N/CM/CM	P 3 N/CM/CM	P 4 N/CM/CM	P 5 N/CM/CM	P 1,T N/CM/CM	P 2,T N/CM/CM	P 3,T N/CM/CM	P 4,T N/CM/CM	P 5,T N/CM/CM
292F	8.43	8.73	9.66	11.52	11.62	8.67	8.78	9.02	9.17	9.17
292H	8.05	8.40	8.42	8.40	8.60	8.46	8.32	8.31	8.43	8.61
292J	8.35	8.59	8.64	9.42	10.94	8.50	8.46	8.55	8.85	9.09
293A	8.94	9.00	9.87	24.07	32.89	8.98	9.27	9.76	10.28	10.27
293B	8.62	8.58	8.76	10.34	24.91	8.52	8.70	8.96	9.61	10.08
293C	8.23	8.07	8.09	8.28	8.52	8.05	7.97	8.00	8.11	8.31
293D	8.82	8.78	9.13	12.33	26.37	8.82	9.03	9.64	10.08	10.38
293F	8.95	8.50	9.60	9.12	10.67	9.17	9.26	9.29	9.77	10.48
294C	10.29	9.97	9.97	10.31	11.42	9.69	9.69	9.69	10.03	10.45
294D	10.22	9.95	9.97	10.19	10.47	9.68	9.62	9.61	9.86	10.18
294E	10.43	10.16	10.18	11.40	13.40	9.84	9.91	10.00	10.45	10.75
294F	10.51	10.31	10.94	13.66	15.19	9.90	10.13	10.37	10.69	10.75
294H	10.38	10.18	10.18	11.14	12.56	10.13	10.13	10.18	10.64	10.95
295B	15.80	15.89	15.86	16.44	20.55	15.11	15.29	15.15	16.18	17.47
295C	16.10	16.17	16.31	18.34	33.82	15.41	15.75	15.94	17.36	18.63
295D	16.81	16.90	17.83	28.52	38.22	15.96	16.59	17.63	18.99	18.99
295E	15.71	15.66	15.78	16.29	18.12	14.67	14.78	14.67	15.33	16.45
295F	16.11	16.11	16.71	18.92	36.62	15.29	15.75	15.99	17.74	18.69
295G	16.78	16.89	17.94	33.40	38.85	15.80	16.45	17.47	18.65	18.67
296B	26.98	27.57	32.79	47.20	48.13	26.50	28.13	30.41	31.48	31.37
296C	24.84	24.55	24.55	25.01	28.80	23.74	24.10	23.33	24.70	28.03
296D	25.96	26.15	27.37	39.60	45.90	25.29	26.40	27.52	30.79	31.26
296E	25.38	25.16	25.76	30.41	41.82	24.52	25.29	25.53	28.89	30.87
296F	26.59	27.11	32.87	45.79	46.73	25.67	27.27	29.76	31.15	31.43
298C	24.83	25.25	27.17	32.46	34.54	25.41	26.67	28.11	30.65	31.48
298D	25.28	26.28	30.27	34.69	35.86	26.01	27.93	30.11	31.46	31.71
298F	25.35	26.22	29.69	34.41	35.48	25.96	27.62	29.65	31.26	31.76
298G	25.97	27.79	33.58	35.62	36.65	26.42	28.62	30.57	31.40	31.71
298H	25.53	26.50	29.81	34.58	35.54	25.82	27.60	29.76	31.29	31.76

Table A-1b. (cont'd)

RUN NO.	P 1 N/CM/CM	P 2 N/CM/CM	P 3 N/CM/CM	P 4 N/CM/CM	P 5 N/CM/CM	P 1,T N/CM/CM	P 2,T N/CM/CM	P 3,T N/CM/CM	P 4,T N/CM/CM	P 5,T N/CM/CM
299B	16.04	16.02	16.84	22.70	26.08	16.59	16.87	17.52	19.21	19.75
299C	15.48	15.29	15.50	16.04	17.37	16.14	15.84	15.70	16.52	17.67
299D	15.69	15.58	16.01	17.48	22.99	15.97	16.01	15.99	17.47	18.78
299E	16.31	16.69	21.07	25.69	26.79	16.45	17.18	18.63	19.21	19.19
299F	15.90	16.00	16.90	21.28	25.48	16.23	16.29	16.95	18.54	19.11
299H	15.52	15.45	15.62	16.28	18.42	15.62	15.42	15.16	16.01	17.33
300A	17.86	18.17	21.52	23.10	23.66	17.63	18.54	19.46	19.89	19.89
300B	17.00	16.93	17.17	18.38	20.84	16.80	16.92	16.94	18.16	19.13
300C	17.42	17.49	18.28	21.87	22.86	17.33	17.83	18.65	19.87	20.11
300D	17.96	18.36	22.15	23.26	23.70	17.71	18.78	19.60	19.95	19.97
300E	17.40	17.36	18.17	21.38	22.64	17.45	17.78	18.43	19.77	20.15
300F	17.22	17.20	17.47	19.80	21.97	17.06	17.22	17.51	19.01	19.81
300G	17.62	17.83	18.80	22.48	22.93	17.65	18.28	19.15	20.15	20.39
301B	9.90	9.94	10.54	16.43	18.06	9.86	10.16	10.64	10.98	11.01
301C	9.72	9.64	9.67	10.45	13.49	9.65	9.75	9.90	10.30	10.82

Table A-1b. (cont'd)

RUN NO.	H 1 M	H 2 M	H 3 M	H 4 M	H 5 M	H 1,T M	H 2,T M	H 3,T M	H 4,T M	H 5,T M
282B	10.5	10.3	10.4	10.4	10.6	10.4	10.3	10.3	10.4	10.7
282E	10.7	10.5	10.6	10.7	12.2	10.5	10.5	10.5	10.8	11.2
283B	11.7	11.6	11.8	12.1	14.6	11.5	11.5	11.5	12.1	12.6
283C	12.0	12.2	14.4	22.8	23.8	12.0	12.5	12.9	13.5	13.5
284B	10.5	10.3	10.4	12.1	22.6	11.2	11.3	11.4	12.6	13.2
284C	10.2	9.9	10.4	11.5	23.3	11.0	11.2	11.2	12.4	13.1
284D	10.5	10.5	11.3	38.1	39.0	11.2	11.8	12.5	13.4	13.3
284E	11.1	11.1	13.1	40.1	40.6	11.8	12.4	13.3	13.6	13.5
285B	18.7	18.7	19.0	19.7	21.6	18.5	18.2	17.8	19.5	20.3
285C	20.1	20.7	23.9	32.1	35.1	20.2	20.5	21.8	23.8	23.5
285D	19.8	19.7	20.0	21.2	24.5	19.4	19.3	18.9	20.8	22.1
285E	20.8	21.0	22.1	29.2	34.2	20.9	21.1	21.2	23.8	25.0
285G	22.1	22.3	24.0	32.4	36.7	23.0	23.7	24.8	27.1	27.7
286B	33.4	33.8	36.7	44.0	46.7	34.9	36.5	38.7	42.6	43.5
286C	34.8	37.6	45.6	49.4	50.4	36.7	39.7	42.6	44.1	44.3
288A	23.3	24.1	28.8	31.1	31.7	23.5	25.1	26.2	26.5	26.7
288B	22.6	22.9	24.4	29.6	30.5	22.5	23.2	24.4	25.8	26.1
288C	22.2	22.4	22.7	26.1	29.3	22.0	22.4	22.7	24.9	26.0
288D	22.6	23.0	24.4	29.5	30.6	23.0	23.7	25.1	26.6	26.9
289A	33.2	33.1	33.2	35.9	50.9	32.1	32.9	32.4	35.9	40.4
289B	34.0	34.2	34.7	45.6	62.2	32.6	33.8	34.1	39.0	41.7
289C	34.3	34.5	35.4	50.5	64.7	33.3	34.7	35.8	40.6	42.4
290C	21.5	21.9	23.0	47.3	52.8	19.9	20.8	22.0	24.0	24.2
290D	20.4	20.5	20.6	21.0	22.4	18.8	18.9	18.8	19.6	20.9
290E	21.6	22.6	26.3	53.6	52.6	20.3	21.7	23.8	24.5	24.6
291A	12.7	12.8	12.8	12.9	13.2	12.2	12.0	12.1	12.2	12.5
292C	10.2	10.6	10.5	10.5	10.9	10.3	10.2	10.2	10.4	10.6
292D	10.5	10.8	10.9	12.8	14.7	10.7	10.8	11.0	11.4	11.5
292E	10.4	10.7	10.8	11.4	13.5	10.6	10.6	10.7	11.1	11.3

Table A-1b. (cont'd)

RUN NO.	H 1 M	H 2 M	H 3 M	H 4 M	H 5 M	H 1,T M	H 2,T M	H 3,T M	H 4,T M	H 5,T M
292F	10.6	10.9	12.2	14.6	14.8	10.9	11.0	11.3	11.5	11.5
292H	10.1	10.5	10.5	10.5	10.8	10.6	10.4	10.4	10.5	10.8
292J	10.5	10.8	10.8	11.9	13.9	10.6	10.6	10.7	11.1	11.4
293A	11.2	11.3	12.4	31.9	44.7	11.3	11.7	12.3	13.0	13.0
293B	10.8	10.8	11.0	13.1	33.1	10.7	10.9	11.2	12.1	12.7
293C	10.3	10.1	10.1	10.4	10.7	10.1	10.0	10.0	10.1	10.4
293D	11.1	11.0	11.5	15.7	35.2	11.1	11.3	12.1	12.7	13.1
293F	11.2	10.6	12.1	11.5	13.5	11.5	11.6	11.7	12.3	13.3
294C	13.0	12.6	12.6	13.0	14.5	12.2	12.2	12.2	12.7	13.2
294D	12.9	12.6	12.6	12.9	13.2	12.2	12.1	12.1	12.4	12.9
294E	13.2	12.8	12.9	14.5	17.2	12.4	12.5	12.6	13.2	13.6
294F	13.3	13.0	13.9	17.5	19.6	12.5	12.8	13.1	13.5	13.6
294H	13.1	12.9	12.9	14.1	16.0	12.8	12.8	12.9	13.5	13.9
295B	20.4	20.5	20.5	21.3	27.0	19.5	19.7	19.5	20.9	22.7
295C	20.8	20.9	21.1	23.9	46.0	19.9	20.4	20.6	22.6	24.3
295D	21.8	21.9	23.2	38.3	52.5	20.6	21.5	22.9	24.8	24.8
295E	20.3	20.2	20.4	21.1	23.6	18.9	19.0	18.9	19.8	21.3
295F	20.9	20.9	21.7	24.7	50.1	19.7	20.4	20.7	23.1	24.4
295G	21.8	21.9	23.4	45.4	53.5	20.4	21.3	22.7	24.4	24.4
296B	36.1	36.9	44.5	66.1	67.5	35.4	37.7	41.0	42.6	42.4
296C	33.0	32.6	32.6	33.3	38.7	31.5	32.0	30.9	32.8	37.6
296D	34.6	34.9	36.7	54.6	64.1	33.7	35.3	36.9	41.6	42.3
296E	33.8	33.5	34.3	41.0	57.9	32.6	33.7	34.0	38.8	41.7
296F	35.5	36.3	44.6	64.0	65.4	34.2	36.5	40.1	42.1	42.5
298C	33.0	33.6	36.4	44.0	47.1	33.8	35.7	37.7	41.4	42.6
298D	33.7	35.1	40.8	47.3	49.0	34.7	37.5	40.6	42.6	42.9
298F	33.8	35.0	40.0	46.9	48.5	34.6	37.0	39.9	42.3	43.0
298G	34.6	37.3	45.7	48.7	50.2	35.3	38.5	41.3	42.5	42.9
298H	34.0	35.4	40.2	47.1	48.6	34.4	37.0	40.1	42.3	43.0

Table A-1b. (cont'd)

RUN NO.	H 1 M	H 2 M	H 3 M	H 4 M	H 5 M	H 1,T M	H 2,T M	H 3,T M	H 4,T M	H 5,T M
299B	20.8	20.7	21.8	30.0	34.8	21.5	21.9	22.8	25.1	25.9
299C	20.0	19.7	20.0	20.8	22.6	20.9	20.5	20.3	21.4	23.0
299D	20.3	20.1	20.7	22.7	30.4	20.7	20.7	20.7	22.7	24.5
299E	21.1	21.6	27.7	34.2	35.8	21.3	22.3	24.3	25.1	25.1
299F	20.6	20.7	21.9	28.0	34.0	21.0	21.1	22.0	24.2	25.0
299H	20.0	20.0	20.2	21.1	24.0	20.2	19.9	19.6	20.7	22.5
300A	23.3	23.7	28.3	30.6	31.4	22.9	24.2	25.5	26.1	26.1
300B	22.1	22.0	22.3	24.0	27.4	21.8	22.0	22.0	23.7	25.0
300C	22.7	22.7	23.8	28.8	30.2	22.5	23.2	24.4	26.0	26.4
300D	23.4	23.9	29.2	30.8	31.4	23.0	24.5	25.7	26.2	26.2
300E	22.6	22.6	23.7	28.2	29.9	22.7	23.1	24.0	25.9	26.4
300F	22.4	22.3	22.7	25.9	29.0	22.2	22.4	22.8	24.9	26.0
300G	22.9	23.2	24.5	29.7	30.3	23.0	23.8	25.0	26.4	26.8
301B	12.5	12.5	13.3	21.3	23.5	12.4	12.8	13.5	13.9	14.0
301C	12.3	12.1	12.2	13.2	17.3	12.2	12.3	12.5	13.0	13.7

Table A-2a. Experimental cavitation data for 0.312-inch hydrofoil using liquid hydrogen (English Units).

RUN NO.	CAVITY INCHES	TO DEG R	VO FT/SEC	PO PSIA	PV PSIA	HO FT	HV FT	KV	T 1 DEG R	T 2 DEG R	T 3 DEG R	T 4 DEG R	T 5 DEG R
228A*		36.83	106.5	23.60	15.55	770.5	508.2	1.49					
228B	1.31	36.83	122.4	20.90	15.55	682.6	508.2	0.75	34.24	34.38	34.60	35.24	36.02
228C	0.75	36.77	118.8	21.70	15.41	708.3	503.5	0.93	34.47	34.87	35.59	36.22	36.04
228E**		36.81	112.8	24.60	15.50	802.9	506.6	1.50					
229B	0.90	37.15	135.8	24.80	16.37	812.0	536.8	0.96	33.70	34.02	34.42	35.66	36.16
229C	0.35	37.12	132.6	26.10	16.28	854.1	533.6	1.17	35.37	36.32	36.65	36.54	36.72
229D**		37.15	121.0	29.70	16.37	971.7	536.8	1.91					
230B	1.25	37.15	132.7	24.20	16.37	792.4	536.8	0.93	35.17	35.03	35.01	36.14	36.59
230C	0.82	37.15	133.0	24.55	16.37	803.8	536.8	0.97	35.41	35.51	35.96	36.77	37.04
230D	0.52	37.08	133.4	25.00	16.19	817.9	530.4	1.04	35.44	35.77	36.49	36.90	36.97
231B	1.60	37.03	170.0	33.90	16.05	1107.2	525.6	1.30	34.60	34.78	34.56	35.35	36.04
231C	0.70	37.13	168.7	34.50	16.33	1127.8	535.2	1.34	35.01	35.59	36.04	37.33	37.35
231D	0.40	37.10	165.2	35.40	16.23	1156.7	532.0	1.47	35.48	34.67	37.13	37.42	37.31
232B	1.10	37.73	212.8	52.05	17.93	1706.9	590.9	1.59	33.89	34.20	33.82	35.35	36.36
233A*		36.99	149.7	43.66	15.96	1423.6	522.4	2.59					
233B	1.70	37.06	172.0	34.70	16.14	1133.6	528.8	1.31	32.65	32.69	32.62	32.33	33.73
233C	1.00	37.01	171.0	35.20	16.00	1149.2	524.0	1.38	33.19	33.55	33.71	34.45	35.73
233D**		37.48	152.2	44.23	17.23	1448.6	566.7	2.45					
235B	1.70	37.58	193.7	42.57	17.53	1396.0	577.0	1.41	33.26	33.50	33.05	33.75	34.65
235C	1.03	37.58	191.4	43.10	17.53	1413.2	577.0	1.47	33.88	34.20	33.93	35.37	36.32
236 *		40.00	119.4	33.60	25.08	1130.8	845.2	1.29					
237B	1.20	39.62	155.7	33.26	23.76	1114.9	797.8	0.84	36.05	36.97	37.08	38.61	38.75
237C	0.80	39.62	154.9	33.60	23.76	1126.2	797.8	0.88	36.34	37.53	38.11	38.70	38.93
237D	0.45	39.73	153.5	34.36	24.13	1152.9	811.2	0.93	37.12	38.57	39.02	39.13	39.26

* DENOTES AN INCIPIENT RUN
** DENOTES A DESINENT RUN

Table A-2a. (cont'd)

RUN NO.	CAVITY INCHES	T0 DEG R	V0 FT/SEC	P0 PSIA	PV PSIA	H0 FT	HV FT	KV	T 1 DEG R	T 2 DEG R	T 3 DEG R	T 4 DEG R	T 5 DEG R
239A*		40.46	163.4	52.50	26.77	1770.2	906.8	2.08					
239B	1.20	40.59	179.5	43.50	27.24	1471.1	924.0	1.09	36.04	36.47	36.14	37.69	39.19
239C	0.80	40.54	180.5	44.06	27.04	1489.0	916.6	1.13	36.81	37.44	37.80	39.42	39.83
240B	0.75	38.25	218.6	53.30	19.42	1756.3	643.3	1.50	35.05	35.06	34.99	36.85	36.79
240C	1.40	38.61	218.0	53.65	20.50	1774.0	681.5	1.48	34.99	34.83	34.20	34.83	36.25
241B	1.12	38.29	181.5	38.95	19.53	1286.7	647.0	1.25	34.49	34.96	34.58	35.77	37.01
242A*		37.24	181.7	51.70	16.61	1687.8	545.0	2.23					
242B	1.75	37.26	194.9	43.20	16.66	1412.2	546.7	1.47	33.97	33.66	33.17	32.96	33.86
243B	0.80	37.26	192.5	43.90	16.66	1434.9	546.7	1.54	33.66	34.00	34.13	35.08	35.59
244A*		36.68	106.4	23.50	15.19	766.2	495.8	1.54					
244B	1.30	36.52	116.4	20.40	14.79	664.4	482.2	0.87	34.15	34.22	35.05	35.01	35.14
244C	0.45	36.47	114.5	21.10	14.66	686.8	477.7	1.03	34.15	34.65	35.23	35.78	35.60
244D	0.40	36.54	113.2	21.40	14.83	697.0	483.7	1.07	34.78	35.42	35.73	36.16	35.91
244E	1.20	36.54	115.9	20.62	14.83	671.7	483.7	0.90	34.27	34.58	35.01	35.77	36.05
245A*		36.77	117.9	28.40	15.41	926.1	503.5	1.96					
245B	1.68	36.77	129.9	23.75	15.41	775.0	503.5	1.03	33.21	33.16	33.07	33.93	33.82
245C	1.40	36.83	129.2	23.85	15.55	778.6	508.2	1.04	33.25	33.28	33.26	34.07	34.49
245D	0.75	36.90	128.5	24.40	15.73	797.0	514.4	1.10	34.09	34.49	35.08	36.00	35.82
245E**		37.06	113.3	29.00	16.14	948.1	528.8	2.10					
246A	1.25	37.51	210.0	51.65	17.33	1690.4	570.1	1.64	34.92	35.23	34.60	35.30	36.88
247B	0.60	37.24	213.9	53.20	16.61	1736.4	545.0	1.68	35.08	35.57	36.14	36.36	36.88
247C	1.05	37.42	217.9	52.26	17.09	1708.8	561.7	1.56	34.38	34.69	34.11	35.41	36.72
248B	1.25	36.88	171.1	36.05	15.68	1175.5	512.9	1.46	33.52	33.71	33.43	34.25	35.28
248C	0.55	36.83	168.0	37.10	15.55	1209.0	508.2	1.60	35.01	35.46	36.14	36.76	36.72

* DENOTES AN INCIPIENT RUN
** DENOTES A DESINENT RUN

Table A-2a. (cont'd)

RUN NO.	CAVITY INCHES	T0 DEG R	V0 FT/SEC	P0 PSIA	PV PSIA	H0 FT	HV FT	KV	T 1 DEG R	T 2 DEG R	T 3 DEG R	T 4 DEG R	T 5 DEG R
249B	1.57	37.08	191.5	42.25	16.19	1379.0	530.4	1.49	33.68	33.93	33.48	34.06	34.67
249C	0.45	37.13	189.5	44.67	16.33	1458.2	535.2	1.65	35.39	36.00	36.54	36.79	36.67
249D	0.75	37.26	190.6	43.82	16.66	1432.3	546.7	1.57	34.99	35.37	35.55	36.47	37.04
251A*		39.73	168.8	52.00	24.13	1739.6	811.2	2.10					
251B	0.80	39.76	185.3	44.00	24.26	1474.5	815.6	1.23	35.69	36.20	36.34	37.69	38.65
251C	0.42	39.76	181.5	45.70	24.26	1531.0	815.6	1.40	37.08	38.16	38.84	39.29	39.06
252A*		38.43	179.5	56.07	19.96	1850.1	662.2	2.37					
252B	1.15	38.34	198.7	46.40	19.69	1531.9	652.7	1.43	34.31	34.74	34.22	35.48	36.83
252C	0.80	38.54	198.1	47.27	20.28	1563.4	673.7	1.46	35.55	36.05	36.00	37.60	38.20
253A*		40.21	137.8	41.80	25.85	1408.1	873.2	1.81					
254B	0.50	36.79	166.6	35.30	15.46	1150.2	505.1	1.50	35.14	35.71	36.45	36.77	37.01
254C	0.72	36.95	167.2	35.10	15.86	1145.4	519.2	1.44	35.06	35.59	36.04	36.85	37.15
254D	1.58	36.81	167.0	34.32	15.50	1118.6	506.6	1.41	33.95	34.13	33.91	34.15	35.23
255A*		39.91	199.9	67.86	24.76	2268.7	833.7	2.31					
255B	1.60	39.87	219.1	55.80	24.63	1868.4	829.2	1.39	35.28	35.75	34.88	35.46	37.15
255C	0.72	39.96	217.9	57.82	24.95	1937.3	840.6	1.49	36.92	37.48	38.03	39.38	39.55
256A	0.40	37.94	194.2	47.60	18.53	1565.2	612.1	1.63	35.82	36.59	37.44	37.69	37.93
257B	0.92	38.02	218.6	54.60	18.74	1794.8	619.4	1.58	34.90	35.26	34.83	36.22	37.40
258A*		38.21	200.5	65.40	19.31	2150.5	639.6	2.42					
258B	0.90	38.29	218.7	54.72	19.53	1803.4	647.0	1.56	34.67	34.99	34.58	36.04	37.22
258C	0.42	38.43	214.1	56.70	19.96	1870.7	662.2	1.70	36.40	37.12	38.00	38.32	38.21
259A*		39.69	123.5	35.20	24.01	1180.4	806.7	1.58					
260A*		37.26	156.3	42.03	16.66	1374.2	546.7	2.18					
260B	1.12	37.30	170.8	35.80	16.75	1171.9	550.0	1.37	33.93	33.98	33.79	35.26	35.87

* DENOTES AN INCIPIENT RUN
** DENOTES A DESINENT RUN

Table A-2a. (cont'd)

RUN NO.	CAVITY INCHES	T0 DEG R	V0 FT/SEC	P0 PSIA	PV PSIA	H0 FT	HV FT	KV	T 1 DEG R	T 2 DEG R	T 3 DEG R	T 4 DEG R	T 5 DEG R
260C	0.82	37.30	167.8	36.07	16.75	1180.7	550.0	1.44	34.79	35.14	35.23	36.65	37.13
260D	0.35	37.46	164.6	37.40	17.19	1225.9	565.0	1.57	35.95	36.90	3 .46	37.40	37.51
261A*		36.77	119.2	28.90	15.41	942.3	503.5	1.99					
261B	1.10	36.83	128.4	24.16	15.55	788.7	508.2	1.09	33.93	34.56	34.60	35.86	36.22
261C	0.75	36.81	127.4	24.27	15.50	792.1	506.6	1.13	34.04	34.83	35.21	35.96	36.34
261D	0.40	36.81	127.4	24.90	15.50	812.6	506.6	1.21	34.61	35.91	36.32	36.31	36.43
262A*		37.06	120.5	28.90	16.14	944.9	528.8	1.84					
262B	1.15	37.03	130.7	24.90	16.05	814.3	525.6	1.09	33.37	33.68	33.86	35.14	35.39
262C	0.72	37.03	128.5	25.17	16.05	823.1	525.6	1.16	34.11	34.67	35.46	36.38	36.14
262D	0.38	37.10	127.2	25.90	16.23	847.4	532.0	1.25	35.03	36.25	36.59	36.95	36.65
263A*		38.21	153.3	47.07	19.31	1551.9	639.6	2.50					
263B	1.55	38.23	172.4	39.00	19.37	1287.6	641.4	1.40	34.04	33.93	33.80	35.05	35.60
263C	0.65	38.16	169.8	39.90	19.16	1316.2	634.0	1.52	35.26	35.73	36.18	37.58	37.49
264A*		40.07	166.7	53.70	25.33	1802.6	854.5	2.20					
264B	1.25	40.16	188.0	45.40	25.65	1527.6	866.1	1.20	35.64	36.18	35.50	36.79	38.61
264C	0.70	40.18	184.5	47.00	25.72	1581.3	868.5	1.35	37.21	37.89	38.65	39.96	39.96
265A*		40.01	139.2	43.30	25.14	1455.2	847.5	2.02					
265B	1.15	40.01	152.9	36.10	25.14	1214.7	847.5	1.01	36.20	36.94	36.61	39.20	39.08
265C	0.77	40.01	153.0	36.80	25.14	1238.1	847.5	1.07	36.47	37.31	38.11	39.22	38.92
265D	0.43	40.05	150.0	37.80	25.27	1272.0	852.1	1.20	37.37	38.54	39.24	39.35	39.49
266A*		36.61	105.2	24.10	15.01	785.2	489.7	1.72					
266B*		36.58	103.7	24.83	14.92	808.6	486.7	1.93					
267A**		36.65	114.9	28.43	15.10	926.0	492.8	2.11					
267B**		36.61	114.9	28.57	15.01	930.2	489.7	2.15					
268A**		36.97	149.6	41.81	15.91	1363.4	520.8	2.42					
269A	1.19	41.44	210.2	54.39	30.55	1853.6	1045.9	1.18	35.62	36.38	35.93	38.66	38.99

* DENOTES AN INCIPIENT RUN
** DENOTES A DESINENT RUN

Table A-2a. (cont'd)

RUN NO.	CAVITY INCHES	T0 DEG R	V0 FT/SEC	P0 PSIA	PV PSIA	H0 FT	HV FT	KV	T 1 DEG R	T 2 DEG R	T 3 DEG R	T 4 DEG R	T 5 DEG R
270A**		41.45	154.2	54.00	30.63	1840.8	1048.7	2.14					
270B	0.75	41.47	174.7	45.23	30.70	1544.8	1051.4	1.04	37.80	38.63	39.44	40.52	40.61
270C	1.17	41.42	176.9	44.26	30.48	1510.9	1043.2	0.96	37.58	38.18	38.34	40.36	40.64
271A**		41.56	154.8	53.20	31.07	1816.1	1065.1	2.02					
272A**		37.44	191.7	59.59	17.14	1946.8	563.4	2.42					
273A*		40.07	149.8	48.10	25.33	1616.1	854.5	2.18					
273B	0.75	40.01	172.2	40.33	25.14	1356.0	847.5	1.10	36.59	37.26	38.05	38.70	39.31
273C*		40.07	149.7	47.43	25.33	1593.8	854.5	2.12					
274D**		41.45	127.6	44.28	30.63	1512.3	1048.7	1.83					
275C**		41.36	107.7	37.63	30.26	1285.4	1035.1	1.39					
278A**		39.56	124.1	36.93	23.58	1236.4	791.2	1.86					
278D**		39.85	120.9	37.48	24.57	1258.6	826.9	1.90					
279A**		41.36	191.8	67.83	30.26	2304.0	1035.1	2.22					
281A	1.08	41.53	214.8	56.63	30.92	1931.2	1059.6	1.22	37.24	37.76	37.19	39.01	40.88
281C**		41.60	193.1	66.83	31.22	2276.6	1070.7	2.08					

* DENOTES AN INCIPIENT RUN
** DENOTES A DESINENT RUN

Table A-2a. (cont'd)

RUN NO.	P 1 PSIA	P 2 PSIA	P 3 PSIA	P 4 PSIA	P 5 PSIA	P 1,T PSIA	P 2,T PSIA	P 3,T PSIA	P 4,T PSIA	P 5,T PSIA
228B	9.35	9.40	10.00	11.68	14.40	9.95	10.22	10.62	11.91	13.60
228C	10.25	10.45	12.40	15.90	16.40	10.38	11.15	12.64	14.06	13.64
229B	9.68	9.90	10.80	14.85	17.15	9.00	9.56	10.28	12.80	13.93
229C	10.80	13.50	18.50	19.23	19.83	12.18	14.31	15.10	14.83	15.28
230B	8.75	9.05	9.80	11.65	15.80	11.77	11.47	11.44	13.89	14.97
230C	9.05	9.55	11.45	16.00	17.50	12.25	12.49	13.48	15.41	16.09
230D	9.35	10.30	13.80	17.45	18.25	12.33	13.04	14.70	15.73	15.91
231B	8.50	8.58	9.00	9.40	12.35	10.62	10.97	10.55	12.14	13.64
231C	9.10	9.65	10.80	19.75	22.85	11.44	12.64	13.64	16.85	16.90
231D	9.85	11.40	19.65	23.75	24.50	12.41	10.76	16.33	17.09	16.80
232B	10.48	9.65	10.25	11.65	25.30	9.34	9.89	9.22	12.14	14.40
233B	7.95	8.15	8.55	8.70	9.85	7.36	7.41	7.30	6.89	9.06
233C	8.45	8.75	9.50	12.85	20.75	8.18	8.76	9.03	10.35	12.96
235B	7.87	8.37	8.62	8.87	10.47	8.29	8.67	7.95	9.09	10.73
235C	8.75	9.10	9.50	12.50	22.60	9.31	9.89	9.40	12.18	14.31
237B	12.41	12.91	14.51	21.16	23.46	13.68	15.91	16.19	20.50	20.95
237C	12.80	13.90	17.80	23.45	24.75	14.36	17.38	19.00	20.78	21.51
237D	13.56	15.46	22.66	24.86	25.76	16.28	20.39	21.80	22.15	22.56
239B	13.40	13.50	14.20	16.70	26.60	13.64	14.66	13.89	17.83	22.32
239C	14.56	14.86	16.31	27.09	30.76	15.50	17.14	18.13	23.09	24.51
240B	11.00	10.60	10.60	22.60	31.50	11.51	11.55	11.40	15.59	15.46
240C	10.45	9.80	10.50	10.55	16.00	11.40	11.08	9.89	11.08	14.14
241B	10.60	10.65	11.10	13.20	21.40	10.42	11.33	10.59	13.04	16.00
242B	8.15	8.65	9.80	9.10	10.35	9.47	8.94	8.15	7.81	9.28
243B	9.40	10.25	10.85	16.15	26.35	8.94	9.53	9.76	11.58	12.64

Table A-2a. (cont'd)

RUN NO.	P 1 PSIA	P 2 PSIA	P 3 PSIA	P 4 PSIA	P 5 PSIA	P 1,T PSIA	P 2,T PSIA	P 3,T PSIA	P 4,T PSIA	P 5,T PSIA
244B	9.25	9.20	9.45	11.05	13.75	9.79	9.92	11.51	11.44	11.69
244C	9.95	10.60	14.15	15.55	16.05	9.79	10.73	11.88	13.08	12.68
244D	10.28	12.07	15.63	16.03	16.58	10.97	12.29	12.96	13.93	13.36
244E	9.32	9.47	10.12	13.17	14.92	10.02	10.59	11.44	13.04	13.68
245B	9.05	9.05	9.15	9.20	10.40	8.20	8.12	7.98	9.40	9.22
245C	9.15	9.18	9.08	9.75	12.45	8.26	8.32	8.29	9.66	10.42
245D	9.95	9.95	11.35	15.80	17.50	9.69	10.42	11.58	13.56	13.16
246A	9.00	8.85	8.05	9.15	16.15	11.26	11.88	10.62	12.03	15.68
247B	10.80	10.45	13.20	32.55	34.45	11.58	12.60	13.89	14.40	15.68
247C	9.36	8.96	8.26	12.11	26.11	10.22	10.80	9.72	12.25	15.28
248B	8.65	8.45	8.05	8.90	14.25	8.70	9.03	8.55	9.98	11.99
248C	10.08	9.90	12.40	23.70	24.80	11.44	12.37	13.89	15.37	15.28
249B	8.30	8.19	7.88	7.95	9.75	8.97	9.40	8.64	9.63	10.76
249C	10.67	11.02	21.84	29.22	30.02	12.22	13.56	14.83	15.46	15.14
249D	9.77	9.32	9.72	19.92	28.07	11.40	12.18	12.56	14.66	16.09
251B	13.30	13.30	13.77	22.37	29.40	12.88	14.02	14.36	17.83	20.61
251C	15.00	16.20	27.50	31.60	32.75	16.19	19.16	21.23	22.68	21.92
252B	10.20	9.70	9.77	11.67	24.20	10.08	10.90	9.92	12.41	15.55
252C	11.32	10.57	11.27	18.72	28.57	12.56	13.68	13.56	17.58	19.26
254B	9.10	9.55	13.20	22.60	23.80	11.69	12.92	14.62	15.41	16.00
254C	9.00	9.05	10.05	18.45	23.10	11.55	12.64	13.64	15.59	16.37
254D	8.07	8.07	8.07	8.42	10.57	9.44	9.76	9.37	9.79	11.88
255B	11.20	11.00	11.15	11.30	15.30	11.99	13.00	11.18	12.37	16.37
255C	15.07	14.67	16.12	34.42	38.12	15.77	17.23	18.79	22.97	23.52
256A	12.20	13.05	23.10	31.55	32.70	13.16	14.97	17.14	17.83	18.48
257B	11.40	11.10	10.30	14.90	27.90	11.22	11.95	11.08	14.06	17.04

Table A-2a. (cont'd)

RUN NO.	P 1 PSIA	P 2 PSIA	P 3 PSIA	P 4 PSIA	P 5 PSIA	P 1,T PSIA	P 2,T PSIA	P 3,T PSIA	P 4,T PSIA	P 5,T PSIA
258B	11.37	11.07	10.72	15.82	29.52	10.76	11.40	10.59	13.64	16.56
258C	13.35	13.50	22.20	36.50	37.75	14.49	16.28	18.69	19.63	19.31
260B	9.85	9.65	9.55	11.30	18.15	9.40	9.50	9.15	11.95	13.28
260C	10.17	10.27	10.62	15.67	23.97	11.01	11.69	11.88	15.10	16.33
260D	11.25	13.27	22.90	25.58	26.55	13.44	15.73	17.19	17.04	17.33
261B	9.11	9.41	9.91	12.76	16.06	9.40	10.55	10.62	13.24	14.06
261C	9.37	9.72	10.97	15.87	17.32	9.59	11.08	11.84	13.48	14.36
261D	10.10	11.40	16.50	18.00	18.50	10.66	13.36	14.31	14.27	14.57
262B	9.45	9.70	10.05	12.65	16.50	8.46	8.97	9.28	11.69	12.22
262C	9.92	10.57	12.67	17.32	18.42	9.72	10.76	12.37	14.44	13.89
262D	10.85	12.95	18.00	18.95	19.60	11.47	14.14	14.97	15.86	15.10
263B	10.40	10.45	10.45	10.70	13.10	9.59	9.40	9.19	11.51	12.68
263C	12.20	12.20	13.34	24.97	27.45	11.95	12.96	13.98	17.53	17.28
264B	13.35	12.95	13.00	13.95	21.55	12.76	13.98	12.45	15.46	20.50
264C	15.83	15.70	17.70	31.10	32.98	16.52	18.38	20.61	24.95	24.95
265B	14.70	14.55	15.00	21.70	25.50	14.02	15.82	15.01	22.38	21.97
265C	15.35	15.50	18.40	25.60	27.20	14.66	16.80	19.00	22.44	21.46
265D	16.27	17.73	24.60	27.95	28.80	16.94	20.28	22.50	22.86	23.34
269A	14.79	14.64	14.49	17.79	31.09	12.72	14.44	13.40	20.67	21.68
270B	17.48	17.98	22.23	31.63	33.38	18.13	20.56	23.15	26.97	27.31
270C	16.16	16.26	17.06	26.56	31.06	17.53	19.21	19.69	26.37	27.45
273B	15.13	15.38	17.13	26.53	28.93	14.97	16.66	18.84	20.78	22.74
281A	16.73	16.53	16.38	21.33	35.63	16.61	18.03	16.47	21.74	28.34

Table A-2a. (cont'd)

RUN NO.	H 1 FT	H 2 FT	H 3 FT	H 4 FT	H 5 FT	H 1,T FT	H 2,T FT	H 3,T FT	H 4,T FT	H 5,T FT
228B	298.1	299.8	319.8	376.2	468.8	318.2	327.0	340.7	384.2	441.5
228C	328.2	334.9	400.6	520.4	537.7	332.7	358.3	408.7	457.1	442.9
229B	309.1	316.5	346.6	484.2	563.8	286.6	305.2	329.3	414.1	452.8
229C	346.6	438.0	611.0	636.6	657.7	393.1	465.9	492.8	483.7	498.9
230B	278.2	288.2	313.1	375.2	517.0	379.1	369.2	368.0	451.4	488.2
230C	288.2	304.8	368.5	523.9	576.0	395.7	403.5	437.3	503.5	527.2
230D	298.1	329.8	448.2	574.3	602.2	398.2	422.2	479.2	514.4	520.8
231B	270.0	272.6	286.5	299.8	398.9	340.7	352.3	338.4	391.8	442.9
231C	289.8	308.1	346.6	654.9	765.1	368.0	408.7	442.9	553.3	555.0
231D	314.8	366.8	651.4	797.4	824.4	400.9	345.3	535.2	561.7	551.6
232B	335.9	308.1	328.2	375.2	853.3	297.9	316.0	293.7	391.8	468.8
233B	251.8	258.4	271.6	276.6	314.8	232.3	234.0	230.5	217.1	288.6
233C	268.3	278.2	303.1	415.9	690.3	259.3	278.6	287.6	331.5	419.4
235B	249.2	265.7	273.9	282.2	335.5	263.0	275.6	251.8	289.6	344.1
235C	278.2	289.8	303.1	404.0	756.1	296.8	316.0	299.9	393.1	465.9
237B	400.9	417.9	472.6	704.8	787.0	444.3	520.8	530.4	681.5	697.3
237C	414.2	451.7	586.5	786.6	833.4	467.3	571.8	628.5	691.3	717.4
237D	440.0	505.2	758.3	837.4	870.0	533.6	677.6	727.6	740.0	754.7
239B	434.6	438.0	461.9	548.2	900.6	442.9	477.7	451.4	587.4	746.2
239C	474.3	484.6	534.6	918.4	1053.6	506.6	563.4	597.9	773.9	824.6
240B	353.3	339.9	339.9	756.1	1081.1	370.4	371.7	366.8	509.7	505.1
240C	334.9	313.1	336.5	338.2	523.9	366.8	355.9	316.0	355.9	460.0
241B	339.9	341.6	356.7	427.8	713.3	333.8	364.3	339.5	422.2	524.0
242B	258.4	274.9	313.1	289.8	331.5	302.1	284.5	258.3	247.3	295.8
243B	299.8	328.2	348.3	529.1	891.5	284.5	304.2	311.6	372.9	408.7

Table A-2a. (cont'd)

RUN NO.	H 1 FT	H 2 FT	H 3 FT	H 4 FT	H 5 FT	H 1,T FT	H 2,T FT	H 3,T FT	H 4,T FT	H 5,T FT
244B	294.8	293.2	301.5	355.0	446.5	312.7	317.1	370.4	368.0	376.6
244C	318.1	339.9	460.2	508.3	525.6	312.7	344.1	382.9	423.5	410.1
244D	329.2	389.4	511.1	524.9	544.0	352.3	397.0	419.4	452.8	433.1
244E	297.1	302.1	323.8	426.7	486.6	320.4	339.5	368.0	422.2	444.3
245B	288.2	288.2	291.5	293.2	333.2	260.2	257.4	252.8	299.9	293.7
245C	291.5	292.5	289.2	311.5	402.3	262.1	264.0	263.0	308.4	333.8
245D	318.1	318.1	365.1	517.0	576.0	309.5	333.8	372.9	440.1	426.2
246A	286.5	281.5	255.1	291.5	529.1	361.9	382.9	340.7	388.0	512.9
247B	346.6	334.9	427.8	1120.3	1191.7	372.9	407.4	451.4	468.8	512.9
247C	298.5	285.2	262.0	390.8	882.7	327.0	346.5	310.6	395.7	498.9
248B	274.9	268.3	255.1	283.2	463.6	276.6	287.6	271.7	319.3	386.7
248C	322.5	316.5	400.6	795.6	835.2	368.0	399.5	451.4	502.0	498.9
249B	263.3	259.7	249.5	251.8	311.5	285.6	299.9	274.6	307.4	345.3
249C	342.2	354.0	729.0	996.6	1026.2	394.4	440.1	483.7	505.1	494.3
249D	312.1	297.1	310.5	660.9	954.3	366.8	393.1	406.1	477.7	527.2
251B	431.2	431.2	447.2	747.9	1003.3	416.8	455.7	467.3	587.4	685.4
251C	489.4	530.8	933.4	1084.8	1127.8	530.4	634.0	707.3	758.9	731.7
252B	326.5	309.8	312.1	375.9	813.6	322.6	350.0	317.1	400.9	508.2
252C	364.1	338.9	362.4	618.7	972.7	406.1	444.3	440.1	578.7	637.7
254B	289.8	304.8	427.8	756.1	799.2	376.6	418.1	476.2	503.5	524.0
254C	286.5	288.2	321.5	609.2	774.0	371.7	408.7	442.9	509.7	536.8
254D	255.8	255.8	255.8	267.3	338.9	301.0	311.6	298.9	312.7	382.9
255B	360.0	353.3	358.4	363.4	499.7	386.7	420.8	359.5	399.5	536.8
255C	491.8	478.0	528.0	1190.6	1331.3	516.0	566.7	621.2	769.6	789.1
256A	393.8	422.7	774.0	1083.0	1125.9	426.2	488.2	563.4	587.4	610.3
257B	366.8	356.7	329.8	485.9	948.1	360.7	385.4	355.9	457.1	560.0

Table A-2a. (cont'd)

RUN NO.	H 1 FT	H 2 FT	H 3 FT	H 4 FT	H 5 FT	H 1,T FT	H 2,T FT	H 3,T FT	H 4,T FT	H 5,T FT
258B	365.8	355.7	343.9	517.7	1007.7	345.3	366.8	339.5	442.9	543.4
258C	432.9	438.0	741.9	1269.4	1317.2	471.7	533.6	617.6	650.8	639.6
260B	314.8	308.1	304.8	363.4	598.7	299.9	303.1	291.7	385.4	430.4
260C	325.5	328.8	340.6	512.5	805.3	353.5	376.6	382.9	492.8	535.2
260D	361.7	430.1	766.9	863.5	898.7	435.9	514.4	565.0	560.0	570.1
261B	290.2	300.1	316.8	412.8	526.0	299.9	338.4	340.7	429.0	457.1
261C	298.8	310.5	352.3	519.4	569.7	306.3	355.9	381.6	437.3	467.3
261D	323.2	366.8	541.2	593.5	611.0	341.8	433.1	465.9	464.4	474.7
262B	301.5	309.8	321.5	409.1	541.2	268.8	285.6	295.8	376.6	394.4
262C	317.1	338.9	409.7	569.7	608.2	310.6	345.3	399.5	470.3	451.4
262D	348.3	419.3	593.5	626.7	649.6	369.2	460.0	488.2	519.2	492.8
263B	333.2	334.9	334.9	343.2	424.4	306.3	299.9	292.7	370.4	410.1
263C	393.8	393.8	432.5	841.4	931.6	385.4	419.4	454.3	577.0	568.4
264B	432.9	419.3	421.0	453.4	718.7	412.7	454.3	402.2	505.1	681.5
264C	518.0	513.5	583.0	1066.2	1136.4	541.7	606.8	685.4	840.6	840.6
265B	479.1	473.9	489.4	724.0	860.6	455.7	517.6	489.7	748.3	733.8
265C	501.4	506.6	607.5	864.2	922.5	477.7	551.6	628.5	750.4	715.3
265D	533.2	584.0	828.0	949.9	981.1	556.6	673.7	752.6	765.3	782.5
269A	482.2	477.0	471.9	586.1	1065.9	411.4	470.3	434.5	687.4	723.5
270B	575.3	592.8	742.9	1086.0	1151.4	597.9	683.5	776.0	914.2	926.5
270C	529.4	532.9	560.7	899.1	1064.7	577.0	635.9	652.7	892.3	931.4
273B	493.9	502.5	563.1	898.0	985.9	488.2	546.7	623.0	691.3	761.0
281A	549.2	542.3	537.1	710.9	1236.4	545.0	594.4	540.1	725.5	964.2

Table A-2b. Experimental cavitation data for 0.312-inch hydrofoil using liquid hydrogen (SI Units).

RUN NO.	CAVITY CM	T0 DEG K	V0 M/SEC	P0 N/CM/CM	PV N/CM/CM	H0 M	HV M	KV	T 1 DEG K	T 2 DEG K	T 3 DEG K	T 4 DEG K	T 5 DEG K
228A*		20.46	32.5	16.27	10.72	234.8	154.9	1.49					
228B	3.32	20.46	37.3	14.41	10.72	208.0	154.9	0.75	19.02	19.10	19.22	19.58	20.01
228C	1.90	20.43	36.2	14.96	10.62	215.9	153.5	0.93	19.15	19.37	19.77	20.12	20.02
228E**		20.45	34.4	16.96	10.69	244.7	154.4	1.50					
229B	2.28	20.64	41.4	17.10	11.29	247.5	163.6	0.96	18.72	18.90	19.12	19.81	20.09
229C	0.88	20.62	40.4	18.00	11.22	260.3	162.6	1.17	19.65	20.18	20.36	20.30	20.40
229D**		20.64	36.9	20.48	11.29	296.2	163.6	1.91					
230B	3.17	20.64	40.5	16.69	11.29	241.5	163.6	0.93	19.54	19.46	19.45	20.08	20.33
230C	2.08	20.64	40.5	16.93	11.29	245.0	163.6	0.97	19.67	19.73	19.98	20.43	20.58
230D	1.32	20.60	40.7	17.24	11.16	249.3	161.7	1.04	19.69	19.87	20.27	20.50	20.54
231B	4.06	20.57	51.8	23.37	11.06	337.5	160.2	1.30	19.22	19.32	19.20	19.64	20.02
231C	1.77	20.63	51.4	23.79	11.26	343.8	163.1	1.34	19.45	19.77	20.02	20.74	20.75
231D	1.01	20.61	50.4	24.41	11.19	352.6	162.1	1.47	19.71	19.26	20.63	20.79	20.73
232B	2.79	20.96	64.9	35.89	12.36	520.3	180.1	1.59	18.83	19.00	18.79	19.64	20.20
233A*		20.55	45.6	30.10	11.00	433.9	159.2	2.59					
233B	4.31	20.59	52.4	23.92	11.13	345.5	161.2	1.31	18.14	18.16	18.12	17.96	18.74
233C	2.54	20.56	52.1	24.27	11.03	350.3	159.7	1.38	18.44	18.64	18.73	19.14	19.85
233D**		20.82	46.4	30.50	11.88	441.5	172.7	2.45					
235B	4.31	20.88	59.0	29.35	12.09	425.5	175.9	1.41	18.48	18.61	18.36	18.75	19.25
235C	2.61	20.88	58.3	29.72	12.09	430.8	175.9	1.47	18.82	19.00	18.85	19.65	20.18
236 *		22.22	36.4	23.17	17.29	344.7	257.6	1.29					
237B	3.04	22.01	47.5	22.93	16.38	339.8	243.2	0.84	20.03	20.54	20.60	21.45	21.53
237C	2.03	22.01	47.2	23.17	16.38	343.3	243.2	0.88	20.19	20.85	21.17	21.50	21.63
237D	1.14	22.07	46.8	23.69	16.64	351.4	247.2	0.93	20.62	21.43	21.68	21.74	21.81

* DENOTES AN INCIPIENT RUN
** DENOTES A DESINENT RUN

Table A-2b. (cont'd)

RUN NO.	CAVITY CM	T0 DEG K	V0 M/SEC	P0 N/CM/CM	PV N/CM/CM	H0 M	HV M	KV	T 1 DEG K	T 2 DEG K	T 3 DEG K	T 4 DEG K	T 5 DEG K
239A*		22.48	49.8	36.20	18.46	539.6	276.4	2.08					
239B	3.04	22.55	54.7	29.99	18.78	448.4	281.6	1.09	20.02	20.26	20.08	20.94	21.77
239C	2.03	22.52	55.0	30.38	18.64	453.9	279.4	1.13	20.45	20.80	21.00	21.90	22.13
240B	1.90	21.25	66.6	36.75	13.39	535.3	196.1	1.50	19.47	19.48	19.44	20.47	20.44
240C	3.55	21.45	66.5	36.99	14.14	540.7	207.7	1.48	19.44	19.35	19.00	19.35	20.14
241B	2.84	21.27	55.3	26.86	13.46	392.2	197.2	1.25	19.16	19.42	19.21	19.87	20.56
242A*		20.69	55.4	35.65	11.45	514.4	166.1	2.23					
242B	4.44	20.70	59.4	29.79	11.48	430.4	166.6	1.47	18.87	18.70	18.43	18.31	18.81
243B	2.03	20.70	58.7	30.27	11.48	437.4	166.6	1.54	18.70	18.89	18.96	19.49	19.77
244A*		20.38	32.4	16.20	10.47	233.5	151.1	1.54					
244B	3.30	20.29	35.5	14.07	10.20	202.5	147.0	0.87	18.97	19.01	19.47	19.45	19.52
244C	1.14	20.26	34.9	14.55	10.11	209.3	145.6	1.03	18.97	19.25	19.57	19.88	19.78
244D	1.01	20.30	34.5	14.75	10.23	212.4	147.4	1.07	19.32	19.68	19.85	20.09	19.95
244E	3.04	20.30	35.3	14.22	10.23	204.7	147.4	0.90	19.04	19.21	19.45	19.87	20.03
245A*		20.43	35.9	19.58	10.62	282.3	153.5	1.96					
245B	4.26	20.43	39.6	16.38	10.62	236.2	153.5	1.03	18.45	18.42	18.37	18.85	18.79
245C	3.55	20.46	39.4	16.44	10.72	237.3	154.9	1.04	18.47	18.49	18.48	18.93	19.16
245D	1.90	20.50	39.2	16.82	10.84	242.9	156.8	1.10	18.94	19.16	19.49	20.00	19.90
245E**		20.59	34.5	19.99	11.13	289.0	161.2	2.10					
246A	3.17	20.84	64.0	35.61	11.95	515.2	173.8	1.64	19.40	19.57	19.22	19.61	20.49
247B	1.52	20.69	65.2	36.68	11.45	529.3	166.1	1.68	19.49	19.76	20.08	20.20	20.49
247C	2.66	20.79	66.4	36.03	11.78	520.8	171.2	1.56	19.10	19.27	18.95	19.67	20.40
248B	3.17	20.49	52.1	24.86	10.81	358.3	156.3	1.46	18.62	18.73	18.57	19.03	19.60
248C	1.39	20.46	51.2	25.58	10.72	368.5	154.9	1.60	19.45	19.70	20.08	20.42	20.40

* DENOTES AN INCIPIENT RUN
* DENOTES A DESINENT RUN

Table A-2b. (cont'd)

RUN NO.	CAVITY CM	T0 DEG K	V0 M/SEC	P0 N/CM/CM	PV N/CM/CM	H0 M	HV M	KV	T 1 DEG K	T 2 DEG K	T 3 DEG K	T 4 DEG K	T 5 DEG K
249B	3.98	20.60	58.4	29.13	11.16	420.3	161.7	1.49	18.71	18.85	18.60	18.92	19.26
249C	1.14	20.63	57.8	30.80	11.26	444.5	163.1	1.65	19.66	20.00	20.30	20.44	20.37
249D	1.90	20.70	58.1	30.21	11.48	436.6	166.6	1.57	19.44	19.65	19.75	20.26	20.58
251A*		22.07	51.5	35.85	16.64	530.2	247.2	2.10					
251B	2.03	22.09	56.5	30.34	16.72	449.4	248.6	1.23	19.83	20.11	20.19	20.94	21.47
251C	1.06	22.09	55.3	31.51	16.72	466.7	248.6	1.40	20.60	21.20	21.58	21.83	21.70
252A*		21.35	54.7	38.66	13.76	563.9	201.8	2.37					
252B	2.92	21.30	60.6	31.99	13.57	466.9	198.9	1.43	19.06	19.30	19.01	19.71	20.46
252C	2.03	21.41	60.4	32.59	13.98	476.5	205.4	1.46	19.75	20.03	20.00	20.89	21.22
253A*		22.34	42.0	28.82	17.82	429.2	266.2	1.81					
254B	1.27	20.44	50.8	24.34	10.66	350.6	153.9	1.50	19.52	19.84	20.25	20.43	20.56
254C	1.82	20.53	51.0	24.20	10.94	349.1	158.2	1.44	19.48	19.77	20.02	20.47	20.64
254D	4.01	20.45	50.9	23.66	10.69	341.0	154.4	1.41	18.86	18.96	18.84	18.97	19.57
255A*		22.17	60.9	46.79	17.07	691.5	254.1	2.31					
255B	4.06	22.15	66.8	38.47	16.98	569.5	252.7	1.39	19.60	19.86	19.38	19.70	20.64
255C	1.82	22.20	66.4	39.87	17.20	590.5	256.2	1.49	20.51	20.82	21.13	21.88	21.97
256A	1.01	21.08	59.2	32.82	12.78	477.1	186.6	1.63	19.90	20.33	20.80	20.94	21.07
257B	2.33	21.12	66.6	37.65	12.92	547.0	188.8	1.58	19.39	19.59	19.35	20.12	20.78
258A*		21.23	61.1	45.09	13.32	655.5	194.9	2.42					
258B	2.28	21.27	66.7	37.73	13.46	549.7	197.2	1.56	19.26	19.44	19.21	20.02	20.68
258C	1.06	21.35	65.3	39.09	13.76	570.2	201.8	1.70	20.22	20.62	21.11	21.29	21.23
259A*		22.05	37.6	24.27	16.55	359.8	245.9	1.58					
260A*		20.70	47.6	28.98	11.48	418.8	166.6	2.18					
260B	2.84	20.72	52.1	24.68	11.55	357.2	167.6	1.37	18.85	18.88	18.77	19.59	19.93

* DENOTES AN INCIPIENT RUN
** DENOTES A DESINENT RUN

Table A-2b. (cont'd)

RUN NO.	CAVITY CM	T0 DEG K	V0 M/SEC	P0 N/CM/CM	PV N/CM/CM	H0 M	HV M	KV	T 1 DEG K	T 2 DEG K	T 3 DEG K	T 4 DEG K	T 5 DEG K
260C	2.08	20.72	51.1	24.87	11.55	359.9	167.6	1.44	19.33	19.52	19.57	20.36	20.63
260D	0.88	20.81	50.2	25.79	11.85	373.6	172.2	1.57	19.97	20.50	20.81	20.78	20.84
261A*		20.43	36.3	19.93	10.62	287.2	153.5	1.99					
261B	2.79	20.46	39.1	16.66	10.72	240.4	154.9	1.09	18.85	19.20	19.22	19.92	20.12
261C	1.90	20.45	38.8	16.73	10.69	241.4	154.4	1.13	18.91	19.35	19.56	19.98	20.19
261D	1.01	20.45	38.8	17.17	10.69	247.7	154.4	1.21	19.23	19.95	20.18	20.17	20.24
262A*		20.59	36.7	19.93	11.13	288.0	161.2	1.84					
262B	2.92	20.57	39.8	17.17	11.06	248.2	160.2	1.09	18.54	18.71	18.81	19.52	19.66
262C	1.82	20.57	39.2	17.35	11.06	250.9	160.2	1.16	18.95	19.26	19.70	20.21	20.08
262D	0.96	20.61	38.8	17.86	11.19	258.3	162.1	1.25	19.46	20.14	20.33	20.53	20.36
263A*		21.23	46.7	32.45	13.32	473.0	194.9	2.50					
263B	3.93	21.24	52.6	26.89	13.35	392.5	195.5	1.40	18.91	18.85	18.78	19.47	19.78
263C	1.65	21.20	51.8	27.51	13.21	401.2	193.2	1.52	19.59	19.85	20.10	20.88	20.83
264A*		22.26	50.8	37.02	17.47	549.4	260.4	2.20					
264B	3.17	22.31	57.3	31.30	17.69	465.6	264.0	1.20	19.80	20.10	19.72	20.44	21.45
264C	1.77	22.32	56.2	32.41	17.73	482.0	264.7	1.35	20.67	21.05	21.47	22.20	22.20
265A*		22.23	42.4	29.85	17.33	443.5	258.3	2.02					
265B	2.92	22.23	46.6	24.89	17.33	370.2	258.3	1.01	20.11	20.52	20.34	21.78	21.71
265C	1.95	22.23	46.6	25.37	17.33	377.4	258.3	1.07	20.26	20.73	21.17	21.79	21.62
265D	1.09	22.25	45.7	26.06	17.42	387.7	259.7	1.20	20.76	21.41	21.80	21.86	21.94
266A*		20.34	32.1	16.62	10.35	239.3	149.3	1.72					
266B*		20.32	31.6	17.12	10.29	246.5	148.3	1.93					
267A**		20.36	35.0	19.60	10.41	282.2	150.2	2.11					
267B**		20.34	35.0	19.70	10.35	283.5	149.3	2.15					
268A**		20.54	45.6	28.83	10.97	415.6	158.7	2.42					
269A	3.02	23.02	64.1	37.50	21.07	565.0	318.8	1.18	19.79	20.21	19.96	21.48	21.66

* DENOTES AN INCIPIENT RUN
** DENOTES A DESINENT RUN

Table A-2b. (cont'd)

RUN NO.	CAVITY CM	T0 DEG K	V0 M/SEC	P0 N/CM/CM	PV N/CM/CM	H0 M	HV M	KV	T 1 DEG K	T 2 DEG K	T 3 DEG K	T 4 DEG K	T 5 DEG K
270A**		23.03	47.0	37.23	21.12	561.1	319.6	2.14					
270B	1.90	23.04	53.3	31.18	21.17	470.8	320.5	1.04	21.00	21.46	21.91	22.51	22.56
270C	2.97	23.01	53.9	30.52	21.02	460.5	318.0	0.96	20.88	21.21	21.30	22.42	22.58
271A**		23.09	47.2	36.68	21.42	553.6	324.7	2.02					
272A**		20.80	58.4	41.09	11.82	593.4	171.7	2.42					
273A*		22.26	45.7	33.16	17.47	492.6	260.4	2.18					
273B	1.90	22.23	52.5	27.81	17.33	413.3	258.3	1.10	20.33	20.70	21.14	21.50	21.84
273C*		22.26	45.6	32.70	17.47	485.8	260.4	2.12					
274D**		23.03	38.9	30.53	21.12	460.9	319.6	1.83					
275C**		22.98	32.8	25.94	20.86	391.8	315.5	1.39					
278A**		21.98	37.8	25.46	16.26	376.9	241.2	1.86					
278D**		22.14	36.9	25.84	16.94	383.6	252.0	1.90					
279A**		22.98	58.4	46.77	20.86	702.3	315.5	2.22					
281A	2.74	23.07	65.5	39.05	21.32	588.6	323.0	1.22	20.69	20.98	20.66	21.67	22.71
281C**		23.11	58.8	46.08	21.52	693.9	326.3	2.08					

* DENOTES AN INCIPIENT RUN
** DENOTES A DESINENT RUN

Table A-2b. (cont'd)

RUN NO.	P 1 N/CM/CM	P 2 N/CM/CM	P 3 N/CM/CM	P 4 N/CM/CM	P 5 N/CM/CM	P 1,T N/CM/CM	P 2,T N/CM/CM	P 3,T N/CM/CM	P 4,T N/CM/CM	P 5,T N/CM/CM
228B	6.45	6.48	6.89	8.05	9.93	6.86	7.04	7.32	8.21	9.38
228C	7.07	7.21	8.55	10.96	11.31	7.16	7.69	8.72	9.69	9.41
229B	6.67	6.83	7.45	10.24	11.82	6.21	6.59	7.09	8.82	9.61
229C	7.45	9.31	12.76	13.26	13.67	8.40	9.87	10.41	10.23	10.53
230B	6.03	6.24	6.76	8.03	10.89	8.11	7.91	7.88	9.58	10.32
230C	6.24	6.58	7.89	11.03	12.07	8.45	8.61	9.29	10.62	11.10
230D	6.45	7.10	9.51	12.03	12.58	8.50	8.99	10.14	10.84	10.97
231B	5.86	5.92	6.21	6.48	8.52	7.32	7.56	7.28	8.37	9.41
231C	6.27	6.65	7.45	13.62	15.75	7.88	8.72	9.41	11.62	11.65
231D	6.79	7.86	13.55	16.38	16.89	8.56	7.42	11.26	11.78	11.58
232B	7.23	6.65	7.07	8.03	17.44	6.44	6.82	6.35	8.37	9.93
233B	5.48	5.62	5.90	6.00	6.79	5.07	5.11	5.04	4.75	6.25
233C	5.83	6.03	6.55	8.86	14.31	5.64	6.04	6.23	7.14	8.93
235B	5.43	5.77	5.94	6.12	7.22	5.72	5.98	5.48	6.27	7.40
235C	6.03	6.27	6.55	8.62	15.58	6.42	6.82	6.48	8.40	9.87
237B	8.56	8.90	10.00	14.59	16.18	9.44	10.97	11.16	14.14	14.44
237C	8.83	9.58	12.27	16.17	17.06	9.90	11.98	13.10	14.33	14.83
237D	9.35	10.66	15.62	17.14	17.76	11.22	14.06	15.03	15.27	15.55
239B	9.24	9.31	9.79	11.51	18.34	9.41	10.11	9.58	12.29	15.39
239C	10.04	10.25	11.25	18.68	21.21	10.69	11.82	12.50	15.92	16.90
240B	7.58	7.31	7.31	15.58	21.72	7.93	7.96	7.86	10.75	10.66
240C	7.21	6.76	7.24	7.27	11.03	7.86	7.64	6.82	7.64	9.75
241B	7.31	7.34	7.65	9.10	14.75	7.18	7.81	7.30	8.99	11.03
242B	5.62	5.96	6.76	6.27	7.14	6.53	6.16	5.62	5.39	6.40
243B	6.48	7.07	7.48	11.14	18.17	6.16	6.57	6.73	7.99	8.72

Table A-2b. (cont'd)

RUN NO.	P 1 N/CM/CM	P 2 N/CM/CM	P 3 N/CM/CM	P 4 N/CM/CM	P 5 N/CM/CM	P 1,T N/CM/CM	P 2,T N/CM/CM	P 3,T N/CM/CM	P 4,T N/CM/CM	P 5,T N/CM/CM
244B	6.38	6.34	6.52	7.62	9.48	6.75	6.84	7.93	7.88	8.06
244C	6.86	7.31	9.76	10.72	11.07	6.75	7.40	8.19	9.01	8.74
244D	7.09	8.32	10.78	11.05	11.43	7.56	8.48	8.93	9.61	9.21
244E	6.43	6.53	6.98	9.08	10.29	6.91	7.30	7.88	8.99	9.44
245B	6.24	6.24	6.31	6.34	7.17	5.66	5.60	5.50	6.48	6.35
245C	6.31	6.33	6.26	6.72	8.58	5.70	5.74	5.72	6.66	7.18
245D	6.86	6.86	7.83	10.89	12.07	6.68	7.18	7.99	9.35	9.07
246A	6.21	6.10	5.55	6.31	11.14	7.76	8.19	7.32	8.29	10.81
247B	7.45	7.21	9.10	22.44	23.75	7.99	8.69	9.58	9.93	10.81
247C	6.45	6.18	5.70	8.35	18.00	7.04	7.44	6.70	8.45	10.53
248B	5.96	5.83	5.55	6.14	9.83	6.00	6.23	5.90	6.88	8.27
248C	6.95	6.83	8.55	16.34	17.10	7.88	8.53	9.58	10.59	10.53
249B	5.72	5.65	5.43	5.48	6.72	6.19	6.48	5.96	6.64	7.42
249C	7.36	7.60	15.06	20.15	20.70	8.42	9.35	10.23	10.66	10.44
249D	6.74	6.43	6.70	13.73	19.35	7.86	8.40	8.66	10.11	11.10
251B	9.17	9.17	9.49	15.42	20.27	8.88	9.67	9.90	12.29	14.21
251C	10.34	11.17	18.96	21.79	22.58	11.16	13.21	14.64	15.64	15.11
252B	7.03	6.69	6.74	8.05	16.69	6.95	7.52	6.84	8.56	10.72
252C	7.80	7.29	7.77	12.91	19.70	8.66	9.44	9.35	12.12	13.28
254B	6.27	6.58	9.10	15.58	16.41	8.06	8.91	10.08	10.62	11.03
254C	6.21	6.24	6.93	12.72	15.93	7.96	8.72	9.41	10.75	11.29
254D	5.56	5.56	5.56	5.81	7.29	6.51	6.73	6.46	6.75	8.19
255B	7.72	7.58	7.69	7.79	10.55	8.27	8.96	7.71	8.53	11.29
255C	10.39	10.11	11.11	23.73	26.28	10.87	11.88	12.96	15.84	16.22
256A	8.41	9.00	15.93	21.75	22.55	9.07	10.32	11.82	12.29	12.74
257B	7.86	7.65	7.10	10.27	19.24	7.74	8.24	7.64	9.69	11.75

Table A-2b. (cont'd)

RUN NO.	P 1 N/CM/CM	P 2 N/CM/CM	P 3 N/CM/CM	P 4 N/CM/CM	P 5 N/CM/CM	P 1,T N/CM/CM	P 2,T N/CM/CM	P 3,T N/CM/CM	P 4,T N/CM/CM	P 5,T N/CM/CM
258B	7.84	7.63	7.39	10.91	20.35	7.42	7.86	7.30	9.41	11.42
258C	9.20	9.31	15.31	25.17	26.03	9.99	11.22	12.89	13.54	13.32
260B	6.79	6.65	6.58	7.79	12.51	6.48	6.55	6.31	8.24	9.15
260C	7.01	7.08	7.32	10.80	16.53	7.59	8.06	8.19	10.41	11.26
260D	7.76	9.15	15.79	17.64	18.31	9.27	10.84	11.85	11.75	11.95
261B	6.28	6.49	6.83	8.80	11.07	6.48	7.28	7.32	9.13	9.69
261C	6.46	6.70	7.56	10.94	11.94	6.62	7.64	8.16	9.29	9.90
261D	6.96	7.86	11.38	12.41	12.76	7.35	9.21	9.87	9.84	10.05
262B	6.52	6.69	6.93	8.72	11.38	5.84	6.19	6.40	8.06	8.42
262C	6.84	7.29	8.74	11.94	12.70	6.70	7.42	8.53	9.96	9.58
262D	7.48	8.93	12.41	13.07	13.51	7.91	9.75	10.32	10.94	10.41
263B	7.17	7.21	7.21	7.38	9.03	6.62	6.48	6.33	7.93	8.74
263C	8.41	8.41	9.20	17.22	18.93	8.24	8.93	9.64	12.09	11.92
264B	9.20	8.93	8.96	9.62	14.86	8.80	9.64	8.58	10.66	14.14
264C	10.91	10.82	12.20	21.44	22.74	11.39	12.67	14.21	17.20	17.20
265B	10.14	10.03	10.34	14.96	17.58	9.67	10.91	10.35	15.43	15.15
265C	10.58	10.69	12.69	17.65	18.75	10.11	11.58	13.10	15.47	14.79
265D	11.22	12.22	16.96	19.27	19.86	11.68	13.98	15.51	15.76	16.09
269A	10.20	10.09	9.99	12.27	21.44	8.77	9.96	9.24	14.25	14.95
270B	12.05	12.40	15.33	21.81	23.01	12.50	14.17	15.96	18.60	18.83
270C	11.14	11.21	11.76	18.31	21.42	12.09	13.24	13.57	18.18	18.92
273B	10.43	10.60	11.81	18.29	19.95	10.32	11.48	12.99	14.33	15.68
281A	11.53	11.40	11.29	14.71	24.57	11.45	12.43	11.35	14.99	19.54

Table A-2b. (cont'd)

RUN NO.	H 1 M	H 2 M	H 3 M	H 4 M	H 5 M	H 1,T M	H 2,T M	H 3,T M	H 4,T M	H 5,T M
228B	90.9	91.4	97.5	114.7	142.9	97.0	99.7	103.8	117.1	134.6
228C	100.0	102.1	122.1	158.6	163.9	101.4	109.2	124.6	139.3	135.0
229B	94.2	96.5	105.6	147.6	171.8	87.3	93.0	100.4	126.2	138.0
229C	105.6	133.5	186.2	194.0	200.5	119.8	142.0	150.2	147.4	152.1
230B	84.8	87.8	95.4	114.4	157.6	115.6	112.5	112.2	137.6	148.8
230C	87.8	92.9	112.3	159.7	175.6	120.6	123.0	133.3	153.5	160.7
230D	90.9	100.5	136.6	175.0	183.6	121.4	128.7	146.1	156.8	158.7
231B	82.3	83.1	87.3	91.4	121.6	103.8	107.4	103.1	119.4	135.0
231C	88.3	93.9	105.6	199.6	233.2	112.2	124.6	135.0	168.6	169.2
231D	96.0	111.8	198.5	243.0	251.3	122.2	105.2	163.1	171.2	168.1
232B	102.4	93.9	100.0	114.4	260.1	90.8	96.3	89.5	119.4	142.9
233B	76.8	78.8	82.8	84.3	96.0	70.8	71.3	70.3	66.2	88.0
233C	81.3	84.8	92.4	126.8	210.4	79.0	84.9	87.7	101.0	127.8
235B	75.9	81.0	83.5	86.0	102.3	80.2	84.0	76.8	88.3	104.9
235C	84.8	88.3	92.4	123.1	230.5	90.5	96.3	91.4	119.8	142.0
237B	122.2	127.4	144.0	214.8	239.9	135.4	158.7	161.7	207.7	212.5
237C	126.2	137.7	178.8	239.8	254.0	142.4	174.3	191.6	210.7	218.7
237D	134.1	154.0	231.1	255.2	265.2	162.6	206.5	221.8	225.5	230.0
239B	132.5	133.5	140.8	167.1	274.5	135.0	145.6	137.6	179.0	227.5
239C	144.6	147.7	163.0	279.9	321.1	154.4	171.7	182.2	235.9	251.4
240B	107.7	103.6	103.6	230.5	329.5	112.9	113.3	111.8	155.4	153.9
240C	102.1	95.4	102.6	103.1	159.7	111.8	108.5	96.3	108.5	140.2
241B	103.6	104.1	108.7	130.4	217.4	101.7	111.0	103.5	128.7	159.7
242B	78.8	83.8	95.4	88.3	101.0	92.1	86.7	78.7	75.4	90.2
243B	91.4	100.0	106.2	161.3	271.7	86.7	92.7	95.0	113.7	124.6

Table A-2b. (cont'd)

RUN NO.	H 1 M	H 2 M	H 3 M	H 4 M	H 5 M	H 1,T M	H 2,T M	H 3,T M	H 4,T M	H 5,T M
244B	89.9	89.4	91.9	108.2	136.1	95.3	96.6	112.9	112.2	114.8
244C	97.0	103.6	140.3	154.9	160.2	95.3	104.9	116.7	129.1	125.0
244D	100.3	118.7	155.8	160.0	165.8	107.4	121.0	127.8	138.0	132.0
244E	90.6	92.1	98.7	130.1	148.3	97.6	103.5	112.2	128.7	135.4
245B	87.8	87.8	88.8	89.4	101.6	79.3	78.5	77.0	91.4	89.5
245C	88.8	89.2	88.1	94.9	122.6	79.9	80.5	80.2	94.0	101.7
245D	97.0	97.0	111.3	157.6	175.6	94.3	101.7	113.7	134.1	129.9
246A	87.3	85.8	77.8	88.8	161.3	110.3	116.7	103.8	118.2	156.3
247B	105.6	102.1	130.4	341.5	363.2	113.7	124.2	137.6	142.9	156.3
247C	91.0	86.9	79.9	119.1	269.1	99.7	105.6	94.7	120.6	152.1
248B	83.8	81.8	77.8	86.3	141.3	84.3	87.7	82.8	97.3	117.9
248C	98.3	96.5	122.1	242.5	254.6	112.2	121.8	137.6	153.0	152.1
249B	80.3	79.2	76.0	76.8	94.9	87.0	91.4	83.7	93.7	105.2
249C	104.3	107.9	222.2	303.8	312.8	120.2	134.1	147.4	153.9	150.7
249D	95.1	90.6	94.6	201.4	290.9	111.8	119.8	123.8	145.6	160.7
251B	131.4	131.4	136.3	228.0	305.8	127.0	138.9	142.4	179.0	208.9
251C	149.2	161.8	284.5	330.7	343.8	161.7	193.2	215.6	231.3	223.0
252B	99.5	94.4	95.1	114.6	248.0	98.3	106.7	96.6	122.2	154.9
252C	111.0	103.3	110.5	188.6	296.5	123.8	135.4	134.1	176.4	194.4
254B	88.3	92.9	130.4	230.5	243.6	114.8	127.4	145.1	153.5	159.7
254C	87.3	87.8	98.0	185.7	235.9	113.3	124.6	135.0	155.4	163.6
254D	78.0	78.0	78.0	81.5	103.3	91.7	95.0	91.1	95.3	116.7
255B	109.7	107.7	109.2	110.8	152.3	117.9	128.3	109.6	121.8	163.6
255C	149.9	145.7	160.9	362.9	405.8	157.3	172.7	189.3	234.6	240.5
256A	120.0	128.8	235.9	330.1	343.2	129.9	148.8	171.7	179.0	186.0
257B	111.8	108.7	100.5	148.1	289.0	109.9	117.5	108.5	139.3	170.7

Table A-2b. (cont'd)

RUN NO.	H 1 M	H 2 M	H 3 M	H 4 M	H 5 M	H 1,T M	H 2,T M	H 3,T M	H 4,T M	H 5,T M
258B	111.5	108.4	104.8	157.8	307.1	105.2	111.8	103.5	135.0	165.6
258C	131.9	133.5	226.1	386.9	401.5	143.8	162.6	188.2	198.4	194.9
260B	96.0	93.9	92.9	110.8	182.5	91.4	92.4	88.9	117.5	131.2
260C	99.2	100.2	103.8	156.2	245.5	107.8	114.8	116.7	150.2	163.1
260D	110.3	131.1	233.7	263.2	273.9	132.9	156.8	172.2	170.7	173.8
261B	88.4	91.5	96.6	125.8	160.3	91.4	103.1	103.8	130.8	139.3
261C	91.1	94.6	107.4	158.3	173.7	93.4	108.5	116.3	133.3	142.4
261D	98.5	111.8	165.0	180.9	186.2	104.2	132.0	142.0	141.5	144.7
262B	91.9	94.4	98.0	124.7	165.0	81.9	87.0	90.2	114.8	120.2
262C	96.7	103.3	124.9	173.7	185.4	94.7	105.2	121.8	143.3	137.6
262D	106.2	127.8	180.9	191.0	198.0	112.5	140.2	148.8	158.2	150.2
263B	101.6	102.1	102.1	104.6	129.3	93.4	91.4	89.2	112.9	125.0
263C	120.0	120.0	131.8	256.5	284.0	117.5	127.8	138.5	175.9	173.3
264B	131.9	127.8	128.3	138.2	219.1	125.8	138.5	122.6	153.9	207.7
264C	157.9	156.5	177.7	325.0	346.4	165.1	184.9	208.9	256.2	256.2
265B	146.0	144.5	149.2	220.7	262.3	138.9	157.8	149.3	228.1	223.7
265C	152.8	154.4	185.2	263.4	281.2	145.6	168.1	191.6	228.7	218.0
265D	162.5	178.0	252.4	289.5	299.1	169.7	205.4	229.4	233.3	238.5
269A	147.0	145.4	143.8	178.6	324.9	125.4	143.3	132.4	209.5	220.5
270B	175.4	180.7	226.4	331.0	351.0	182.2	208.3	236.5	278.6	282.4
270C	161.4	162.4	170.9	274.0	324.5	175.9	193.8	198.9	272.0	283.9
273B	150.5	153.2	171.6	273.7	300.5	148.8	166.6	189.9	210.7	232.0
281A	167.4	165.3	163.7	216.7	376.8	166.1	181.2	164.6	221.1	293.9

Appendix B: Thermocouple fabrication procedure

After the thermocouple sensor ports are drilled into the assembled hydrofoil--see figures 4.2 and 4.5--the thermocouples are fabricated and installed as follows:

I. Deburr thermocouple sensor ports

A. Thread a 0.010-inch (0.0254 cm) piano wire through the sensor port and through the small stainless steel conduit tube.

B. Apply a medium-coarse lapping compound to the wire at the sensor port.

C. Slide the piano wire back-and-forth inside the conduit ~ 200 times to remove any burrs, at the sensor port, that may have resulted from the drilling operation.

D. Repeat this deburring operation for each thermocouple port. When the last port has been deburred, remove the piano wire and flush all conduits with solvent.

E. Rod dead end of each conduit with piano wire and flush with solvent. Repeat this operation, as required, until thermocouple conduits are clean. Dry conduits by blowing compressed air through them.

II. Fabricate thermocouple junctions

A. Cut a length of Chromel[8] wire twice the length required to extend through the conduit. Skin the thermocouple wire insulation at one end and in the center; tin the skinned wire using stainless steel soldering flux and solid core (50/50) solder. Wash off flux.

---

[8] Identification of a manufacturer and a manufacturer's product has been necessary to make the results of this work meaningful and in no way implies a recommendation or endorsement by the National Bureau of Standards, or by the National Aeronautics and Space Administration.

B. Cut a length of Au (0.07 atomic percent Fe) wire one-half as long as the Chromel wire, and skin and tin each end. Use voltage-controlled soldering iron and do not get Au wire too hot--use just enough heat to melt solder.

C. Twist the Chromel-Au wires together to form a junction, at the mid-length of the Chromel wire, and solder using resin-core radio solder. Clean junction with solvent and thoroughly dry junction.

D. Reinforce the enamel insulation on the Chromel-Au wires with polyimide enamel--two coats. Wipe the enamel on with a plastic glove. Do not insulate the junction (stop application of enamel at about 0.6 cm from the junction). Keep the Chromel and Au wires separated until the enamel dries.

III. Installation of junctions

A. Thread the insulated end of the extra-long Chromel wire into the tube-conduit from the sting end of the hydrofoil assembly. The extra length of Chromel wire is used as a fish-wire to pull the thermocouple junction through the conduit. The thermocouple junction is pulled through the sensor port so that all of the uninsulated Chromel-Au extension wire, near the junction, is exposed.

B. Apply polyimide enamel to the uninsulated wires and junctions--two coats--allow the enamel to thoroughly dry.

C. Pull the junctions back into the sensor ports (final desired position is flush with hydrofoil surface) and check for electrical shorts.

D. Attach a transparent vacuum hose to the aft end of the hollow cylindrical sting shaft.

E. Mix epoxy: Emerson and Cuming, Inc., Stycast[9] 2850 GT with room temperature cure activator.

F. Apply epoxy to the sensor ports (being careful not to displace the thermocouple junctions); then use the vacuum assist and carefully manipulate the thermocouple wires until epoxy can no longer be sucked into the conduits through the sensor ports.

G. Remove vacuum hose and excess epoxy from each sensor port; leave the epoxy at each of these ports slightly mounded.

H. Make final placement of the thermocouple junction at each sensor port. Junctions should project slightly from the mounds of epoxy on top of each sensor port, and should be visibly centered in the sensor ports; i. e., the thermocouple junctions should not be in contact with the hydrofoil sensor ports. These soldered junctions should be sufficiently long that they will not be destroyed, later on, when the epoxy mounds, and encapsulated junctions, are filed and sanded flush with the hydrofoil.

I. After the epoxy is thoroughly cured, the thermocouple installation is again checked for electrical shorts. Then tape-mask the hydrofoil, exposing only the epoxy bumps. Use flat Swiss-pattern files and file the bumps and encapsulated junctions until they are nearly flush with the hydrofoil. Then use wet fine-grit sandpaper and sand the epoxied junctions flush with the hydrofoil. Again check for electrical shorts. These sealed and flush mounted junctions are shown in figure 4. 1.

---

[9] Identification of a manufacturer and a manufacturer's product has been necessary to make the results of this work meaningful and in no way implies a recommendation or endorsement by the National Bureau of Standards, or by the National Aeronautics and Space Administration.

J. Wire motion, and consequently chafing, is minimized by pouring an epoxy plug in the conduit support assembly at the aft end of the hollow sting shaft--this minimizes the possibility of electrical shorts developing. The tinned Chromel-Au wires extend to the rear of this epoxy plug--see figure 4.2.

IV. Thermocouple extension wires

A. Thermocouple extension wires are then attached to the tinned junction leads, at the rear end of the sting assembly, using radio solder. These connections are then enamel insulated, and the extension wires are routed through one of the hollow elliptical sting struts, and soldered to a gold-pin electrical connector--see figures 4.1 and 4.2.

B. About 75 cm of each extension wire is bundled and carefully coiled and compactly packed with a stiff vacuum grease, to form an ogival shaped projection, on the rear end of the sting shaft. The hollow ogival sting cap--see figure 4.2-- is then screwed onto the sting shaft, completely protecting the thermocouple wires. The vacuum grease packed wire assembly provides some thermal tempering for the thermocouple extension wires.

C. A low temperature vacuum seal is obtained at the gold-pin electrical connector by casting another epoxy plug.

D. Constant temperature at this electrical connection was ensured by 1) using a low resistance (brass) thermal path between the connector and the sting flange assembly and 2) carefully insulating this connector with multilayer radiation insulation.

Appendix C: Computer program for correlating desinent cavitation data

This appendix outlines the details of the computer program used to correlate the desinent and incipient cavitation data acquired from this study. Because data could not be obtained at constant temperature, a mathematical technique was developed, so that isotherm data could be calculated. While the fluid temperature could not be precisely controlled, the data were obtained in discrete groups that were nearly isothermal; thus, the technique for computing isotherm data need not be too sophisticated.

The technique chosen to correlate these desinent data consists of fitting an equation to a three-dimensional surface, i.e., P_o, V_o, and T_o (at desinence) are the three coordinates, and an equation is derived to fit all of the experimental data. This equation may then be used to predict desinent flow conditions (P_o and V_o), along any isotherm (T_o = constant), within the boundaries of the experimental data. Also, the desinent flow conditions, at each individual experimental data point, may be computed for comparison with each actual experimental data point. Actually, this is the technique used to assure that the equation adequately fits the experimental data, i.e., the equation is derived from a least-squares solution technique that minimizes the differences in calculated P_o, and experimental P_o, at each experimental T_o and V_o. When these differences in P_o are each less than the minimum possible experimental error in P_o, the equation is considered adequate.

The computer program used to derive this correlative equation uses a simplified Bjorck subroutine. This Bjorck technique is programmed to provide a conventional least-squares solution to data-fitting problems. This program always locates the absolute minima in the

selected ordinate--in this case, standard deviation in P_o at desinence. The Bjorck program consumes little machine time and is very reliable. More details concerning the application of the Bjorck program, and its niceties, to data-fitting problems, are given in reference [20].

To enter the Bjorck program, it is necessary to assume an appropriate form for the surface-fitting equation. Previous experience with P_o - V_o - T_o data, and preliminary hand calculations, indicated that a simple polynomial expression would suffice. The general form of this expression is

$$P_o = A_1 T_o + A_2 V_o + A_3 T_o V_o + A_4 T_o^2 + A_5 V_o^2 + A_6 (T_o V_o)^2 + \ldots\ldots + A_n, \qquad \text{(C-1)}$$

where the A_1 to A_n are numerical coefficients. It was soon learned that the first four or five terms, of eq (C-1), provided an adequate fit of the experimental data and the higher order terms were eliminated from the program. The program listing on page C-6 shows that only eight terms were retained in the program; the minimum number of these terms were used to obtain a satisfactory fit of each batch of experimental data.

As expected, the order in which the terms of eq (C-1) are introduced into the Bjorck program influences the number of terms required to obtain a satisfactory fit of the experimental data. Thus, various combinations of terms--where each combination contained not more than eight terms--were tested to obtain the best combination for each batch of data. The Bjorck solution will best fit the data, with the minimum number of terms, when these terms are the most influential of the available terms, and appear first in the mathematical arrangement

of eq (C-1). The best combination and number of terms is readily indicated, by the minimum standard deviation in P_o, i.e., the Bjorck program computes this standard deviation for 1, 2, 3, 4, 5, 6, 7, and 8 terms, for each combination of terms. Once the best arrangement and number of terms are selected, the differences in P_o (calculated minus experimental values) are inspected to see that the data have been fit, within experimental uncertainties. If so, this correlative equation is used to predict P_o, at constant T_o, for various values of V_o, within the boundaries of the experimental data. This equation should not be used to predict desinent cavitation conditions, outside of the confines of the experimental data. As in all surface-fitting cases, it is dangerous to attempt to extrapolate an experimentally defined surface.

If the correlative equation does not fit the experimental data, within experimental uncertainties, it is necessary to try a different combination of terms in eq (C-1), or assume a different general form for the correlative expression. The polynomial expression in eq (C-1) was sufficient for all data acquired in this study.

For desinent nitrogen cavities on the hydrofoil, we obtained

$$P_o = -1.34832\,T_o + 0.81918\,V_o - 0.00911\,T_o V_o + 0.01082\,T_o^2 + 0.01886\,V_o^2 . \qquad \text{(C-2)}$$

Although incipient cavity data are included in the tabulations of appendix A, only desinent data were used in deriving eq (C-2). The incipient data were not included because they exhibited a slight hysteresis effect, relative to the predominantly desinent data.

For desinent (and incipient) hydrogen cavities on the hydrofoil, we obtained

$$P_o = -3.44809\,T_o + 0.57330\,V_o - 0.00488\,T_o V_o + 0.08066\,T_o^2 . \qquad \text{(C-3)}$$

The incipient cavity data, for hydrogen, showed negligible hysteresis and were included in deriving eq (C-3). The data shown on figures 5.3 and 5.4, and in table 5.2, were computed from eq (C-2); likewise eq (C-3) was used to produce figures 5.1 and 5.2, and table 5.1. In eq (C-2) and eq (C-3) the units of P_o, V_o, and T_o are psia, ft/s, and degrees Rankine, respectively.

The Bjorck desinent-data fitting program functions as follows:

(1) A particular combination of polynomial terms is chosen--statement 19; all input data, label (run no.), T_o, V_o, and P_o are read and stored in computer memory--statement 10.

(2) Coefficients for the Bjorck subroutine are computed--statements 11 to 14.

(3) The chosen algebraic terms are used to fit the experimental data by calling the Bjorck subroutine--statement 22 + 2.

(4) Standard deviation and residuals are computed and printed--statements 22 + 3 to 24 + 1.

(5) The number of algebraic terms to be used in the correlative expression are predetermined, along with ranges and intervals for T_o and V_o; the coefficients for the chosen correlative expression are printed--statements 30 to 33.

(6) The differences in calculated and experimental P_o, at each data point, are computed and printed--statements 44 to 47.

(7) Desinent pressures (P_o) corresponding to the chosen isotherms (T_o), at the chosen velocities (V_o), are then computed and printed-- statements 47 + 1 to 57 + 9.

(8) Values of K_{iv}, at each of the coordinate positions computed in step (7), are calculated and returned upon demand-- statement 30 and statements 9 to 90. Metric (SI units) values of P_o, V_o, and T_o, at each of the calculated coordinate positions, are also computed and returned-- statements 61 to 62 + 4.

All pertinent data is printed out as it is generated. Different combinations of polynomial terms, as listed in statements 12 to 14, may be tested, on each batch of experimental data, by cycling the program with appropriately punched data process cards--statements 90 and 19. Use of any linear expression, different from eq (C-1), is made possible by simply replacing the A (I, J) coefficients--statements 12 to 14--with the appropriate terms from the desired expression. The program, as listed, accommodates 10 terms, but is easily altered to handle any desired number of terms.

This program, as listed, requires an NBS fluid property data deck (data processing cards) for hydrogen or nitrogen fluids.

Computer Program Listing

```
!JOB,2750453,HORD,2
!FTN,L,X,R
      PROGRAM PO VO TO
      DIMENSION P(200),V(200),T(200),L(200),PO(50),VO(50),TO(50),KIV(50)
     1,METPO(50),METTO(50),METVO(50)
      COMMON A(200,10),B(200),NP,NF,C(10,10),Y(10),D(10),R(75)
      DOUBLE PRECISION A,B,C,D,R,Y
      REAL KIV,METPO,METTO,METVO
   19 READ 72,ICASE
      IF(EOF,60)92,13
   13 KTR=I=1
      NF=8
      SS=0.
   10 READ 1,L(I),T(I),V(I),P(I)
      IF(EOF,60) 22,11
   11 B(I)=P(I)
      SS=B(I)*B(I)+SS
   20 GO TO(12,15,16,17,18),ICASE
   12 A(I, 1)=V(I)
      A(I, 2)=T(I)
      A(I, 3)=V(I)*V(I)
      A(I, 4)=T(I)*T(I)
      A(I, 5)=T(I)*T(I)*T(I)
      A(I, 6)=V(I)**4*T(I)**2
      A(I, 7)=V(I)**4
      A(I, 8)=1.00
      GO TO (14,44,55),KTR
   15 A(I, 1)=T(I)
      A(I, 2)=T(I)*V(I)
      A(I, 3)=T(I)*T(I)
      A(I, 4)=V(I)*V(I)*T(I)
      A(I, 5)=T(I)*T(I)*T(I)
      A(I, 6)=V(I)**4*T(I)**2
      A(I, 7)=V(I)**4
      A(I, 8)=1.00
      GO TO(14,44,55),KTR
   16 A(I, 1)=T(I)
      A(I, 2)=V(I)
      A(I, 3)=T(I)*V(I)
      A(I, 4)=T(I)*T(I)
      A(I, 5)=V(I)*V(I)
      A(I, 6)=(T(I)*V(I))**2
      A(I, 7)=V(I)**4
      A(I, 8)=1.00
      GO TO(14,44,55),KTR
   17 A(I, 1)=T(I)
      A(I, 2)=V(I)
      A(I, 3)=T(I)*V(I)
      A(I, 4)=V(I)*T(I)*T(I)
      A(I, 5)=T(I)*V(I)*V(I)
      A(I, 6)=(T(I)*V(I))**2
      A(I, 7)=V(I)**4
      A(I, 8)=1.00
      GO TO(14,44,55),KTR
```

```
18 A(I, 1)=V(I)
   A(I, 2)=T(I)
   A(I, 3)=V(I)*V(I)*T(I)
   A(I, 4)=V(I)*V(I)
   A(I, 5)=T(I)*T(I)
   A(I, 6)=(T(I)*V(I))**2
   A(I, 7)=V(I)**4
   A(I, 8)=1.00
   GO TO(14,44,55),KTR
14 I=I+1
   GO TO 10
22 NP=I-1
   KTR=2
   CALL BJORCK
   DO 24 I=1,10
   SS=SS-Y(I)*Y(I)
   FN=NP-I
   D(I)=SQRT(SS/FN)
   R(I)=D(I)*(((((1.870027491/FN+1.062820556)/FN+2.63502131)/FN
  1 +2.800533017)/FN+2.377926828)/FN+1.959670711)
24 CONTINUE
   PRINT 2,(I,Y(I),R(I),D(I),I=1,10)
30 READ 6,NF,TZ,TM,DT,VZ,VM,DV,KK
   IF(EOF,60) 9,33
33 PRINT 3,(C(NF,J),J=1,NF)
   PRINT 4,NF
   DO 47 I=1,NP
   GO TO(12,15,16,17,18),ICASE
44 PC=0.
   DO 45 J=1,NF
45 PC=PC+A(I,J)*C(NF,J)
   DIFF=P(I)-PC
47 PRINT 5,L(I),T(I),V(I),P(I),PC,DIFF
   KTR=3
   I=NP+1
   LL=1
   T(I)=TZ
50 PRINT 7,T(I),NF
   V(I)=VZ
   GO TO(12,15,16,17,18),ICASE
55 PC=0.
   DO 57 J=1,NF
57 PC=PC+A(I,J)*C(NF,J)
   PRINT 8,V(I),PC
   VO(LL)=V(I)
   PO(LL)=PC
   TO(LL)=T(I)
   LL=LL+1
   V(I)=V(I)+DV
   IF(V(I).LE.VM) GO TO 20
   T(I)=T(I)+DT
   IF(T(I).LE.TM) 50,30
 1 FORMAT(A8,F12.0,2F10.0)
 2 FORMAT(*1THE NUMBER OF TERMS, INTERNAL COEFFICIENTS, THEIR ESTIMAT
```

```
     1ED ERROR, AND THE STANDARD DEVIATION FOR THAT MANY TERMS ARE AS FO
     2LLOWS9*/*0*/(*0A(*I2,*) =* E17.10,* +/-*E9.2,*, STD. DEV. =*E9.2))
    3 FORMAT(*1CALCULATED  PO  IS THE SUM OF THE FOLLOWING TERMS9*/*0*/
     1 /*0 PO  =*E17.10,8H*A(I, 1) E17.10,8H*A(I, 2) E17.10,8H*A(I, 3)
     2 /*0       *E17.10,8H*A(I, 4) E17.10,8H*A(I, 5) E17.10,8H*A(I, 6)
     3 /*0       *E17.10,8H*A(I, 7) E17.10,8H*A(I, 8) E17.10,8H*A(I, 9)
     4 /*0       *E17.10,8H*A(I,10) E17.10,8H*A(I,11) E17.10,8H*A(I,12)
     5 /*0       *E17.10,8H*A(I,13) E17.10,8H*A(I,14) E17.10,8H*A(I,15)
     6 /*0       *E17.10,8H*A(I,16) E17.10,8H*A(I,17) E17.10,8H*A(I,18)
     7 /*0       *E17.10,8H*A(I,19) E17.10,8H*A(I,20) E17.10,8H*A(I,21)
     8 /*0       *E17.10,8H*A(I,22) E17.10,8H*A(I,23) E17.10,8H*A(I,24)
     9 /*0       *E17.10,8H*A(I,25))
    4 FORMAT(*1*I2,* FUNCTIONS GIVES THE FOLLOWING FIT9*/*0*/
     1 * LABEL      T        V       P     P CALC  DIFF*/* *)
    5 FORMAT(*  *A4,F8.2,F7.1,F8.1,F8.1,F6.1)
    6 FORMAT(I10,6F10.0,I10)
    7 FORMAT(*1THE*F6.2,* DEGREE R. ISOTHERM USING*I3,* FUNCTIONS IS9*
     1 /*0*/*       V        PO *)
    8 FORMAT(*0*2F8.1)
    9 LL=LL-1
   60 IF(KK.EQ.1)90,61
C      THIS BRANCHES TO KIV CALC IF KK NOT EQUAL TO 1
   61 DO 62 J=1,LL
      METPO(J)=0.6894757*PO(J)
      METTO(J)=(5./9.)*TO(J)
      METVO(J)=0.3048*VO(J)
      ATMPO=PO(J)/14.6959494
      PSAT=VPRESS(METTO(J))
      RHOLIQ=FIND DH(ATMPO,METTO(J))
      IF(RHOLIQ.GT.0.0) GO TO 63
      KIV(J)=0.0
      GO TO 62
   63 KIV(J)=(PO(J)-14.6959494*PSAT)*144.*2.*32.1725/(RHOLIQ*VO(J)**2)
   62 CONTINUE
      WRITE(61,70)
      WRITE(62,70)
      WRITE (61,71)(TO(J),VO(J),PO(J),KIV(J),METPO(J),METVO(J),METTO(J),
     1J=1,LL)
      WRITE (62,71)(TO(J),VO(J),PO(J),KIV(J),METPO(J),METVO(J),METTO(J),
     1J=1,LL)
   70 FORMAT(*1*, 4X,*TEMPERATURE-COMPENSATED DESINENT DATA(HYDROGEN90.4
     120-IN(1.067-CM)OGIVE)*    /// 7X,*TO*,8X,*VO*,8X,*PO*,10X,*KIV*,10
     2X,*PO*,8X,*VO*,8X,*TO*/ 6X,*DEG R*,4X,*FT/SEC*,5X,*PSIA*,20X,*N/CM
     3/CM*,4X,*M/SEC*,5X,*DEG K*//)
   71 FORMAT(6( 1X,F10.2,F9.1,F11.2,F12.2,F13.2,F9.1,F11.2,/)/)
   72 FORMAT(I1)
   90 GO TO 19
   92 CALL EXIT
      END
      FUNCTION FIND DH(PATM,TDK)
C     CALCULATES THERMOFUNCTIONS OF H2 ACCORDING TO MONO 94
C     INPUT , P IN ATM, T IN DEG K, OUTPUT UNITS AS IN MONO 94
C     EXCEPT THAT DENSITY IN MOLES/CC IS RETURNED, NOT VOLUME, AND
C     INTERNAL ENERGY HAS TO BE CALC. FROM H AND P-V.
```

```
C       INPUT LIMITATIONS, P LESS THAN 350.1, T BETWEEN 13.803 AND 100.0
C       SUBROUTINES REQUIRED, THERMO, CASEI,CASEII,CASEA,ISOTHM,C214TAPE
C       DIRECT ANY QUESTIONS TO HANS RODER
        COMMON /C214TAPE/CT(43,15),CR(90,5),RR(90),TT(43),CW(100),SW(100),
       1 HW(100),PST(28,8),TTT(66),CVSP(66),C(2,6),PP(90),DPDT(90),
       2 DPDT2(90),B1,B2,B3,B4,CA,CB,CC,CD,CE,DPDR,DPDR2,DPDR3,PI,MI,II,
       3 JJ,ISTOP,ISTOP1,JSTOP,CPDTDR,CPDTD1,P,T,RL,RV,H,S,CV,CP,SVEL,
       4 CSLOPE,P1ST(28,7),P2ST(28,7),P3ST(28,6)
        P=PATM
        T=TDK
        MI=1
        CALL CASE A
        FIND DH=RL*125.83728
        RETURN
        END
        SUBROUTINE BJORCK
        COMMON A(200,10),B(200),NP,NF,C(10,10),Y(10),D(10),R(75)
        DOUBLE PRECISION A,B,C,D,R,Y
        D(1)=Y(1)=0.D
        DO 1 I=1,NP
        D(1)=A(I,1)*A(I,1)+D(1)
      1 Y(1)=A(I,1)*B(I)+Y(1)
        Y(1)=Y(1)/D(1)
        IR=0
        DO 5 K=2,NF
        DO 3 J=K,NF
        IR=IR+1
        R(IR)=0.D
        DO 2 I=1,NP
      2 R(IR)=A(I,K-1)*A(I,J)+R(IR)
        R(IR)=R(IR)/D(K-1)
        DO 3 I=1,NP
      3 A(I,J)=A(I,J)-A(I,K-1)*R(IR)
        D(K)=Y(K)=0.D
        DO 4 I=1,NP
        B(I)=B(I)-A(I,K-1)*Y(K-1)
        Y(K)=A(I,K)*B(I)+Y(K)
      4 D(K)=A(I,K)*A(I,K)+D(K)
      5 Y(K)=Y(K)/D(K)
        IRS=-NF
        DO 7 K=1,NF
        IR=IRS=IRS+NF-K+1
        DO 7 JJ=1,K
        J=K-JJ+1
        C(K,J)=Y(J)
        DO 6 I=2,JJ
        C(K,J)=C(K,J)-C(K,K-I+2)*R(IR)
      6 IR=IR-1
      7 IR=IR-NF+K
        DO 8 I=1,NF
      8 Y(I)=Y(I)*D(I)**0.5
        RETURN
        END
           SCOPE
```